Rigorous Higher Order Methods, The Demon of Darkness and Chaos, And Henon's Brain

Kyoko Makino and Martin Berz

Center for Dynamical Systems
Department of Physics and Astronomy
Michigan State University

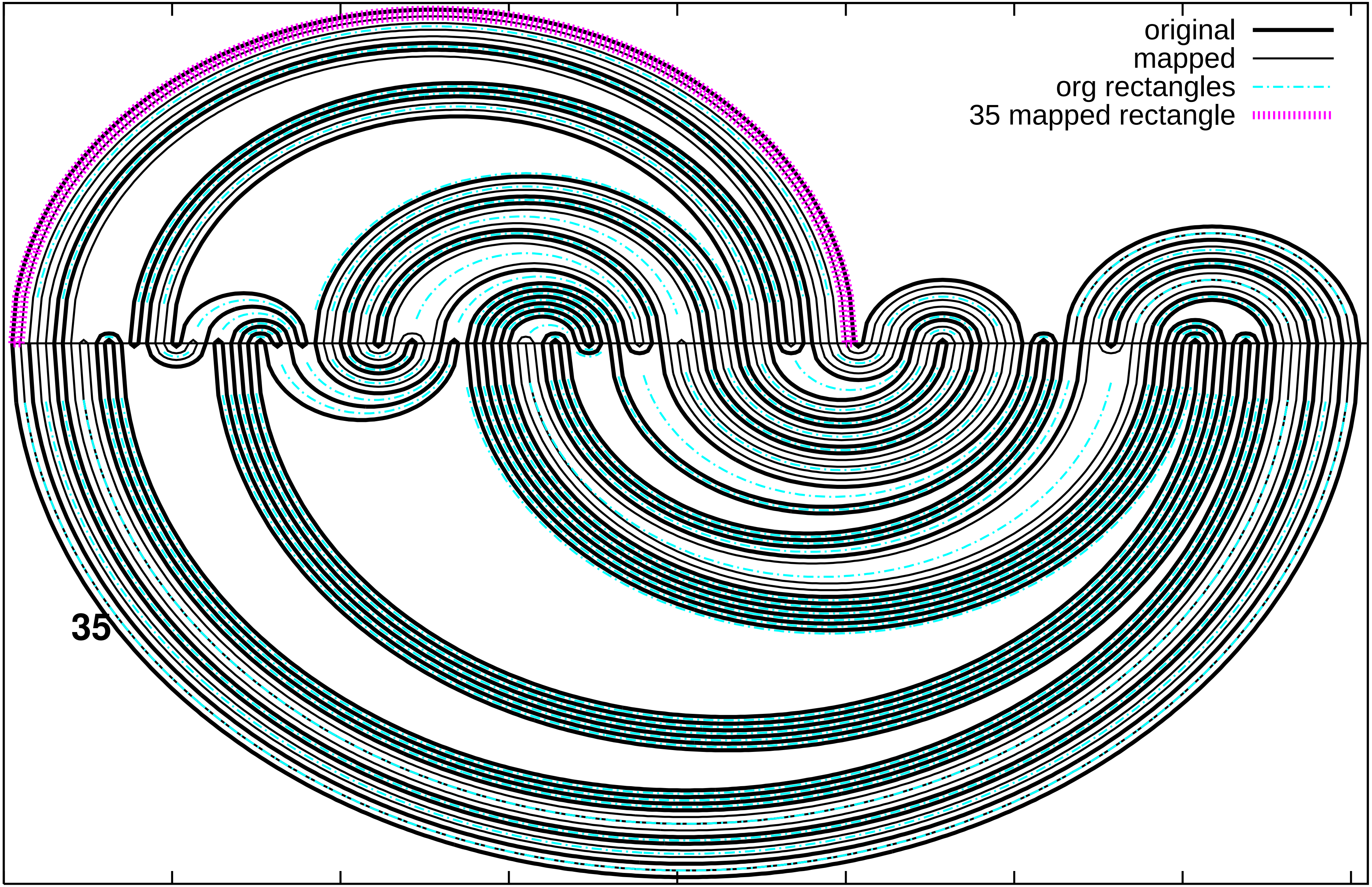
original
mapped
org rectangles
35 mapped rectangle
35

The Henon Map

Henon Map: frequently used elementary example that exhibits many of the well-known effects of nonlinear dynamics, including chaos, periodic fixed points, islands and symplectic motion. The dynamics is two-dimensional, and given by

$$\begin{aligned} x_{n+1} &= 1 - \alpha x_n^2 + y_n \\ y_{n+1} &= \beta x_n. \end{aligned}$$

It can easily be seen that the motion is area preserving for $|\beta| = 1$.We consider

$$\alpha = 2.4 \text{ and } \beta = -1,$$

and concentrate on initial boxes of the from $(x_0, y_0) \in (0.4, -0.4) + [-d, d]^2$.

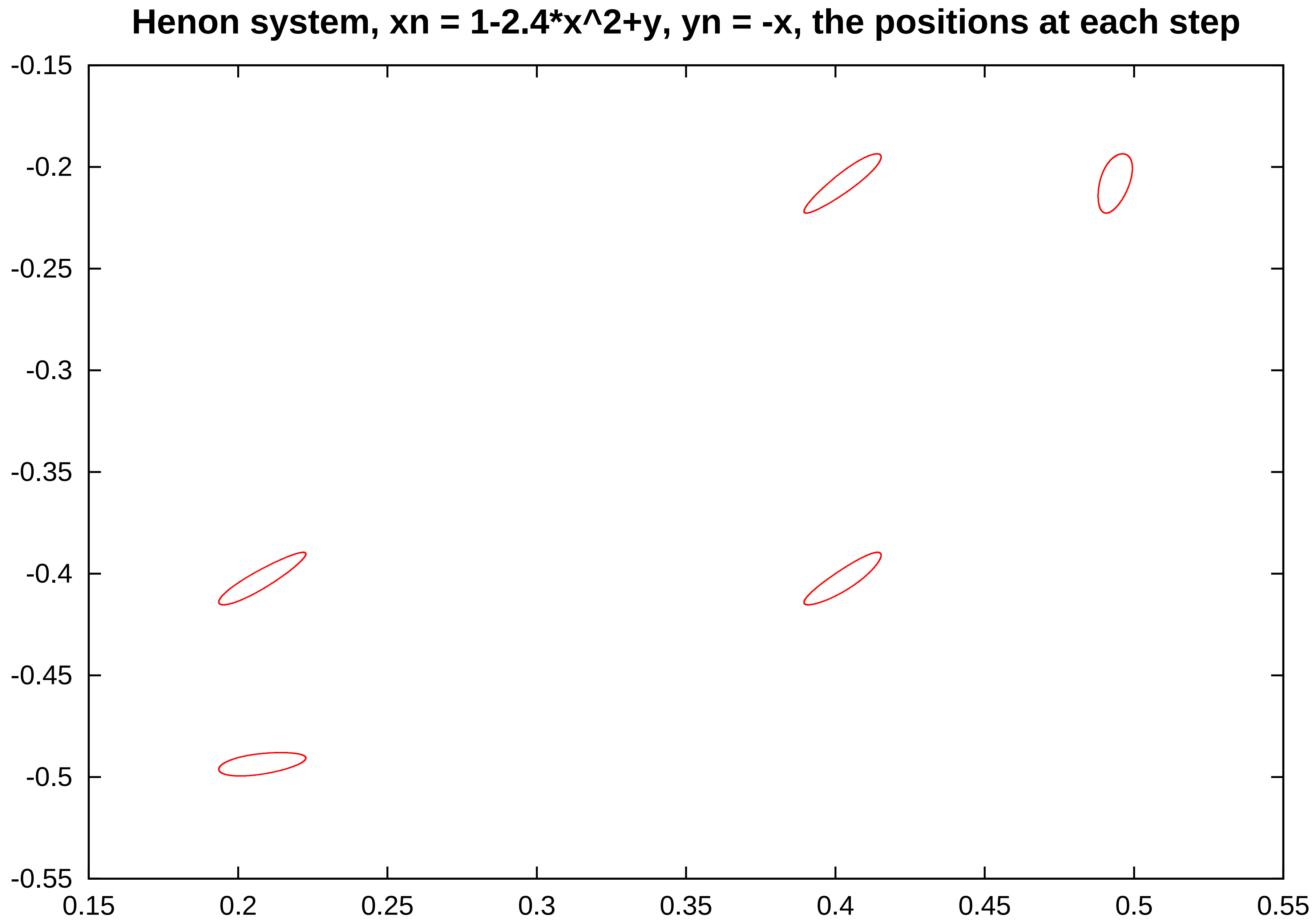
Henon system, xn = 1-2.4*x^2+y, yn = -x, the positions at each step
-0.15
-0.2
-0.25
-0.3
-0.35
-0.4
-0.45
-0.5
-0.55
0.15
0.2
0.25
0.3
0.35
0.4
0.45
0.5
0.55

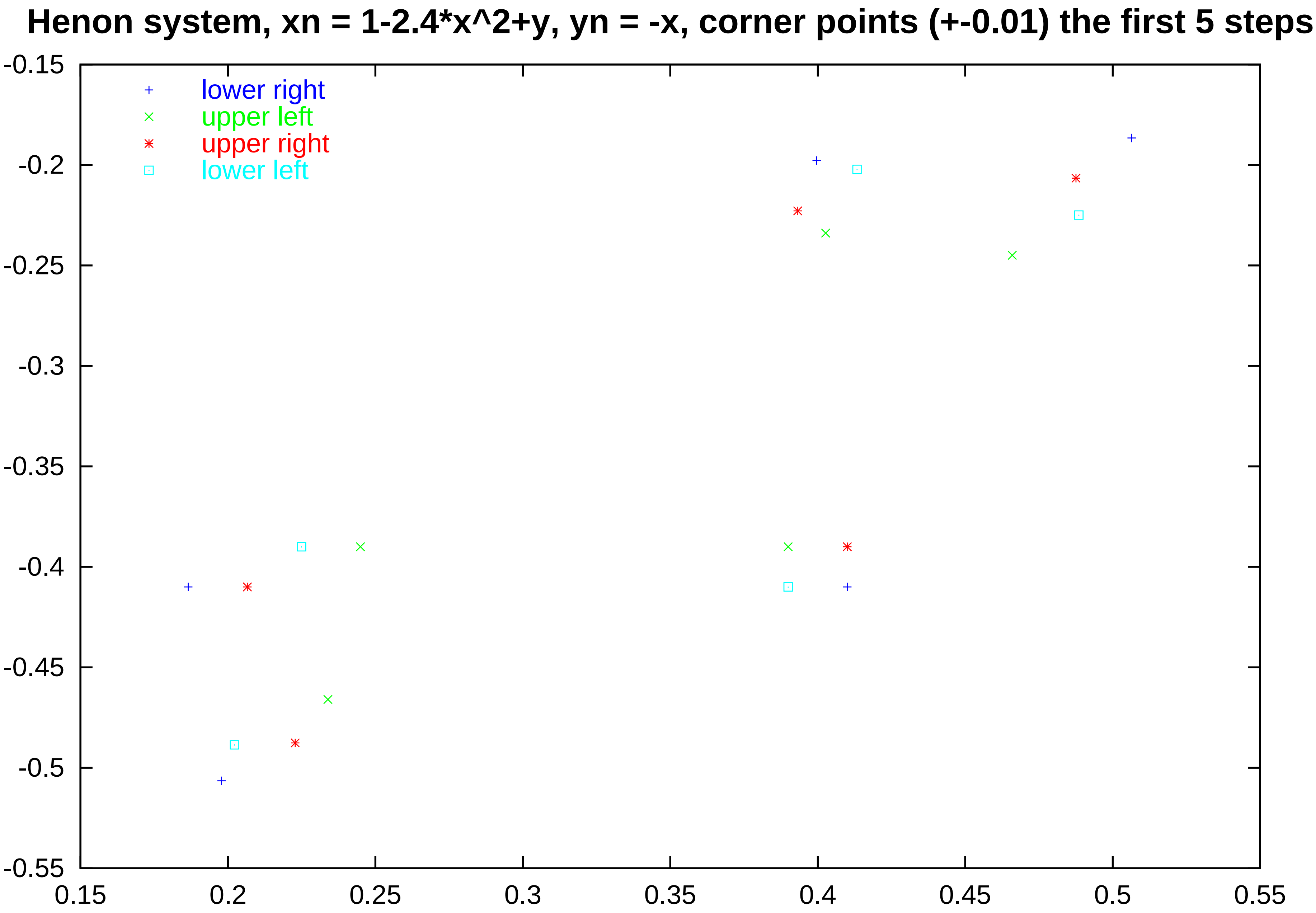
Henon system, xn = 1-2.4*x^2+y, yn = -x, corner points (+-0.01) the first 5 steps
lower right
upper left
upper right
lower left
-0.15
-0.2
-0.25
-0.3
-0.35
-0.4
-0.45
-0.5
-0.55
0.15
0.2
0.25
0.3
0.35
0.4
0.45
0.5
0.55

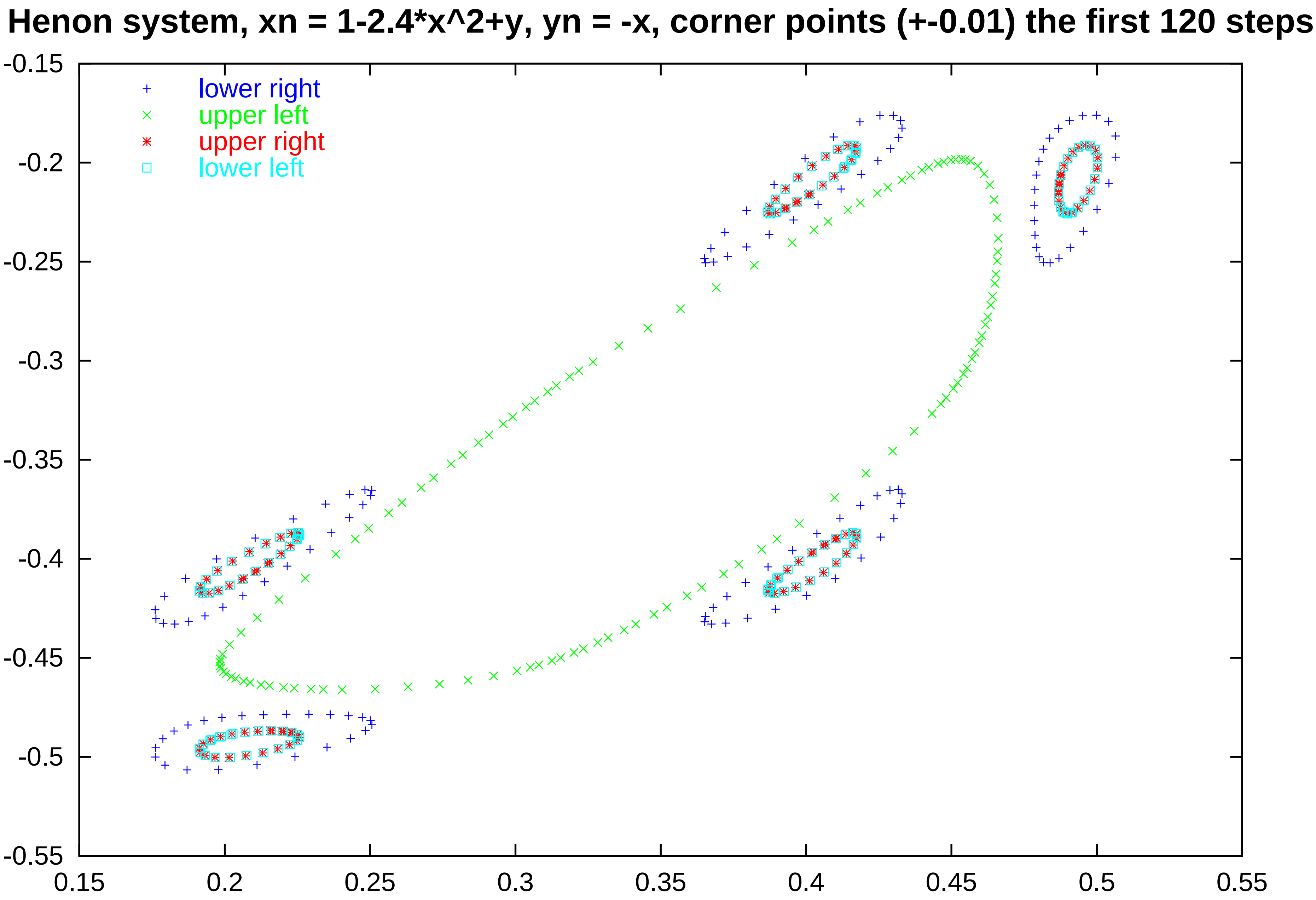
Henon system, xn = 1-2.4*x^2+y, yn = -x, corner points (+-0.01) the first 120 steps
lower right
upper left
upper right
lower left
-0.15
-0.2
-0.25
-0.3
-0.35
-0.4
-0.45
-0.5
-0.55
0.15
0.2
0.25
0.3
0.35
0.4
0.45
0.5
0.55

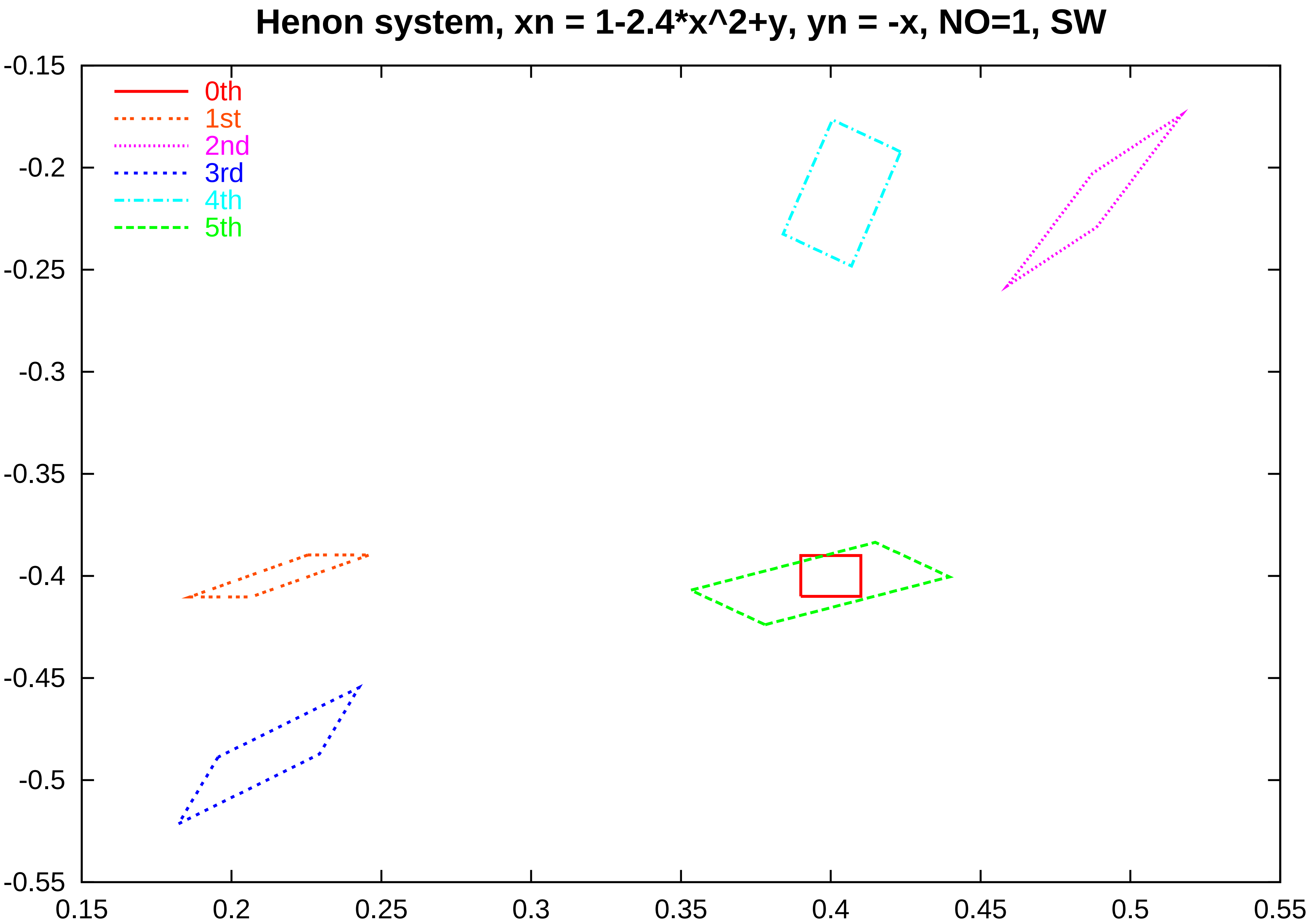
Henon system, xn = 1-2.4*x^2+y, yn = -x, NO=1, SW
0th
1st
2nd
3rd
4th
5th
-0.15
-0.2
-0.25
-0.3
-0.35
-0.4
-0.45
-0.5
-0.55
0.15
0.2
0.25
0.3
0.35
0.4
0.45
0.5
0.55

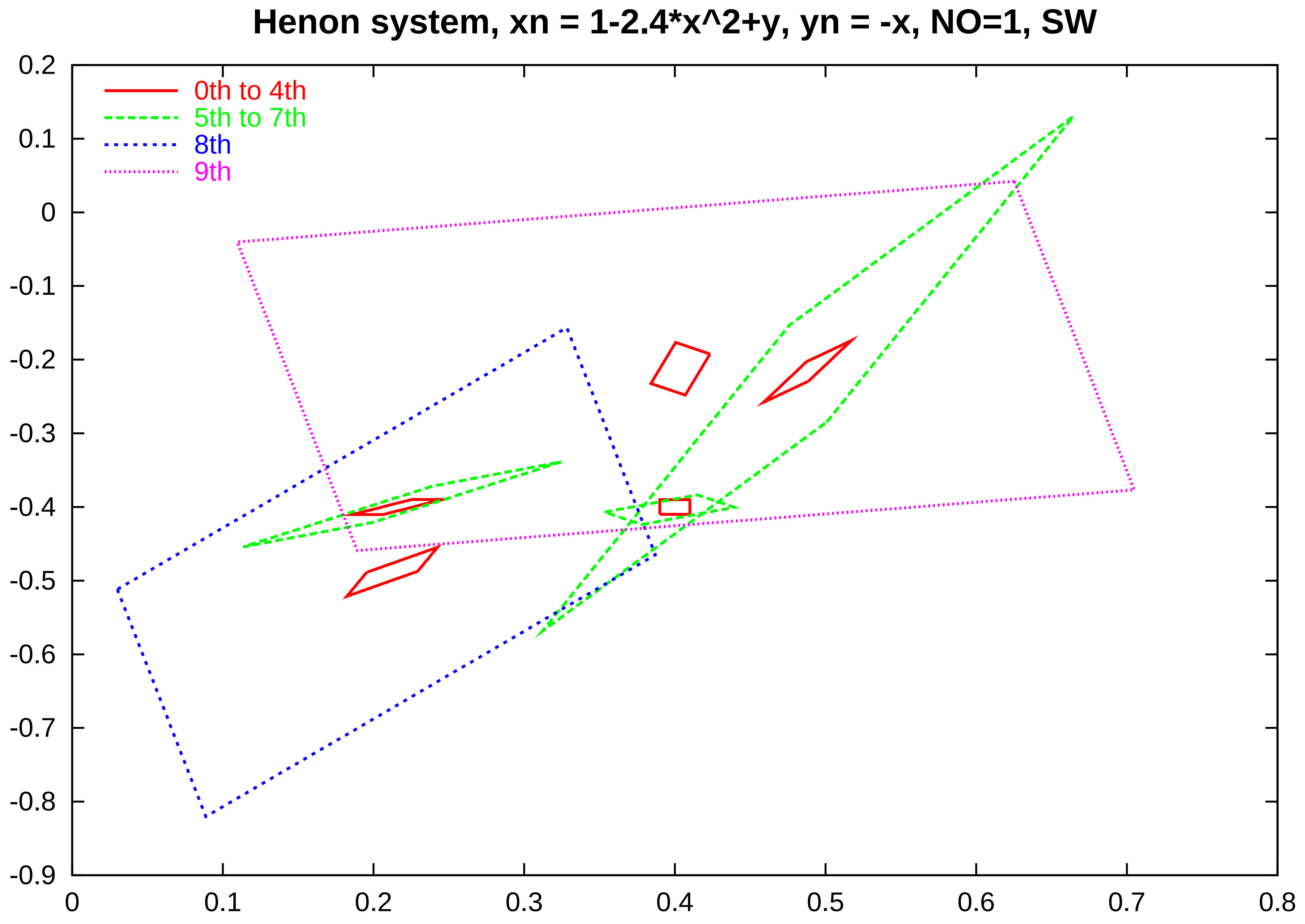

Henon system, xn = 1-2.4*x^2+y, yn = -x, NO=1, SW
0th to 4th
5th to 7th
8th
9th
0.2
0.1
0
-0.1
-0.2
-0.3
-0.4
-0.5
-0.6
-0.7
-0.8
-0.9
0
0.1
0.2
0.3
0.4
0.5
0.6
0.7
0.8

Taylor Models and Operations

Definition (Taylor Model) Let $f : D \subset R^v \to R$ be a function that is $(n+1)$ times continuously partially differentiable on an open set containing the domain v-dimensional domain D. Let x_0 be a point in D and P the n-th order **Taylor polynomial** of f around x_0. Let I be an interval such that

$$f(x) \in P(x - x_0) + I \text{ for all } x \in D.$$

Then we call the pair (P, I) an n-th order Taylor model of f around x_0 on D.

Definition (Addition and Multiplication) Let $T_{1,2} = (P_{1,2}, I_{1,2})$ be n-th order Taylor models around x_0 over the domain D. We define

$$\begin{aligned} T_1 + T_2 &= (P_1 + P_2, I_1 + I_2) \\ T_1 \cdot T_2 &= (P_{1\cdot 2}, I_{1\cdot 2}) \end{aligned}$$

where $P_{1\cdot 2}$ is the part of the polynomial $P_1 \cdot P_2$ up to order n and

$$I_{1\cdot 2} = B(P_e) + B(P_1) \cdot I_2 + B(P_2) \cdot I_1 + I_1 \cdot I_2$$

where P_e is the part of the polynomial $P_1 \cdot P_2$ of orders $(n+1)$ to $2n$, and $B(P)$ denotes a bound of P on the domain D. We demand that $B(P)$ is at least as sharp as direct interval evaluation of $P(x - x_0)$ on D.

Taylor Model Intrinsics

Let $T = (P, I)$ be a Taylor model of order n over the v-dimensional domain $D = [a, b]$ around the point x_0.

Intrinsic functions: We define intrinsic functions for the Taylor models by performing various manipulations that will allow the computation of Taylor models for the intrinsics g from those of the arguments T; $g(T)$.

The strategy depends on g, but **usually** consisting of using

- an addition theorem for g
- the Taylor formula with remainder for g
- the treatment of constant and non-constant parts of T separately

Antiderivation:

$$\partial_i^{-1} T = \partial_i^{-1}(P, I) = \left(\int_0^{x_i} P_{n-1}(x) dx_i \, , \; (B(P - P_{n-1}) + I) \cdot (b_i - a_i) \right) .$$

Taylor Models for the Flow

Goal: Determine a Taylor model, consisting of a Taylor Polynomial and an interval bound for the remainder, for the flow of the differential equation

$$\frac{d}{dt}\vec{r}(t) = \vec{F}(\vec{r}(t), t)$$

where $\vec{F}$ is sufficiently differentiable. The Remainder Bound should be fully rigorous for all initial conditions $\vec{r}_0$ and times t that satisfy

$$\begin{aligned} \vec{r}_0 &\in [\vec{r}_{01}, \vec{r}_{02}] = \vec{B} \\ t &\in [t_0, t_1]. \end{aligned}$$

In particular, $\vec{r}_0$ itself may be a Taylor model, as long as its range is known to lie in $\vec{B}$.

Old Taylor Model based Integrators (–2004)

- High order expansion not only in time t but also in transversal variables $\vec{x}$.
- Capability of weighted order computation, allowing to suppress the expansion order in transversal variables $\vec{x}$.
- Shrink wrapping algorithm including blunting to control ill-conditioned cases.
- Pre-conditioning algorithms based on the Curvilinear, QR decomposition, and blunting pre-conditioners.

Preconditioning the Flow

It can be viewed as a coordinate transformation.

Definition (Preconditioning the Flow) Let $(P + I)$ be a Taylor model. We say that $(P_l + I_l), (P_r + I_r)$ is a factorization of $(P + I)$ if $B(P_r + I_r) \in [-1, 1]$ and

$$(P + I) \in (P_l + I_l) \circ (P_r + I_r) \text{ for all } x \in D$$

where D is the domain of the Taylor model $(P_r + I_r)$.

Proposition Let $(P_{l,n} + I_{l,n}) \circ (P_{r.n} + I_{r,n})$ be a factored Taylor model that encloses the flow of the ODE at time t_n. Let $(P^*_{l,n+1}, I^*_{l,n+1})$ be the result of integrating $(P_{l,n} + I_{l,n})$ from t_n to t_{n+1}. Then

$$(P^*_{l,n+1}, I^*_{l,n+1}) \circ (P_{r.n} + I_{r,n})$$

is a factorization of the flow at time t_{n+1}.

Example Preconditionings: QR, Blunted, Curvilinear.

2 Rössler equations

The Rössler equations are given by

$$\begin{aligned} x' &= -(y+z) \\ y' &= x + 0.2y \\ z' &= 0.2 + z(x-a), \end{aligned} \tag{4}$$

where a is a real parameter. We focus here at the value of $a = 5.7$, where numerical simulations suggest an existence of a strange attractor.

On section $x = 0$ we consider the following initial condition $(y, z) \in (-8.38095, 0.0295902) + [-\delta, \delta]^2$, where δ should be considerably larger than 10^{-3}. The integration time should be around $T = 6$.

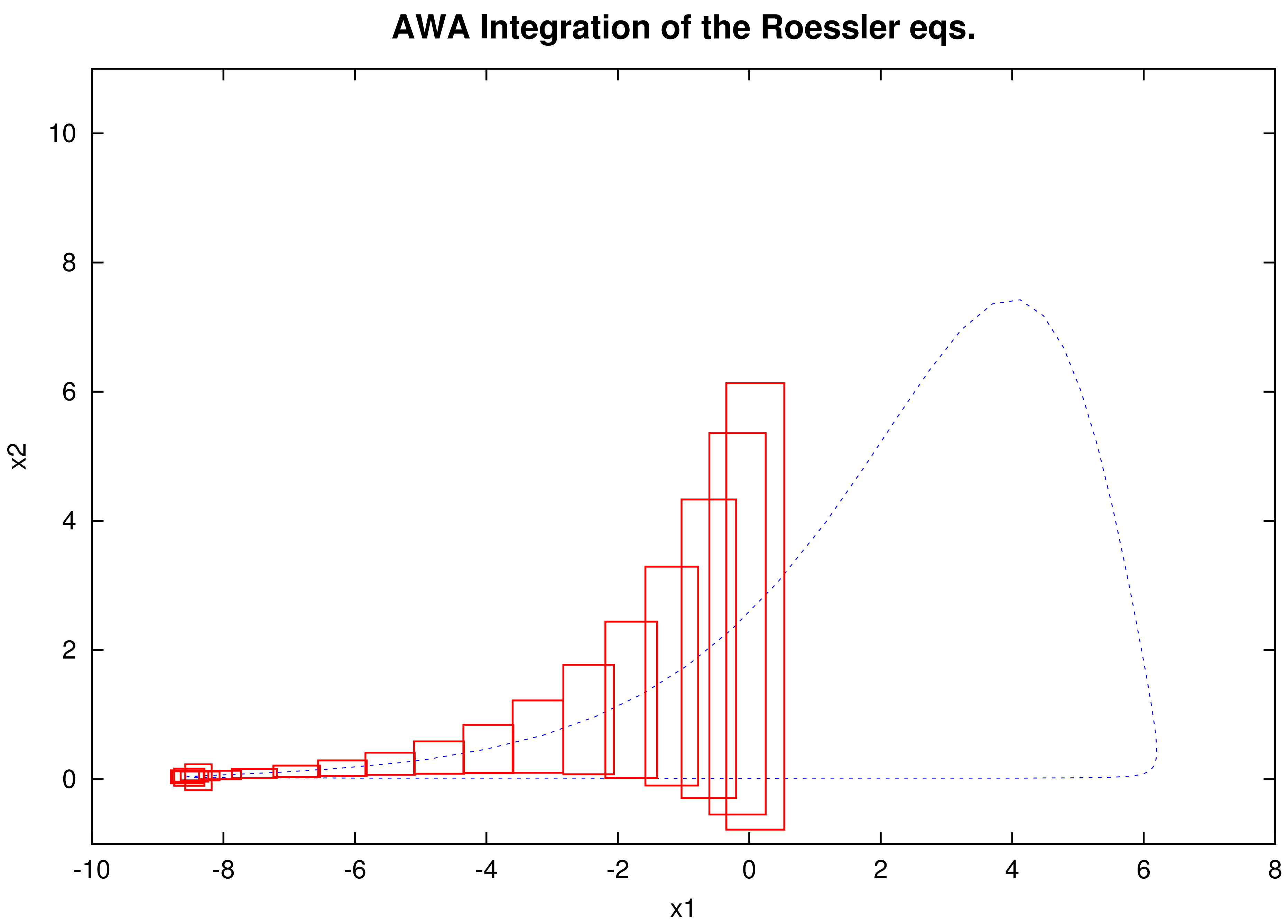
AWA Integration of the Roessler eqs.
x2
x1
10
8
6
4
2
0
-10
-8
-6
-4
-2
0
2
4
6
8

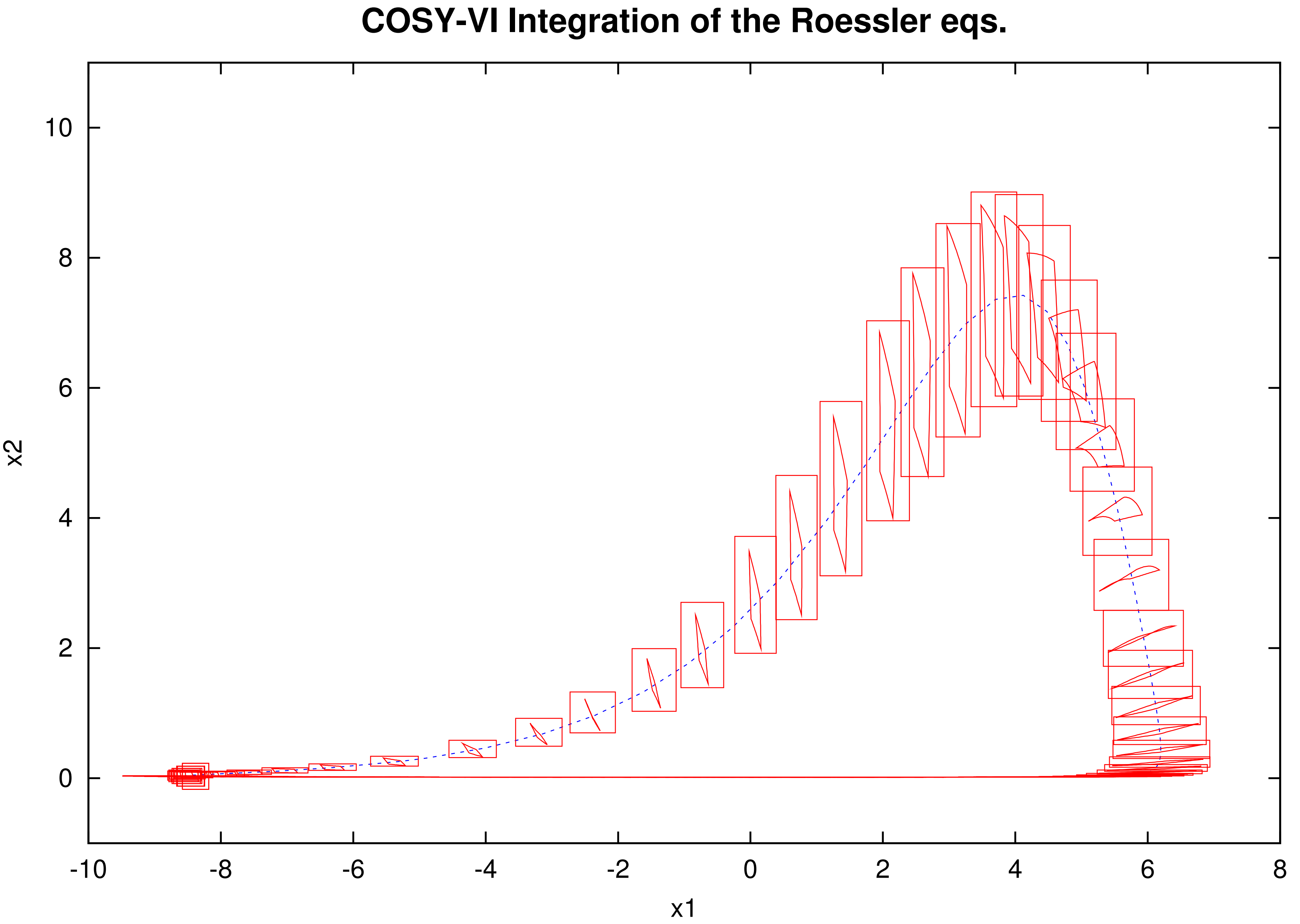
COSY-VI Integration of the Roessler eqs.
x1
x2
-10
-8
-6
-4
-2
0
2
4
6
8
10

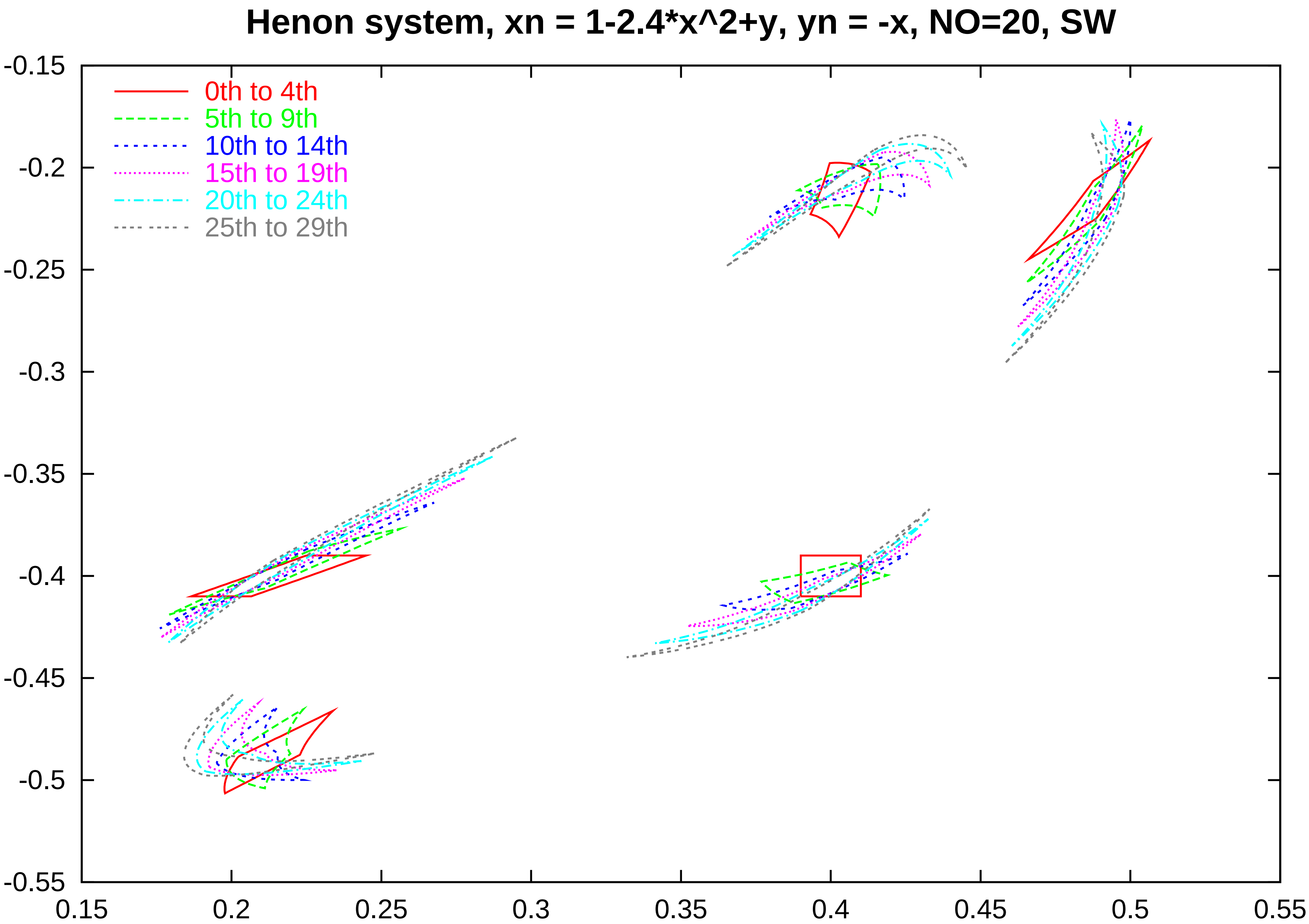
Henon system, xn = 1-2.4*x^2+y, yn = -x, NO=20, SW
0th to 4th
5th to 9th
10th to 14th
15th to 19th
20th to 24th
25th to 29th
-0.15
-0.2
-0.25
-0.3
-0.35
-0.4
-0.45
-0.5
-0.55
0.15
0.2
0.25
0.3
0.35
0.4
0.45
0.5
0.55

TM Integrator: Pushing Further...

- The Reference Trajectory and the Flow Operator
- Improvements of Step Size Control
- Error Parametrization of Taylor Models
- Dynamic Domain Decomposition

The Reference Trajectory

First Step: Obtain Taylor expansion in time of solution of ODE of center point c, i.e. obtain

$$c(t) = c_0 + c_1 \cdot (t - t_0) + c_2 \cdot (t - t_0)^2 + ... + c_n \cdot (t - t_0)^n$$

Very well known from day one how to do this with automatic differentiation. Rather convenient way: can be done by n iterations of the Picard Operator

$$c(t) = c_0 + \int_0^t f(r(t'), t) dt'$$

in one-dimensional Taylor arithmetic. Each iteration raises the order by one; so in each iteration i, only need to do Taylor arithmetic in order i. In either way, this step is **cheap** since it involves only **one-dimensional** operations.

The Nonlinear Flow

Second Step: The goal is to obtain Taylor expansion in time to order n **and** initial conditions to order k. Note:

1. This is usually the most **expensive** step. In the original Taylor model-based algorithm, it is done by n **iterations** of the Picard Operator in multi-dimensional Taylor arithmetic, where c_0 is now a polynomial in initial conditions.
2. The case $k = 1$ has been known for a long time. Traditionally solved by setting up **ODEs for sensitivities** and solving these as before.
3. The case of higher k goes back to Beam Physics (M. Berz, Particle Accelerators 1988)
4. Newest Taylor model arithmetic naturally supports different expansions orders k for initial conditions and n for time.

Goal: Obtain flow with one **single evaluation** of right hand side.

The Nonlinear Relative ODE

We now develop a better way for second step.
First: introduce new "perturbation" variables $\tilde{r}$ such that

$$r(t) = c(t) + A \cdot \tilde{r}(t).$$

The matrix A provides **preconditioning**. ODE for $\tilde{r}(t)$:

$$\tilde{r}' = A^{-1}\left[f(c(t) + A \cdot \tilde{r}(t)) - c'(t)\right]$$

Second: evaluate ODE for $\tilde{r}'$ in Taylor arithmetic. Obtain a Taylor expansion of the ODE, i.e.

$$\tilde{r}' = P(\tilde{r}, t)$$

up to order n in time and k in $\tilde{r}$. **Very important** for later use: the polynomial P will have no constant part, i.e.

$$P(0, t) = 0.$$

Reminder: The Lie Derivative

Let

$$r' = f(r, t)$$

be a dynamical system. Let g be a variable in state space, and let us study $g(r(t))$, i.e. along a solution of the ODE. We have

$$\frac{d}{dt} g(t) = f \cdot \nabla g + \frac{\partial g}{\partial t}$$

Introducing the **Lie Derivative** $L_f = f \cdot \nabla + \partial / \partial t$, we have

$$\frac{d^n}{dt^n} g = L_f^n g \text{ and } g(t) \approx \sum_{i=0}^{n} \frac{(t - t_0)^i}{i!} \, L_f^i g \Big/_{t=t_0}$$

Polynomial Flow from Lie Derivative

Remember the ODE for $\tilde{r}'$:

$$\tilde{r}' = P(\tilde{r}, t)$$

up to order n in time and k in $\tilde{r}$. And remember $P(0,t) = 0$. Thus we can obtain the n-th order expansion of the flow as

$$\tilde{r}(t) = \sum_{i=0}^{n} \frac{(t-t_0)^i}{i!} \cdot \left(P \cdot \nabla + \frac{\partial}{\partial t} \right)^i \tilde{r}_0 \Big/_{t=t_0}$$

- The fact that $P(0,t) = 0$ restores the derivatives lost in ∇
- The fact that $\partial/\partial t$ appears without origin-preserving factor limits the expansion to order n.

Performance of Lie Derivative Flow Methods

Apparently we have the following:

- Each term in the Lie derivative sum requires $v+1$ derivations (very cheap, just re-shuffling of coefficients)
- Each term requires v multiplications
- We need **one** evaluation of f in ${}_nD_v$ (to set up ODE)

Compare this with the conventional algorithm, which requires n evaluations of the function f of the right hand side. Thus, roughly, if the evaluation of f requires more than v multiplications, the new method is more efficient.

- Many practically appearing right hand sides f satisfy this.
- But on the other hand, if the function f does not satisfy this (for example for the linear case), then also P will be simple (in the linear case: P will be linear), and thus less operations appear

Step Size Control

Step size control to maintain approximate error ε in each step. Based on a suite of tests:

1. Utilize the **Reference Orbit.** Extrapolate the size of coefficients for estimate of remainder error, scale so that it reaches and get Δt_1. Goes back to Moore in 1960s. This is one of conveniences when using Taylor integrators.
2. Utilize the **Flow.** Compute flow time step with Δt_1.Extrapolate the contributions of each order of flow for estimate of remainder error to get update Δt_2.
3. Utilize a **Correction factor** c to account for overestimation in TM arithmetic as $c = \sqrt[n+1]{|R|/\varepsilon}$. Largely a measure of complexity of ODE. Dynamically update the correction factor.
4. Perform verification attempt for $\Delta t_3 = c \cdot \Delta t_2$

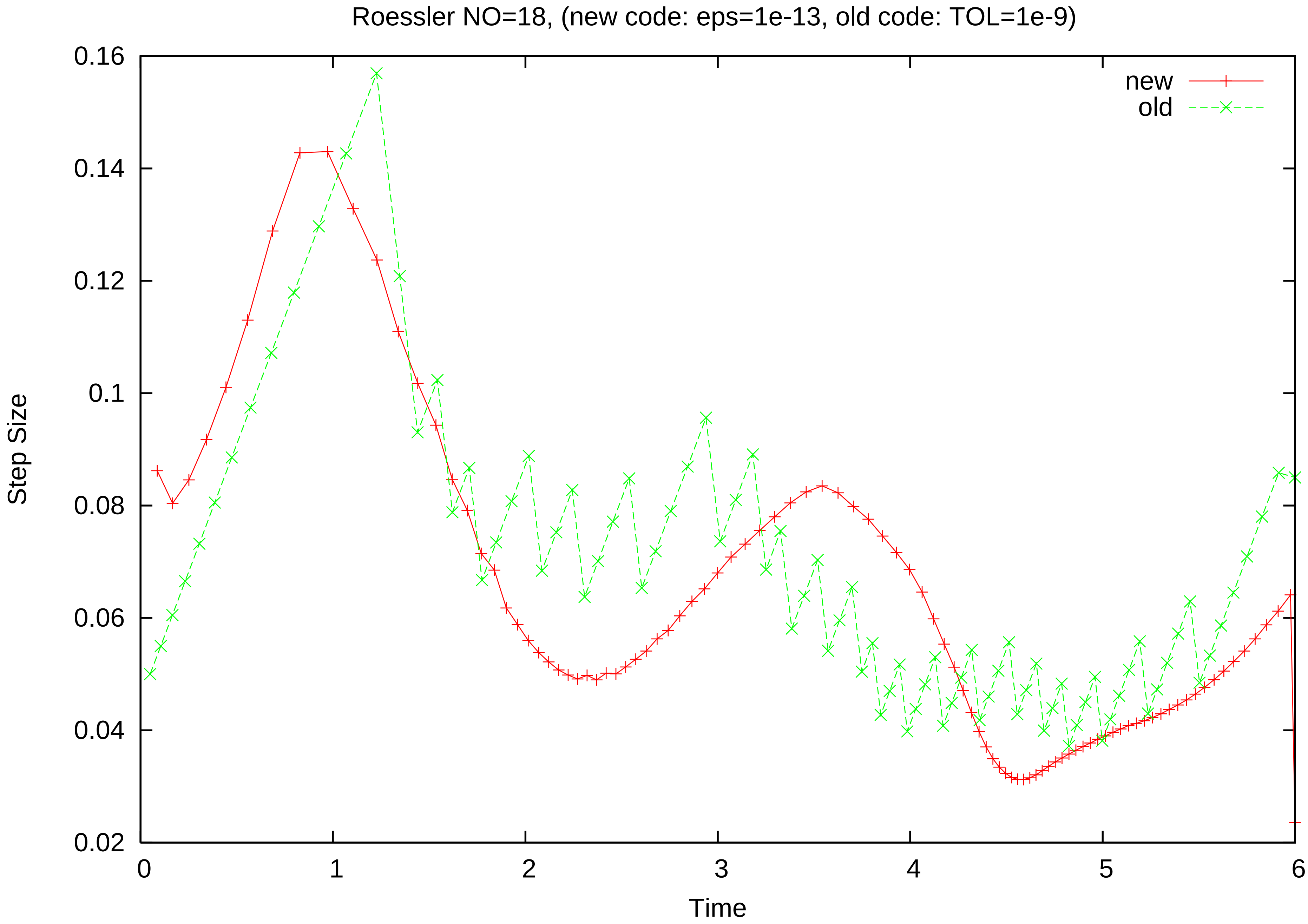

Roessler NO=18, (new code: eps=1e-13, old code: TOL=1e-9)
new
old
Step Size
Time
0.16
0.14
0.12
0.1
0.08
0.06
0.04
0.02
0
1
2
3
4
5
6

Error Parametrization of Taylor models

Motivation: Is it possible to absorb the remainder error bound intervals of Taylor models into the polynomial parts using additional parameters?

Phrase the question as the following problem:

1. Have Taylor models with 0 remainder error interval, which depend on the independent variables $\vec{x}$ and the parameters $\vec{\alpha}$.
$$\vec{T}_0 = \vec{P}_0(\vec{x}, \vec{\alpha}) + \overrightarrow{[0, 0]}.$$
2. Perform Taylor model arithmetic on $\vec{T}_0$, namely $\vec{F}(\vec{T}_0)$
$$\vec{F}(\vec{T}_0) = \vec{P}(\vec{x}, \vec{\alpha}) + \vec{I}_F, \text{ where } \vec{I}_F \neq \overrightarrow{[0, 0]}.$$
3. Try to absorb $\vec{I}_F$ into the polynomial part that depends on $\vec{\alpha}$
$$\vec{P}(\vec{x}, \vec{\alpha}) + \vec{I}_F \subseteq \vec{P}'(\vec{x}, \vec{\alpha}) + \overrightarrow{[0, 0]}. \qquad \text{(A)}$$

Error Absorption

We limit the explicitly $\vec{\alpha}$-dependent part $\vec{P}_\alpha(\vec{x},\vec{\alpha})$ to be only **linearly** dependent on $\vec{\alpha}$, and express $\vec{I}_F$ by the matrix form.

$$\vec{P}_\alpha(\vec{x},\vec{\alpha}) + \vec{I}_F \subseteq \left(\widehat{M} + \widehat{\bar{M}}(\vec{x})\right) \cdot \vec{\alpha} + \left(\widehat{I}_F + \widehat{\bar{\bar{I}}}_F(\vec{x})\right) \cdot \vec{\beta}.$$

where $(\widehat{I}_F)_{ii} = |I_{Fi}|$, $\widehat{\bar{\bar{I}}}_F(\vec{x}) = 0$. The problem is now to find a **set sum of two parallelepipeds**. Choose a favoured collection of v column vectors $\widehat{L} + \widehat{\bar{\bar{L}}}(\vec{x})$ using the **Psum algorithm.**

$$\begin{aligned}\vec{P}_\alpha(\vec{x},\vec{\alpha}) + \vec{I}_F &\subseteq \left(\widehat{L} + \widehat{\bar{\bar{L}}}(\vec{x})\right) \cdot \vec{\alpha} + \left(\widehat{E} + \widehat{\bar{\bar{E}}}(\vec{x})\right) \cdot \vec{\beta} \\ &\subseteq \widehat{L} \circ \left[\left(\widehat{I} + \widehat{L}^{-1} \circ \widehat{\bar{\bar{L}}}(\vec{x})\right) \cdot \vec{\alpha} + \widehat{B} \cdot \vec{\beta}\right]\end{aligned}$$

where $\widehat{B}$ is diagonal, $(\widehat{B})_{ii} = |\text{bound}((\widehat{L}^{-1} \circ (\widehat{E} + \widehat{\bar{\bar{E}}}(\vec{x})) \cdot \vec{\beta})_i)|$.

If the **diagonal terms** of $\left(\widehat{I} + \widehat{L}^{-1} \circ \widehat{\bar{\bar{L}}}(\vec{x})\right)$ are **positive**,

$$\vec{P}_\alpha(\vec{x},\vec{\alpha}) + \vec{I}_F \subseteq \left(\widehat{L} + \widehat{\bar{\bar{L}}}(\vec{x}) + \widehat{L} \circ \widehat{B}\right) \cdot \vec{\alpha}.$$

Psum Algorithm for Choosing Vectors

Task: Choose v vectors out of n vectors $\vec{s}_i$, $i = 1, ..., n$, $n \geq v$.

1. Choose the longest vector $\vec{s}_k$, and assign it as $\vec{t}_1$. Normalize it as $\vec{e}_1 = \vec{t}_1 / \left| \vec{t}_1 \right|$.
2. Out of the remaining vectors $\vec{s}_i$, choose the j-th vector $\vec{t}_j = \vec{s}_k$ such that
$$\frac{\left|\vec{s}_k\right|^2 - \sum_{m=1}^{j-1} \left|\vec{s}_k \cdot \vec{e}_m\right|^2}{\left|\vec{s}_k\right|^{2p}}$$
is largest. Compute $\vec{e}_j$, the orthonormalized vector of $\vec{t}_j$ to $\vec{e}_1, ..., \vec{e}_{j-1}$. (Gram-Schmidt)
3. Repeat the process 2 until $j = v$.

Experimentally, $p = 0.5$ is found to be efficient and robust for obtaining a set sum of two parallelepipeds

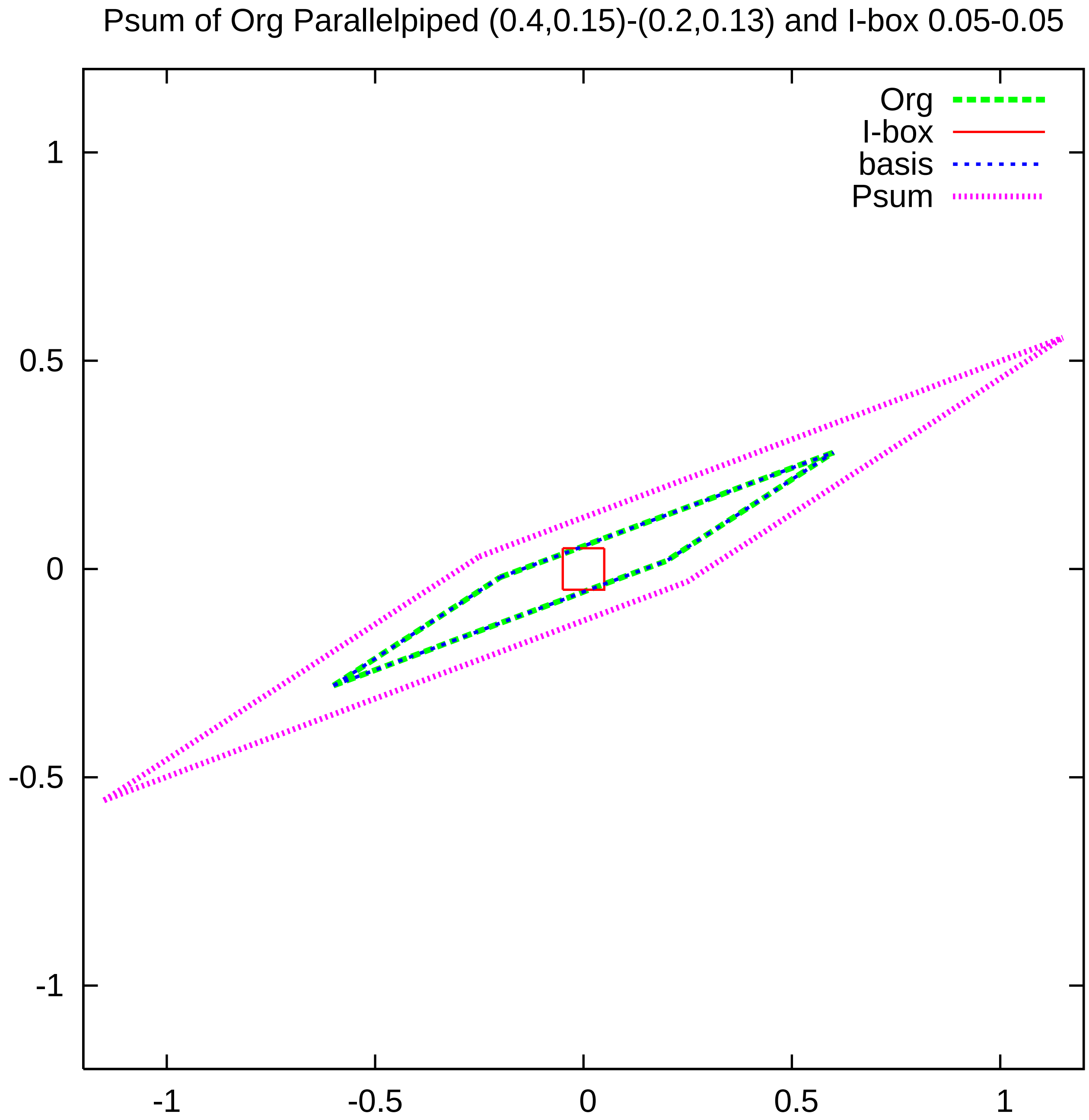
Psum of Org Parallelpiped (0.4,0.15)-(0.2,0.13) and I-box 0.05-0.05
Org
I-box
basis
Psum
1
0.5
0
-0.5
-1
-1
-0.5
0
0.5
1

Psum of Org Parallelpiped (0.4,0.15)-(0.2,0.13) and I-box 0.07-0.07

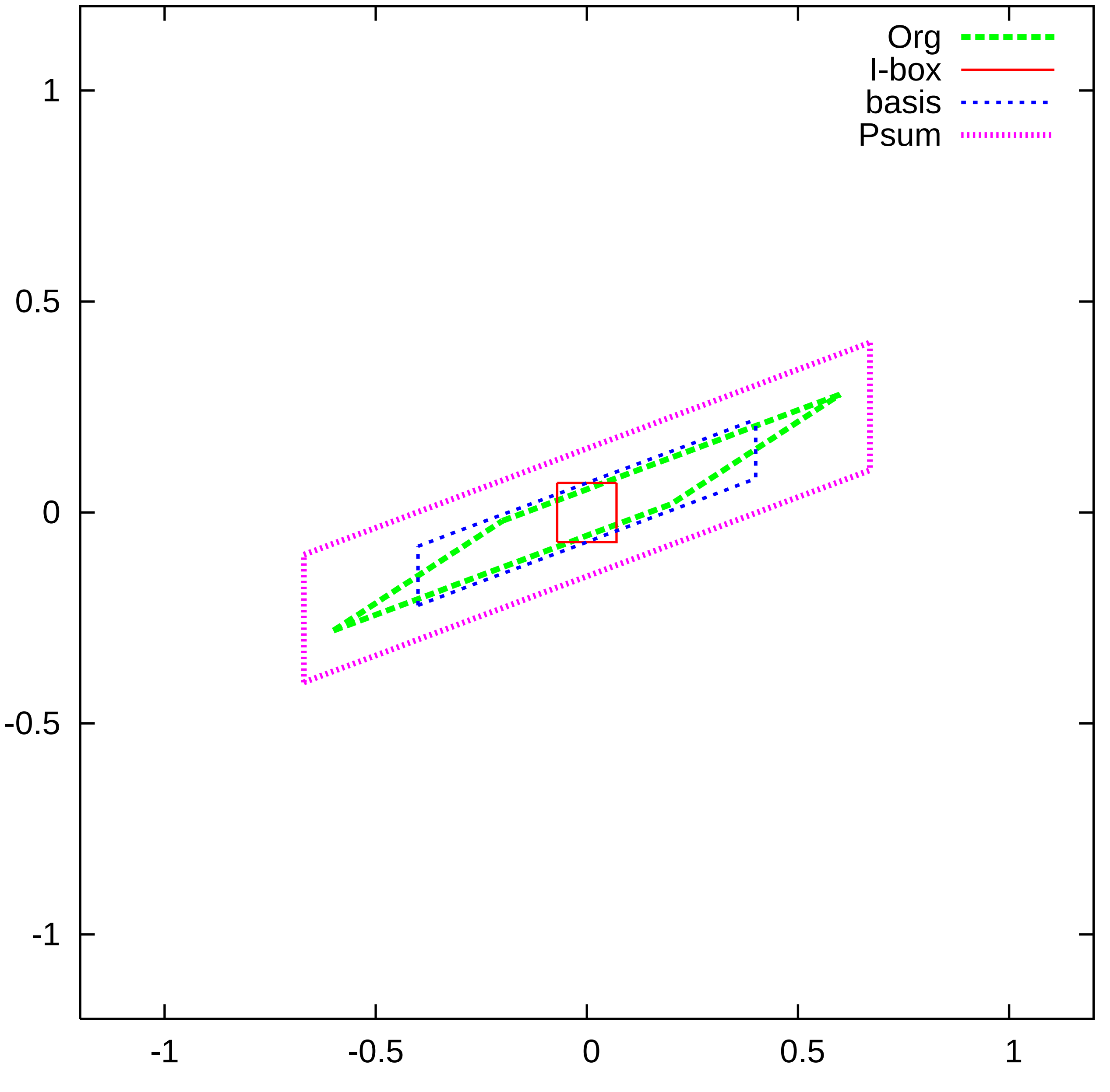

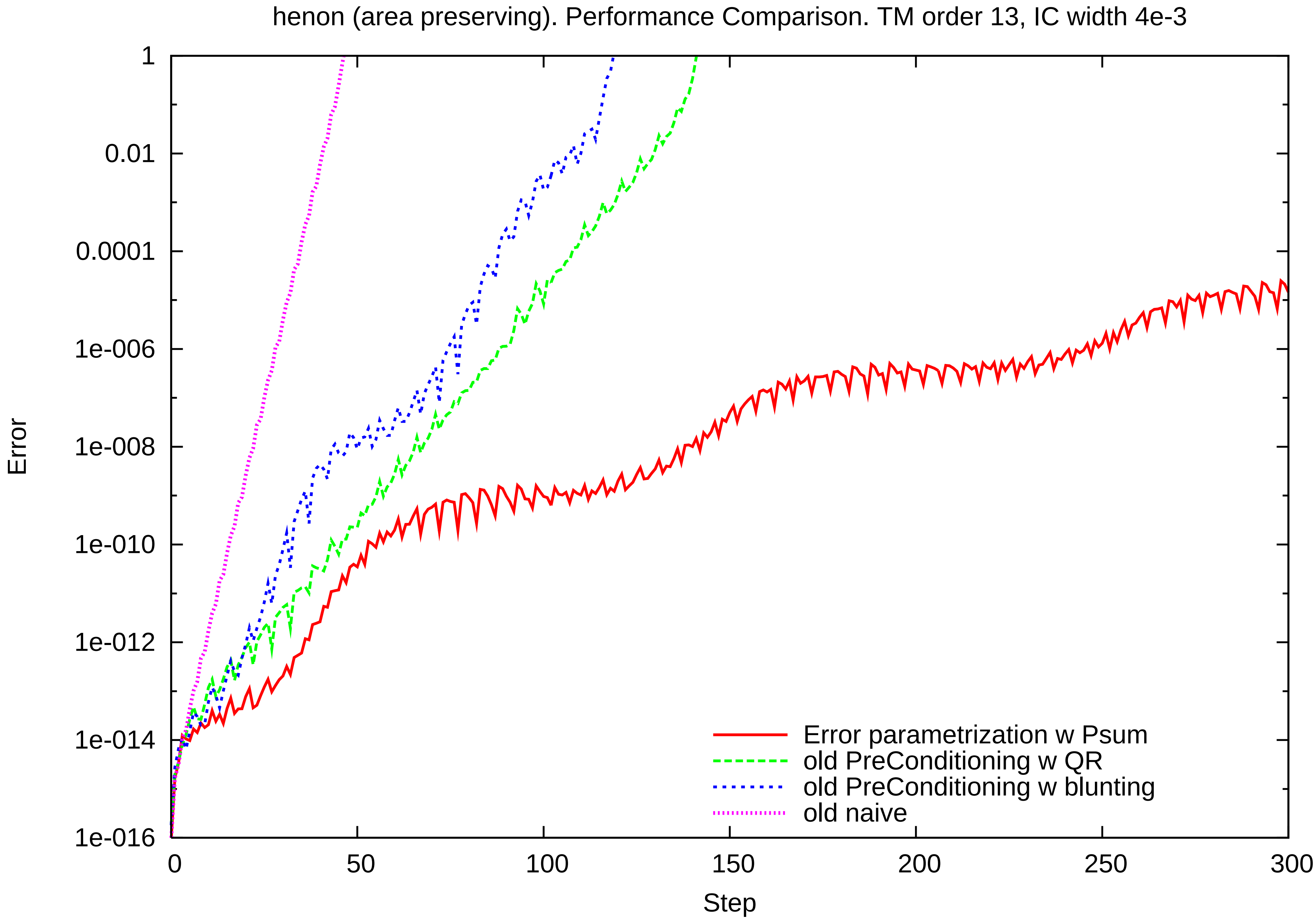

henon (area preserving). Performance Comparison. TM order 13, IC width 4e-3
1
0.01
0.0001
1e-006
1e-008
1e-010
1e-012
1e-014
1e-016
0
50
100
150
200
250
300
Error
Step
Error parametrization w Psum
old PreConditioning w QR
old PreConditioning w blunting
old naive

Cost of Additional Parameters

For a v dimensional system, we need v parameters $\vec{\alpha}$ to absorb Taylor model remainder error bound intervals. The dependence on $\vec{\alpha}$ is limited to **linear**. So, we use weighted DA. Choose an appropriate weight order w for $\vec{\alpha}$.

- The dependence on $\vec{\alpha}$ has to be kept linear. Namely $2 \cdot w > n$, where n is the computational order of Taylor models. Choose

$$w = \text{Int}\left(\frac{n}{2}\right) + 1.$$

Maximum size necessary for DA and TM for $v = 2$.

n	v	DA	TM	v	DA	TM		w	v_w	DA	TM
13	2	105	140	$2+2$	2380	2419	$\Rightarrow$	7	$2+2_w$	161	200
21	2	253	304	$2+2$	12650	12705	$\Rightarrow$	11	$2+2_w$	385	440
33	2	595	670	$2+2$	66045	66124	$\Rightarrow$	17	$2+2_w$	901	980

Dynamic Domain Decomposition

For extended domains, this is **natural equivalent** to step size control. Similarity to what's done in global optimization.

1. Evaluate ODE for $\Delta t = 0$ for current flow.
2. If resulting remainder bound R greater than ε, split the domain along variable leading to longest axis.
3. Absorb R in the TM polynomial part using the error parametrization method. If it fails, split the domain along variable leading to largest x dependence of the error.
4. Put one half of the box on stack for future work.

Things to consider:

- Utilize "First-in-last-out" stack; minimizes stack length. Special adjustments for stack management in a parallel environment, including load balancing.
- Outlook: also dynamic order control for dependence on initial conditions

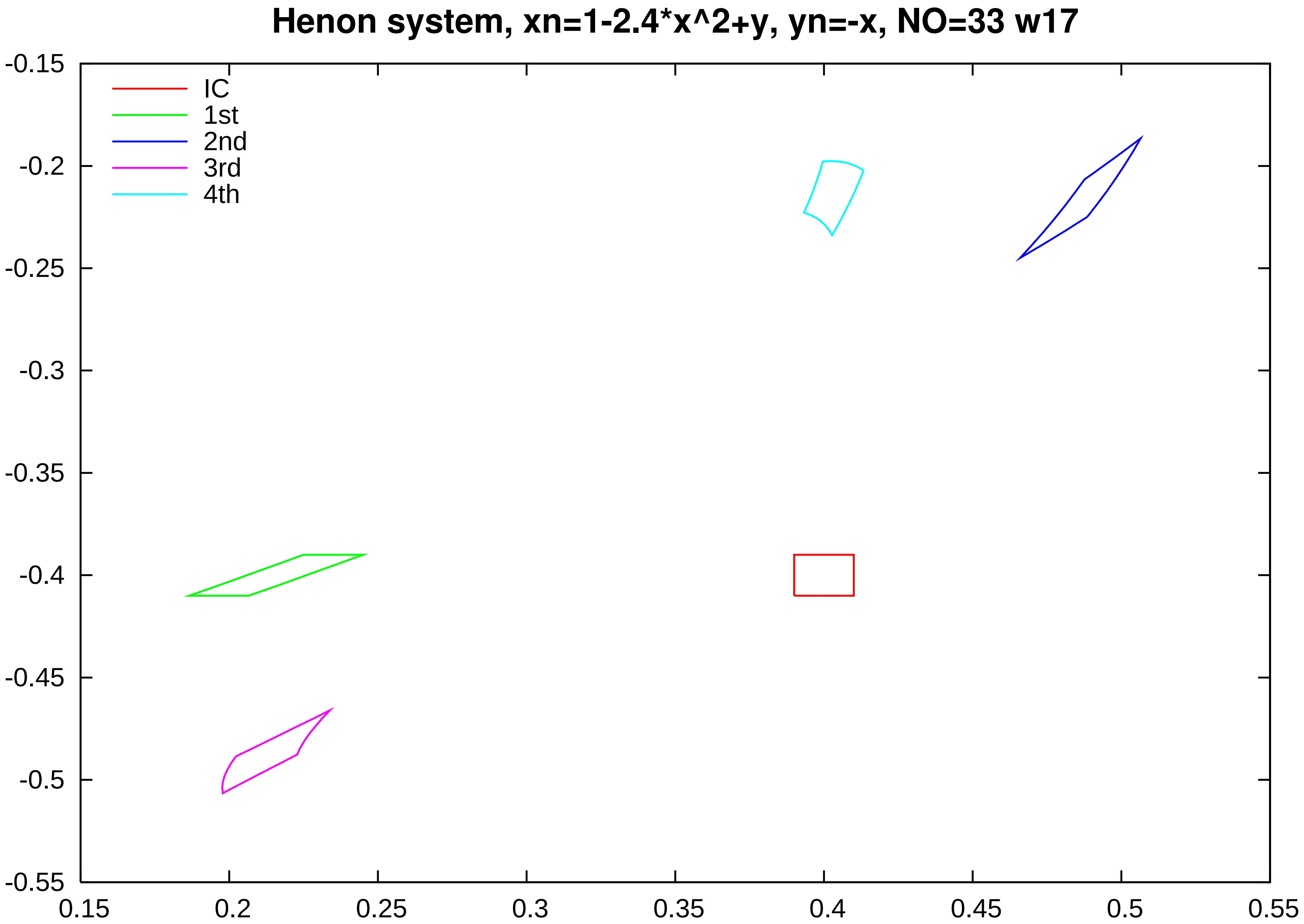

Henon system, xn=1-2.4*x^2+y, yn=-x, NO=33 w17
IC
1st
2nd
3rd
4th
-0.15
-0.2
-0.25
-0.3
-0.35
-0.4
-0.45
-0.5
-0.55
0.15
0.2
0.25
0.3
0.35
0.4
0.45
0.5
0.55

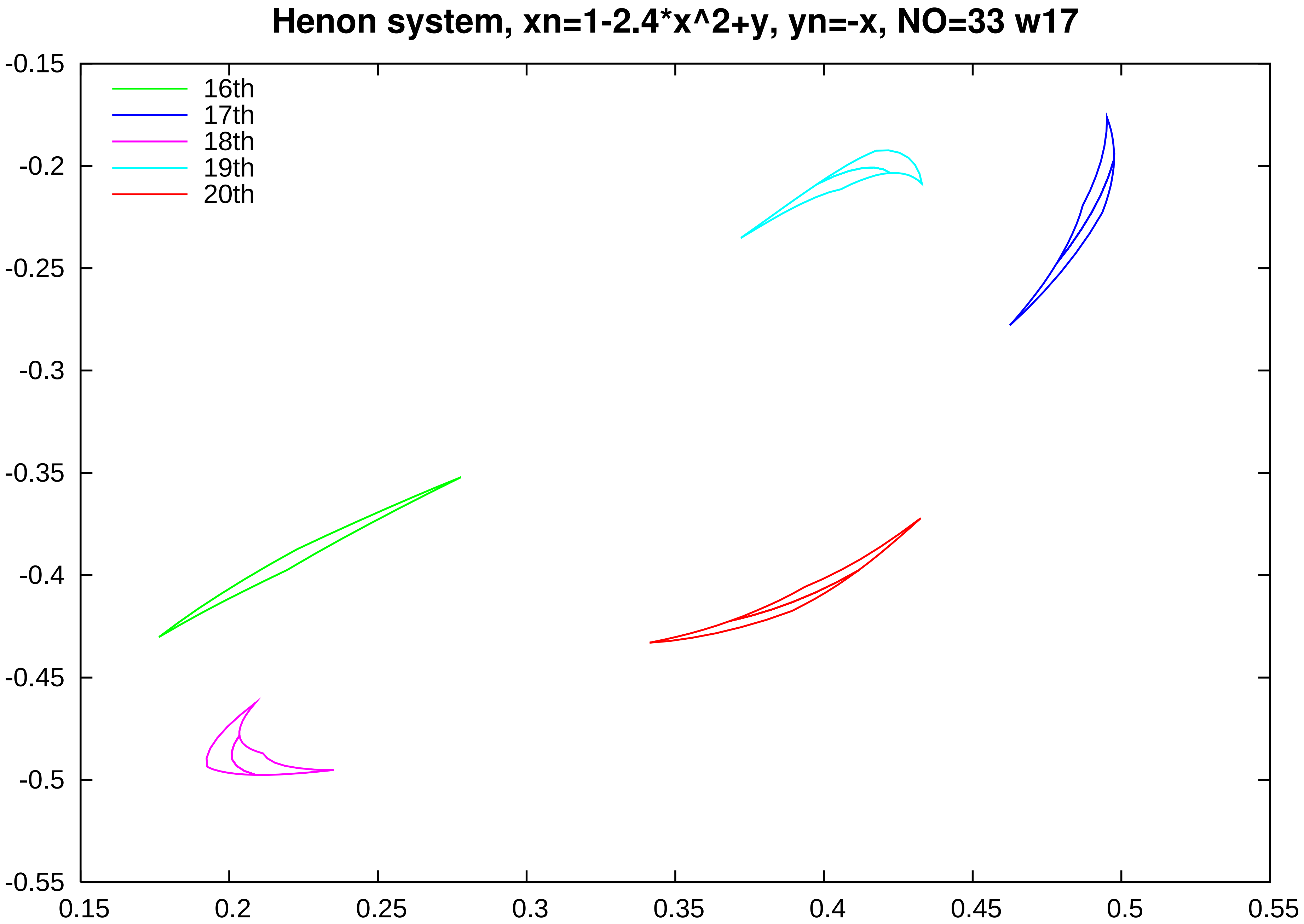
Henon system, xn=1-2.4*x^2+y, yn=-x, NO=33 w17
16th
17th
18th
19th
20th
-0.15
-0.2
-0.25
-0.3
-0.35
-0.4
-0.45
-0.5
-0.55
0.15
0.2
0.25
0.3
0.35
0.4
0.45
0.5
0.55

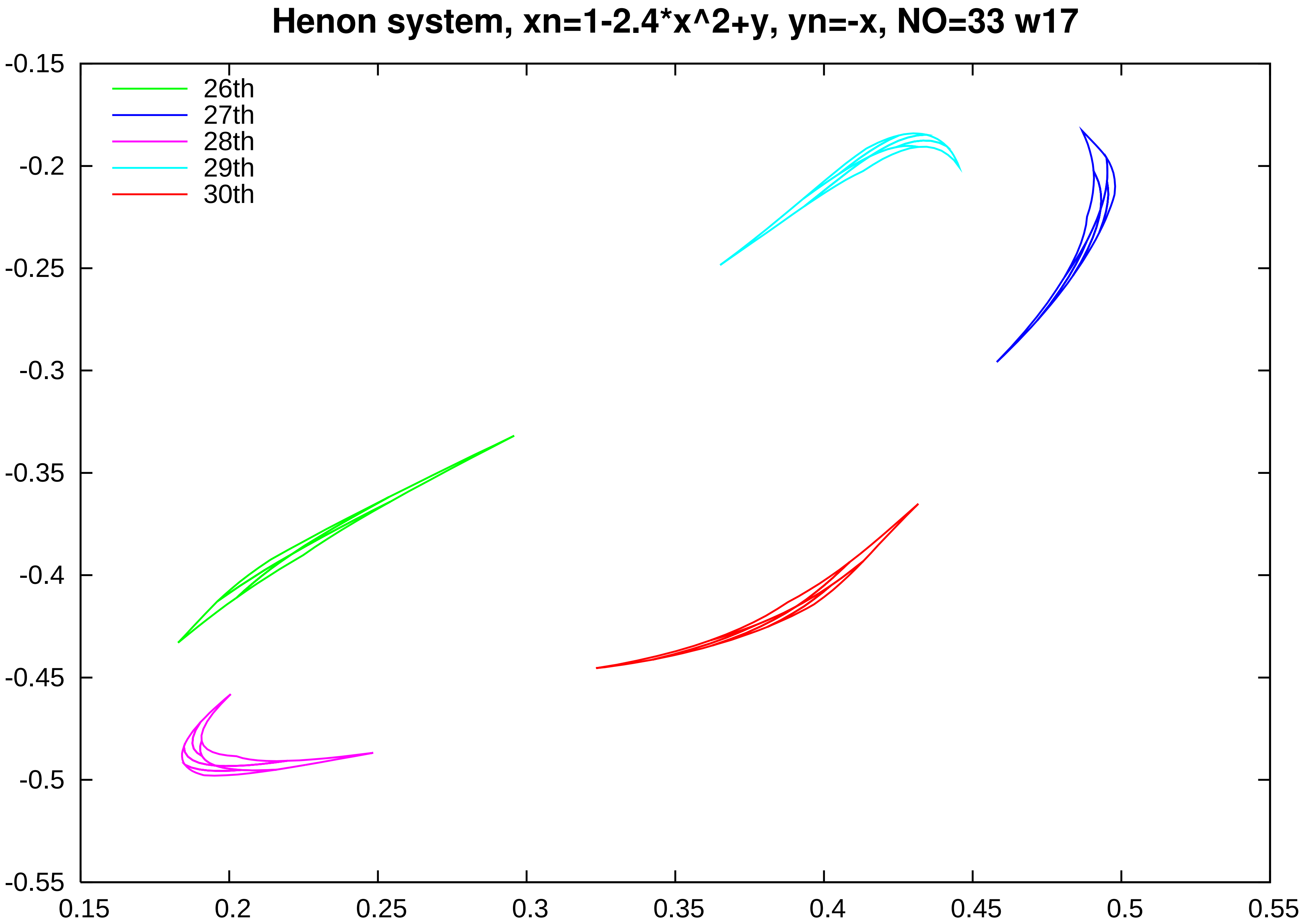
Henon system, xn=1-2.4*x^2+y, yn=-x, NO=33 w17
26th
27th
28th
29th
30th
-0.15
-0.2
-0.25
-0.3
-0.35
-0.4
-0.45
-0.5
-0.55
0.15
0.2
0.25
0.3
0.35
0.4
0.45
0.5
0.55

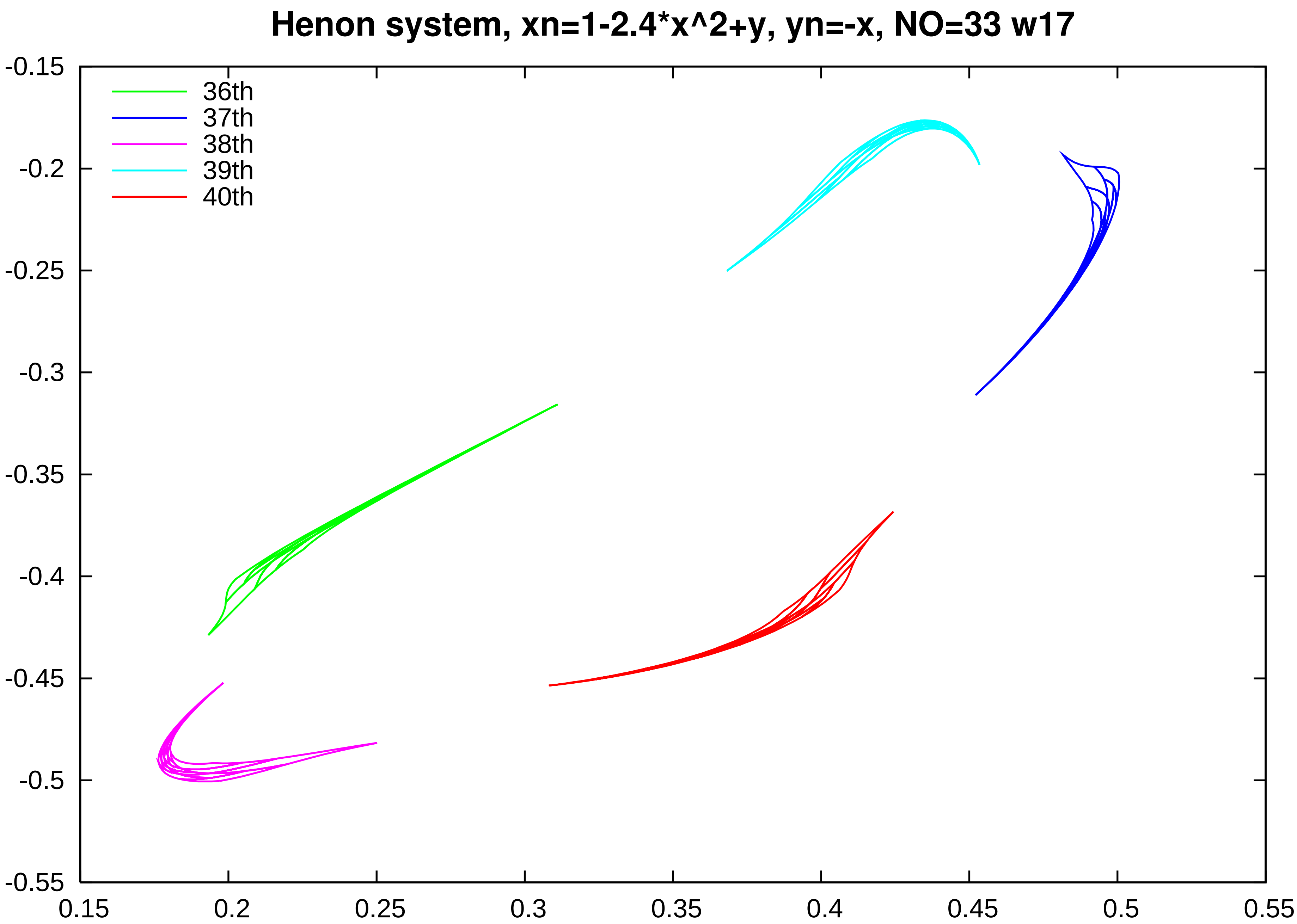
Henon system, xn=1-2.4*x^2+y, yn=-x, NO=33 w17
36th
37th
38th
39th
40th
-0.15
-0.2
-0.25
-0.3
-0.35
-0.4
-0.45
-0.5
-0.55
0.15
0.2
0.25
0.3
0.35
0.4
0.45
0.5
0.55

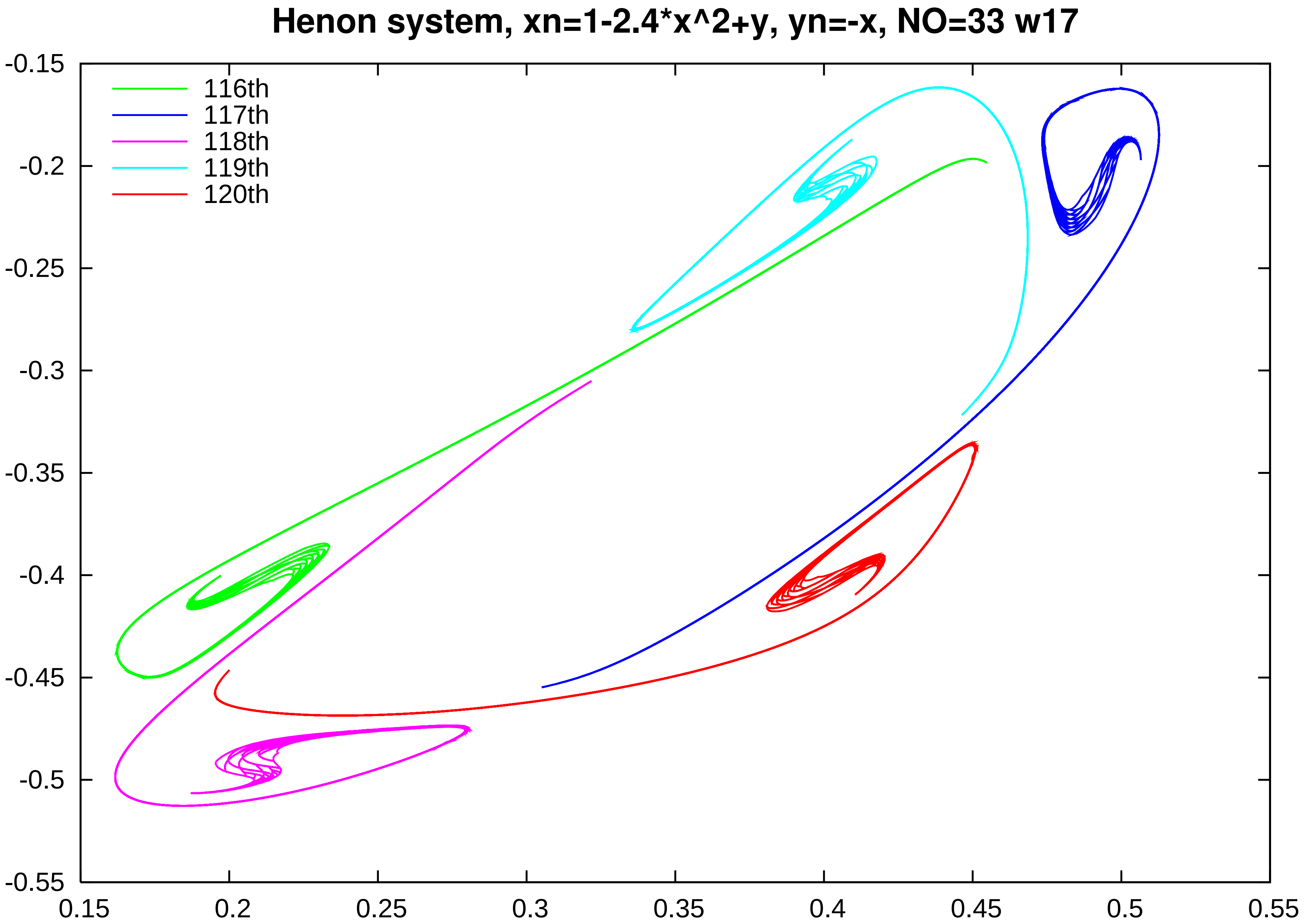
Henon system, xn=1-2.4*x^2+y, yn=-x, NO=33 w17
116th
117th
118th
119th
120th
-0.15
-0.2
-0.25
-0.3
-0.35
-0.4
-0.45
-0.5
-0.55
0.15
0.2
0.25
0.3
0.35
0.4
0.45
0.5
0.55

discrete kepler. 1st revolution, ICw 0.02, NO=13 w7

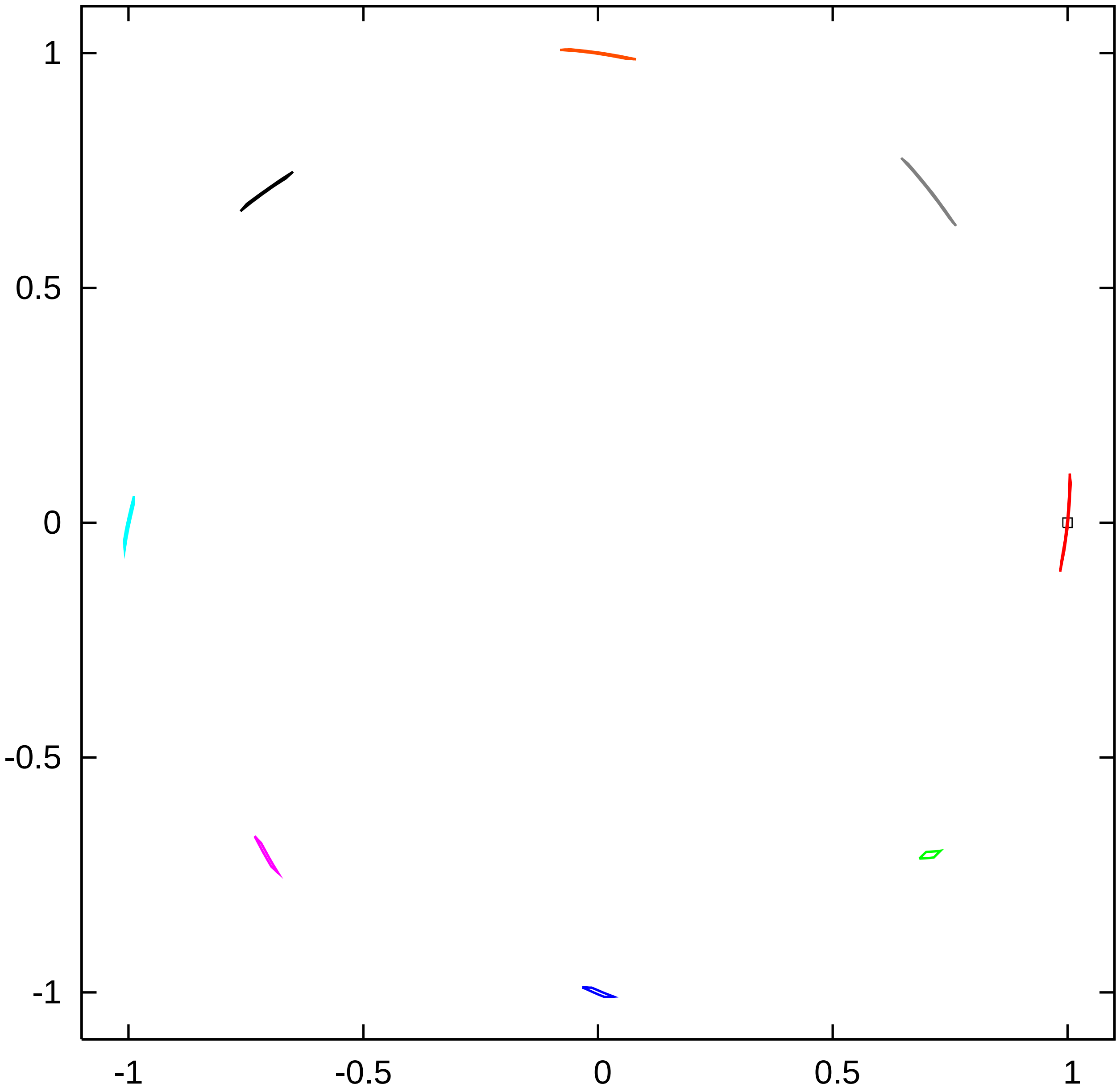

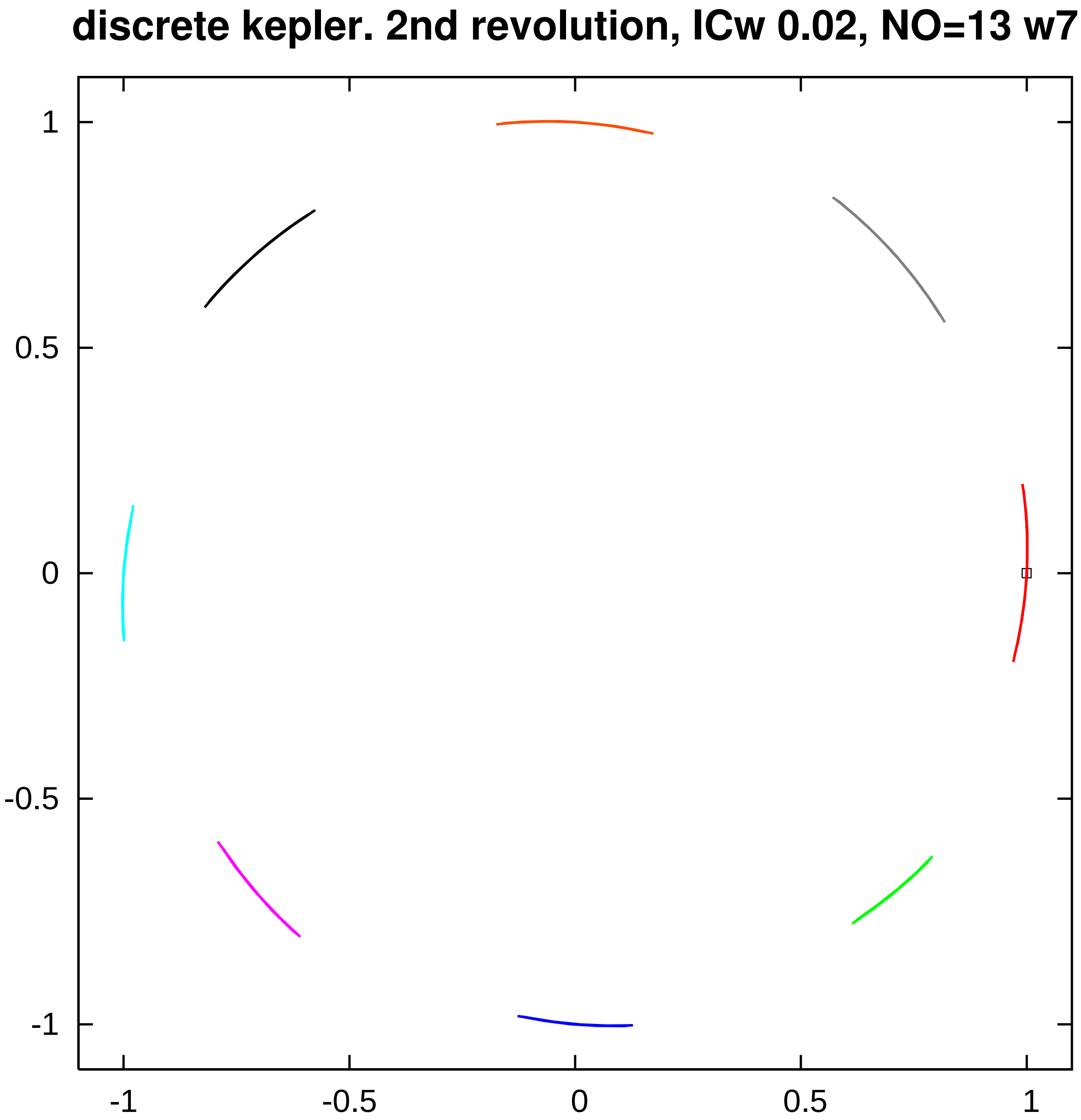
discrete kepler. 2nd revolution, ICw 0.02, NO=13 w7
1
0.5
0
-0.5
-1
-1
-0.5
0
0.5
1

discrete kepler. 3rd revolution, ICw 0.02, NO=13 w7

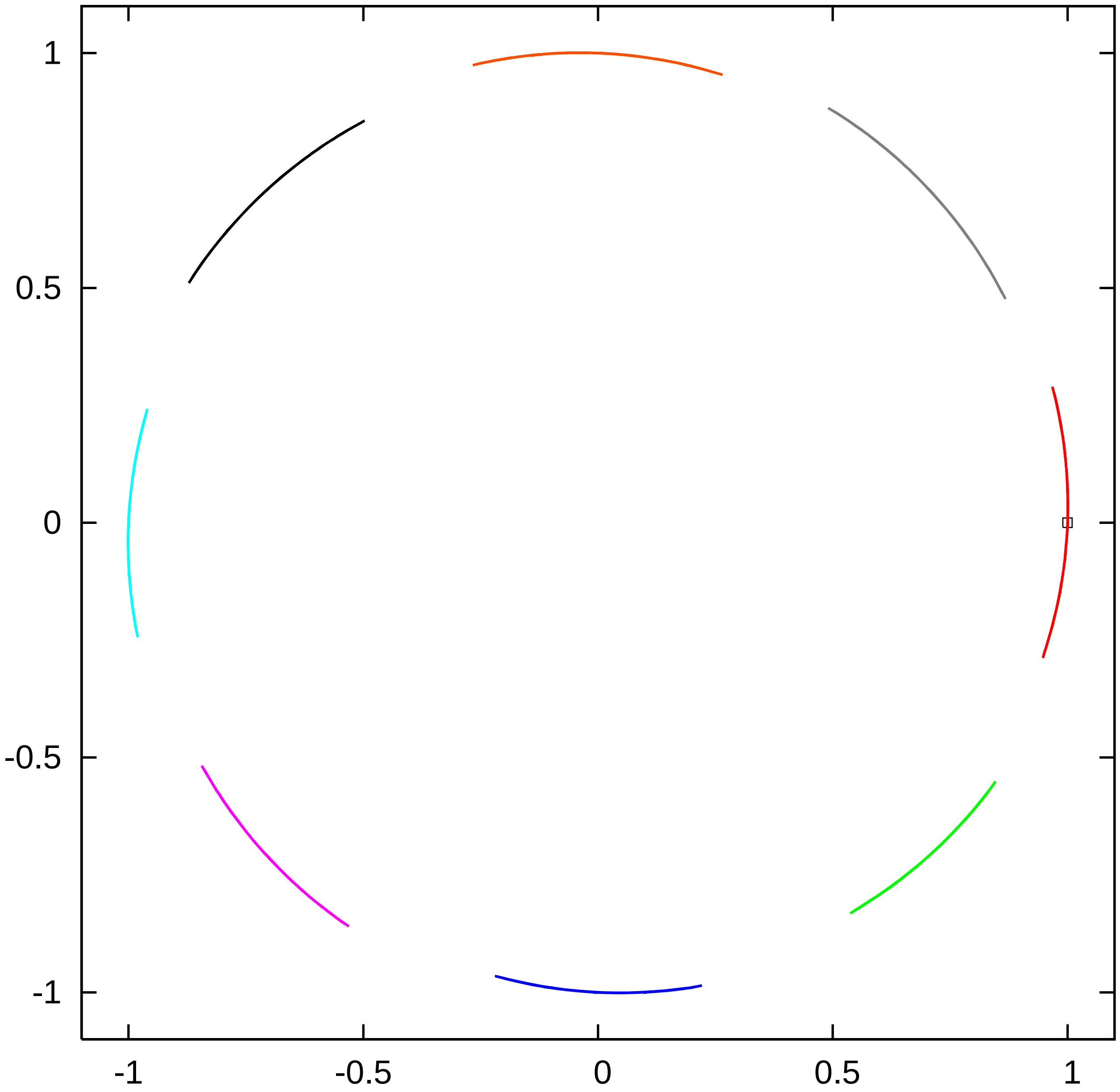

discrete kepler. 4th revolution, ICw 0.02, NO=13 w7

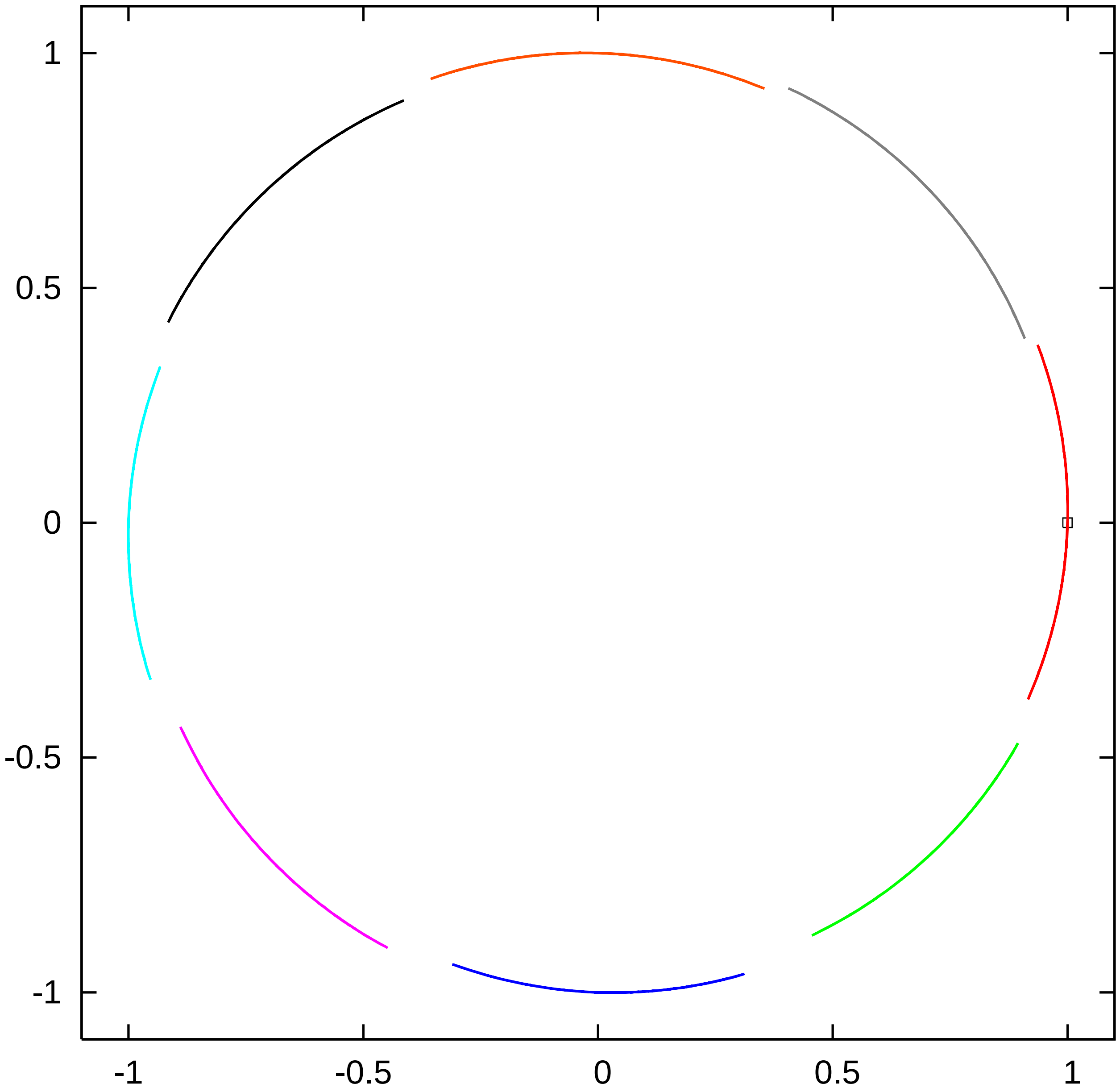

discrete kepler. 5th revolution, ICw 0.02, NO=13 w7

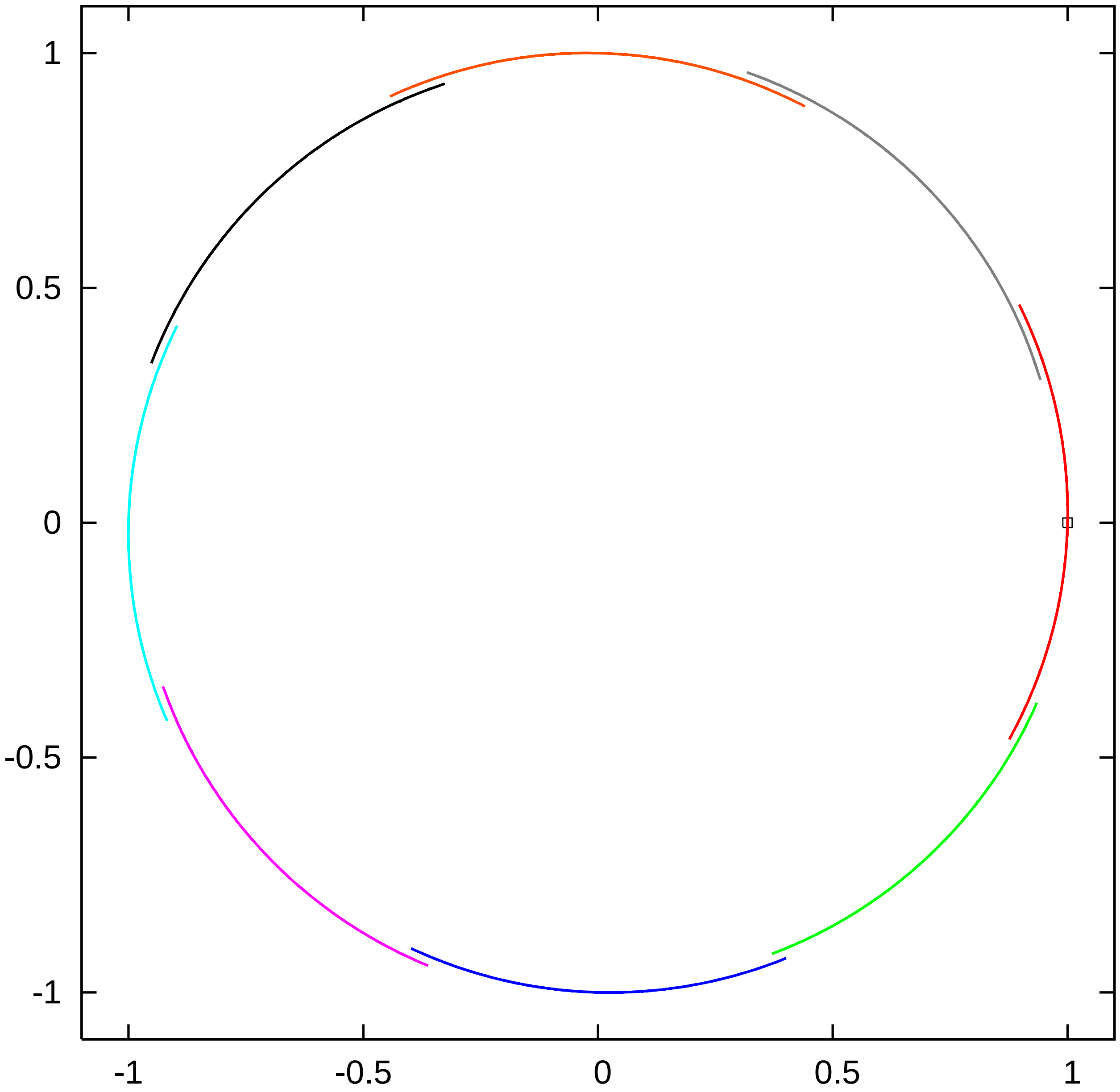

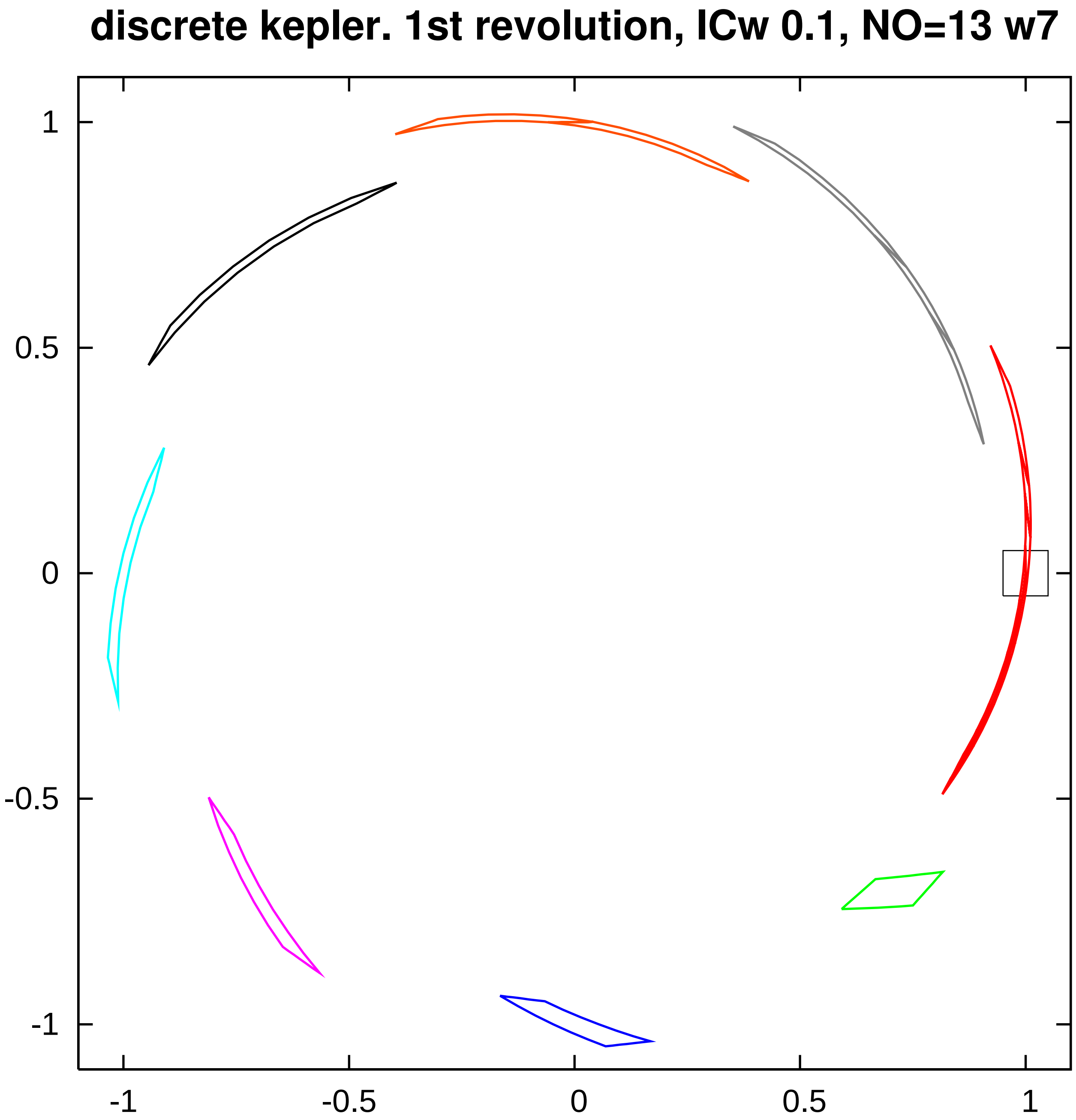
discrete kepler. 1st revolution, ICw 0.1, NO=13 w7
1
0.5
0
-0.5
-1
-1
-0.5
0
0.5
1

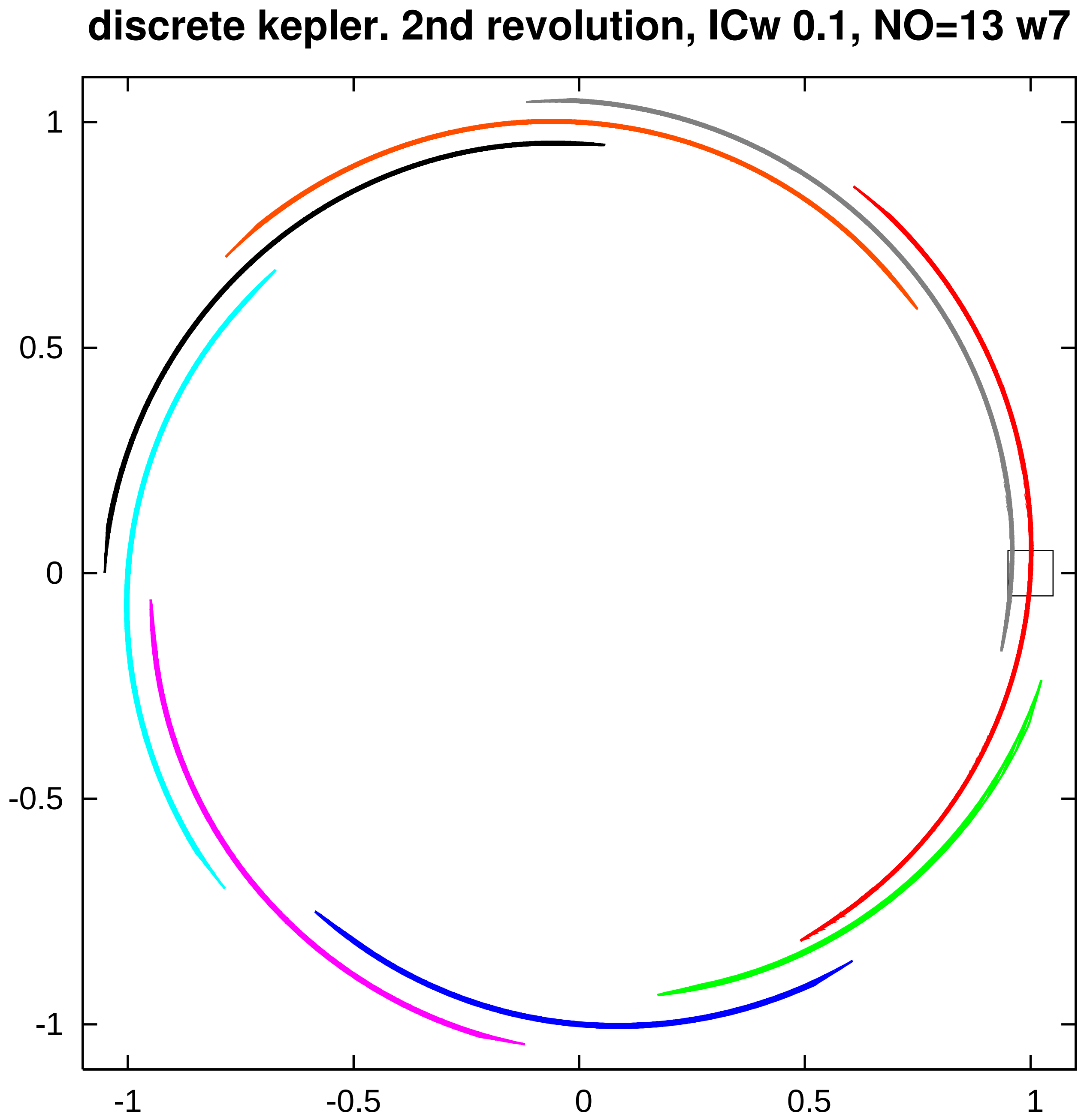
discrete kepler. 2nd revolution, ICw 0.1, NO=13 w7
1
0.5
0
-0.5
-1
-1
-0.5
0
0.5
1

discrete kepler. NO=13 w7

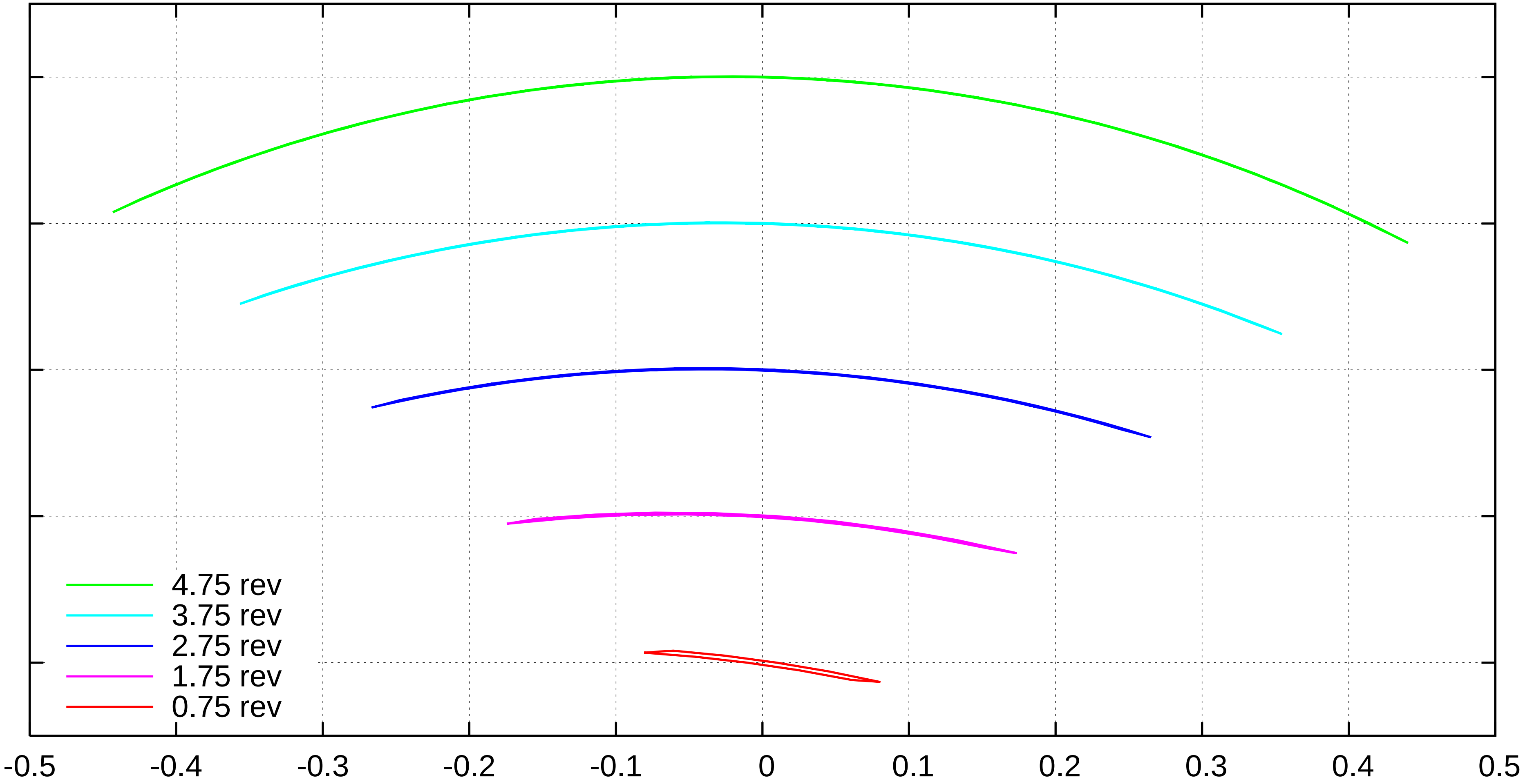

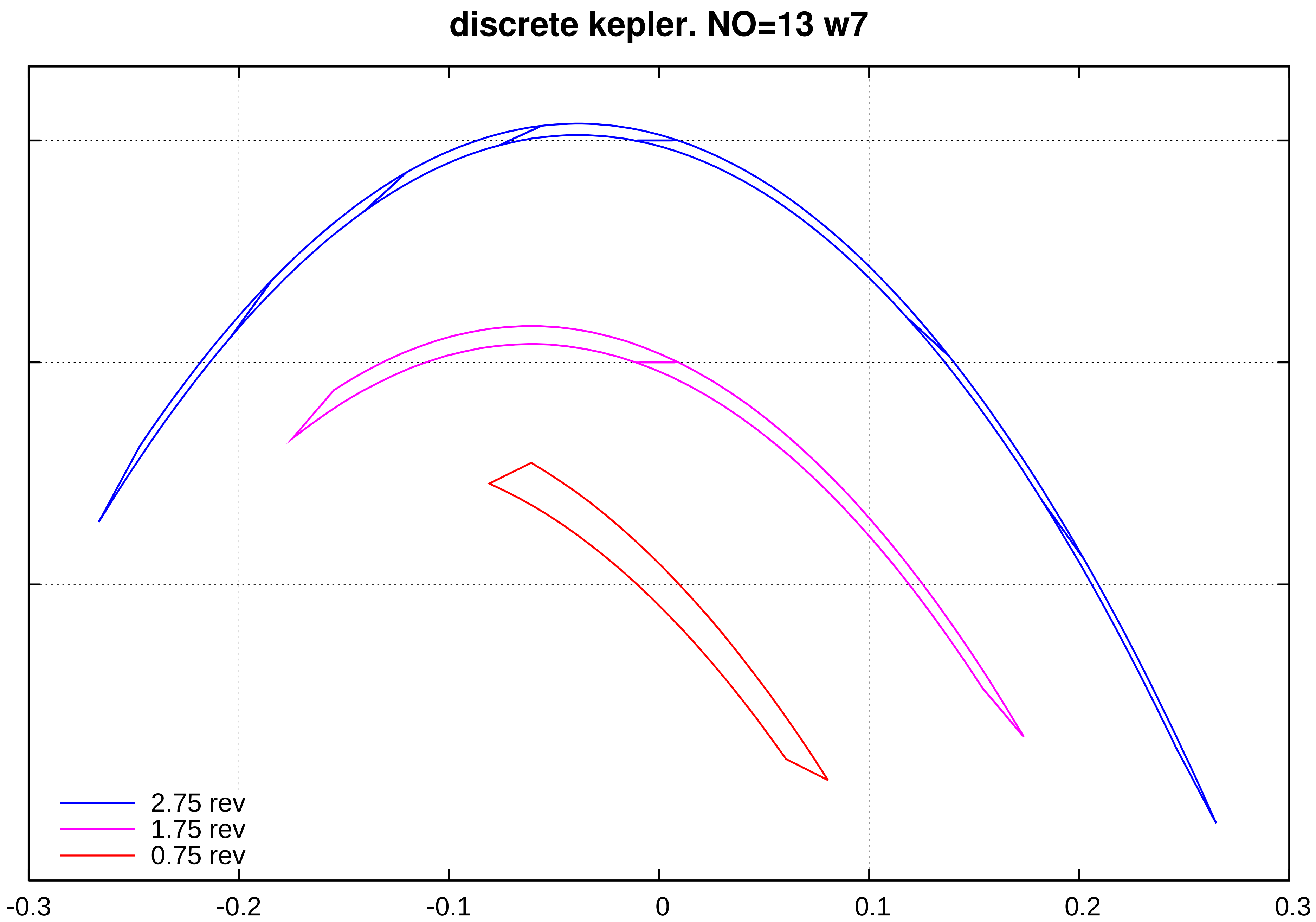
discrete kepler. NO=13 w7
-0.3
-0.2
-0.1
0
0.1
0.2
0.3
2.75 rev
1.75 rev
0.75 rev

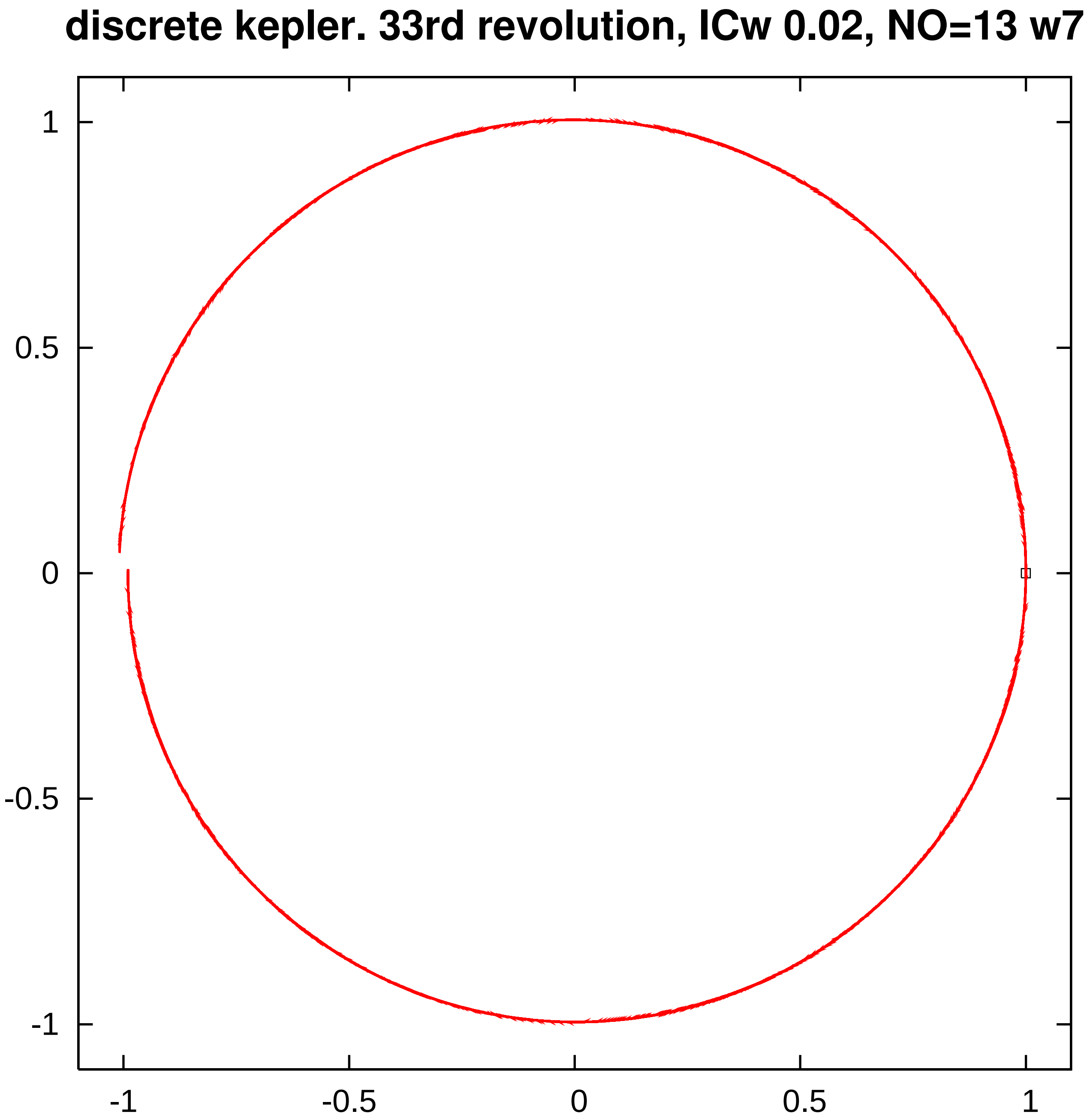

discrete kepler. 33rd revolution, ICw 0.02, NO=13 w7
1
0.5
0
-0.5
-1
-1
-0.5
0
0.5
1

The Milano-Michigan ESA Project

A Collaboration of the Instituto Aerospaziale at Politecnico di Milano and Michigan State University. Currently funded by the European Space Agency to

- Develop a verified integrator for solar system dynamics in a complete model of the solar system
- Includes influences of all planets, major asteroids, general relativity, etc
- Analyze its behavior and abilities
- Apply the integrator to study the dynamics of the Near-Earth Asteroid (99942) Apophis

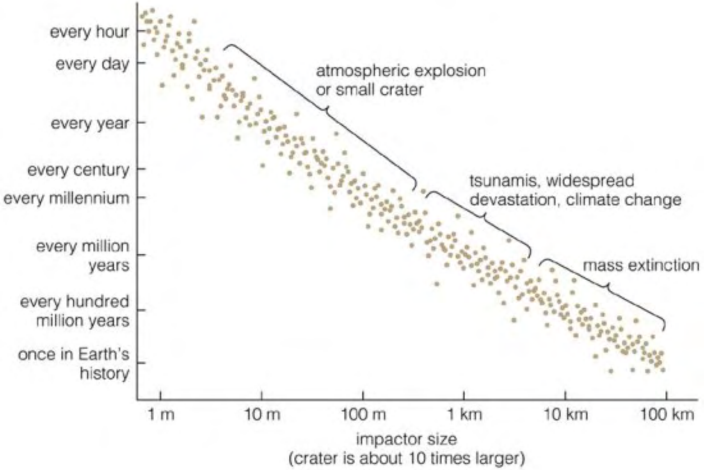

every hour
every day
every year
every century
every millennium
every million years
every hundred million years
once in Earth's history
atmospheric explosion or small crater
tsunamis, widespread devastation, climate change
mass extinction
1 m
10 m
100 m
1 km
10 km
100 km
impactor size
(crater is about 10 times larger)

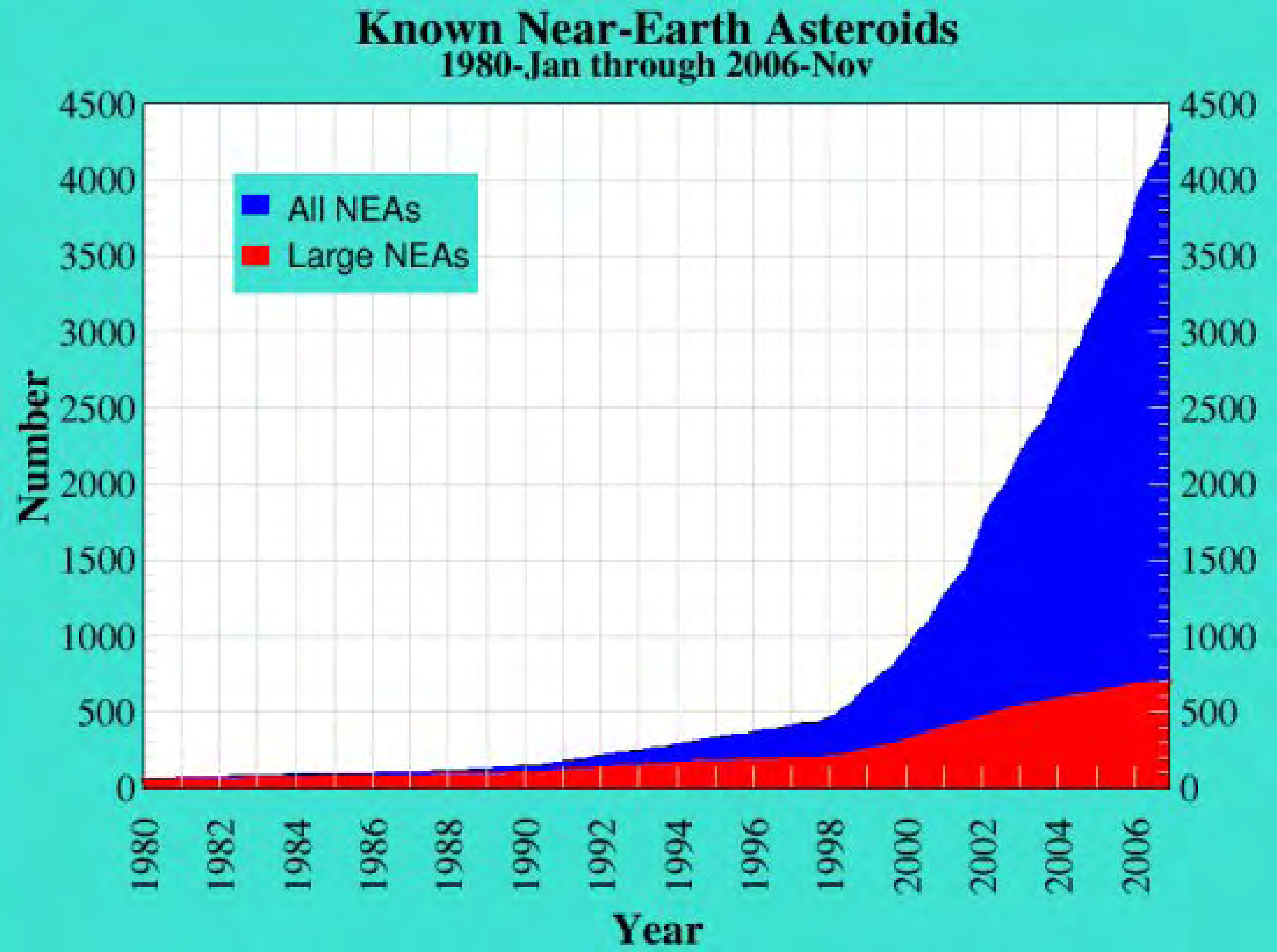
Known Near-Earth Asteroids
1980-Jan through 2006-Nov
All NEAs
Large NEAs
Number
Year
0
500
1000
1500
2000
2500
3000
3500
4000
4500
1980
1982
1984
1986
1988
1990
1992
1994
1996
1998
2000
2002
2004
2006

Near Earth Asteroid (99942) Apophis

- A Near-Earth Asteroid discovered in 2004
- Eccentric orbit between the orbits of Venus and Mars

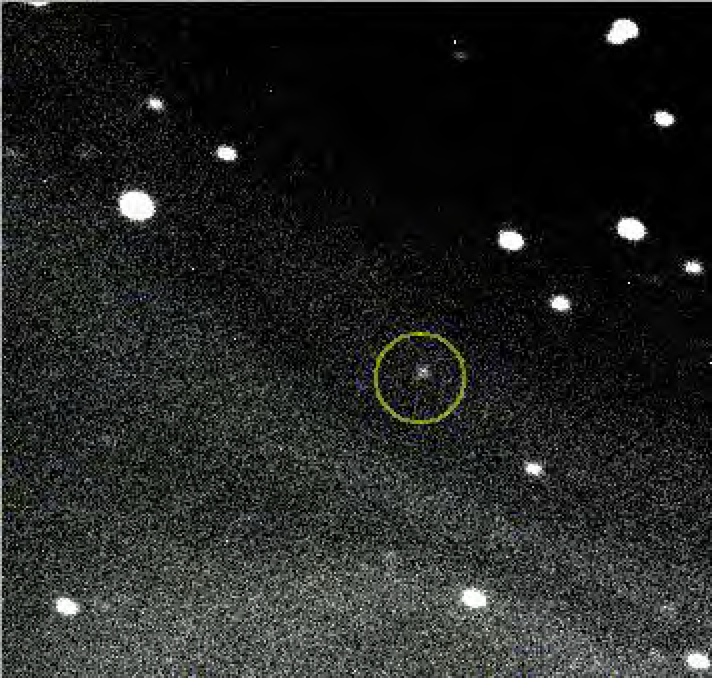

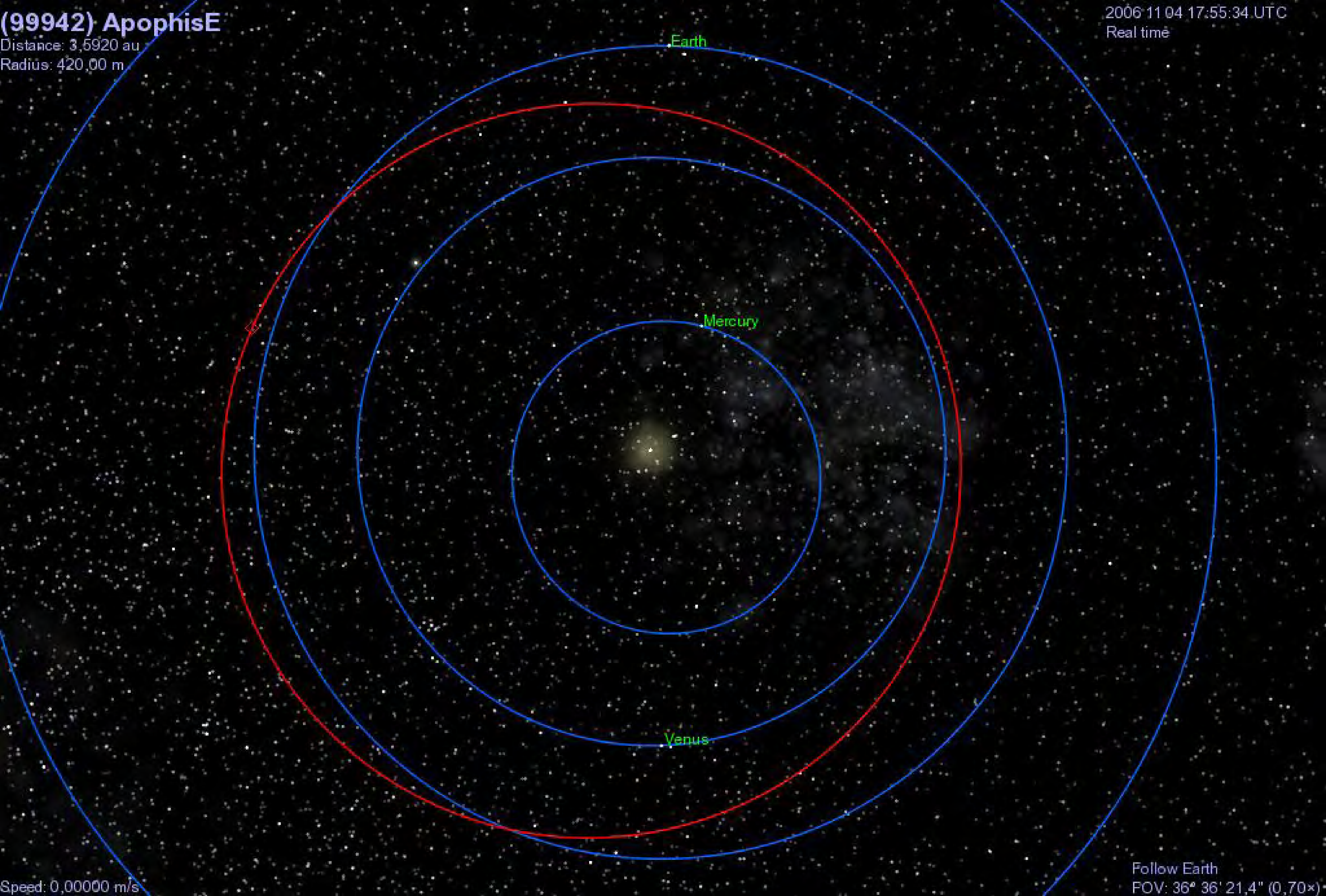
(99942) ApophisE
Distance: 3,5920 au
Radius: 420,00 m
2006 11 04 17:55:34 UTC
Real time
Earth
Mercury
Venus
Speed: 0,00000 m/s
Follow Earth
FOV: 36° 36' 21,4" (0,70×)

Near Earth Asteroid (99942) Apophis

- A Near-Earth Asteroid discovered in 2004
- Eccentric orbit between the orbits of Venus and Mars
- Apophis will have a first near collision with Earth on **Friday, April 13, 2029**

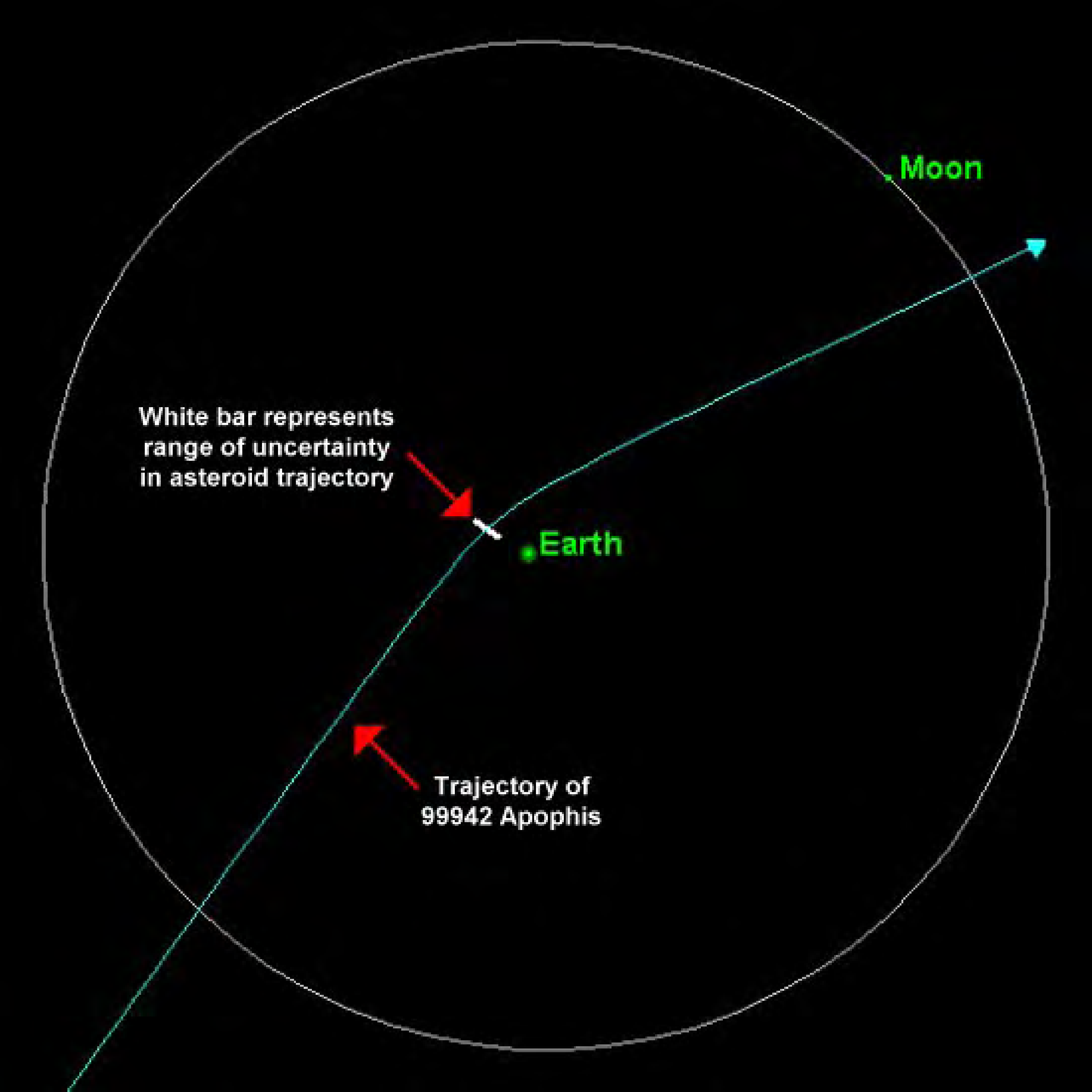

Moon
White bar represents
range of uncertainty
in asteroid trajectory
Earth
Trajectory of
99942 Apophis

Near Earth Asteroid (99942) Apophis

- A Near-Earth Asteroid discovered in 2004
- Eccentric orbit between the orbits of Venus and Mars
- Apophis will have a first near collision with Earth on **Friday, April 13, 2029**
- Apophis will have another near **(???)** collision with Earth on (Monday), **April 13, 2036**

Near Earth Asteroid (99942) Apophis

- A Near-Earth Asteroid discovered in 2004
- Eccentric orbit between the orbits of Venus and Mars
- Apophis will have a first near collision with Earth on **Friday, April 13, 2029**
- Apophis will have another near **(???)** collision with Earth on (Monday), **April 13, 2036**
- The near collision in 2029 very significantly alters Apophis' orbit

The small uncertainties of Apophis' current orbit parameters, amplified by the influence of the near collision in 2029, makes predictions for 2036 **very difficult.**

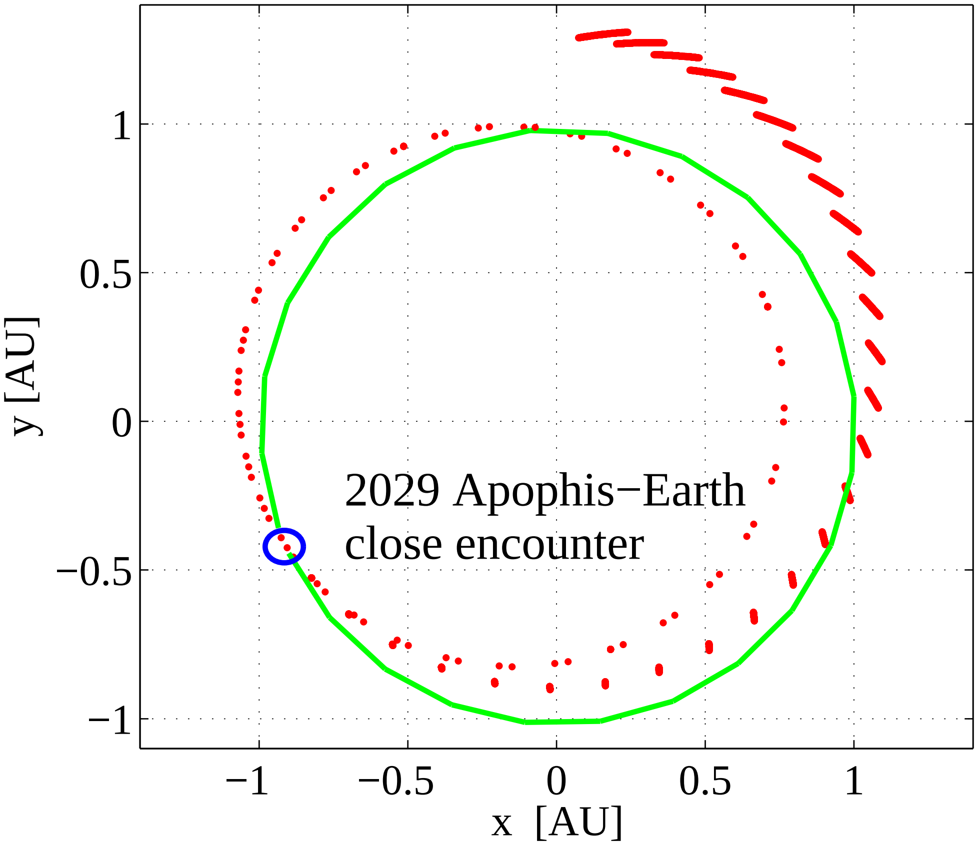

1
0.5
0
−0.5
−1
y [AU]
−1
−0.5
0
0.5
1
x [AU]
2029 Apophis−Earth
close encounter

(99942) Apophis - Encounter 2036

Prediction of motion of Apophis is very difficult. Its orbit is significantly affected by tiny perturbations:

- Detailed shape of Earth's gravitational field (oblateness, mountains)
- Gravitational pull of other asteroids
- Radiation pressure from Sun (even a small reflective shield being applied can deflect the asteroid)
- 64 bit accuracy of numerical integrators (regardless of verification)

All these influences affect the final position to the size of more than one Earth diameter

Apophis - The Demon of Darkness and Chaos

(From http://www.egyptiandreams.co.uk/apep.php)

- In Egyptian mythology, Apep - or **Apophis** in Greek - was an evil demon, the deification of **darkness and chaos**, and thus opponent of light and Ma'at (order/truth), whose existence was believed about from the Middle Kingdom onwards.
- As the personification of all that was evil, Apep was seen as a giant **snake**, or sometimes a crocodile, serpent, or dragon.

Apophis - The Demon of Darkness and Chaos

- Tales of Apep's battles against the Sun God **Ra** were elaborated during the New Kingdom. Since nearly everyone can see that the sun is not attacked by a giant snake during the day, story tellers said that Apep must lie just below the horizon in the underworld, which attacked the sun each night.
- In a bid to explain natural phenomona it was said that occasionally Apep got the upper hand. The damage to order caused **thunderstorms and earthquakes**. It was even thought that sometimes Apep actually managed to briefly swallow Ra during the day, causing a **solar eclipse.**

The Henon Map

$$H(x, y) = (1 - ax^2 + y, bx).$$

We set the parameters $a = 1.4$ and $b = 0.3$, which are originally considered by Henon. The map H has two fixed points.

$$\vec{p}_1 = (0.63135, 0.18940) \quad \text{and} \quad \vec{p}_2 = (-1.13135, -0.33941).$$

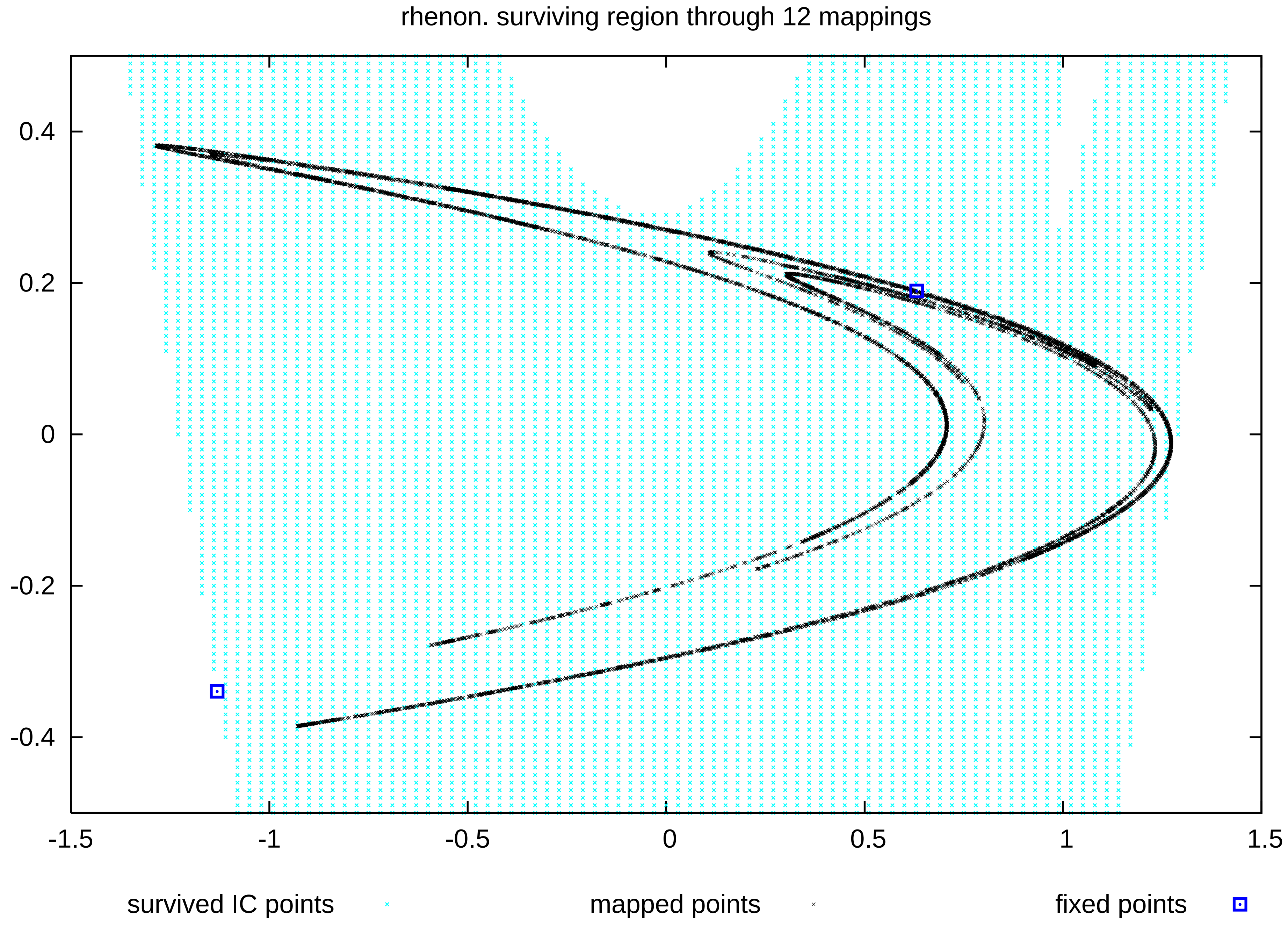
rhenon. surviving region through 12 mappings
0.4
0.2
0
-0.2
-0.4
-1.5
-1
-0.5
0
0.5
1
1.5
survived IC points
mapped points
fixed points

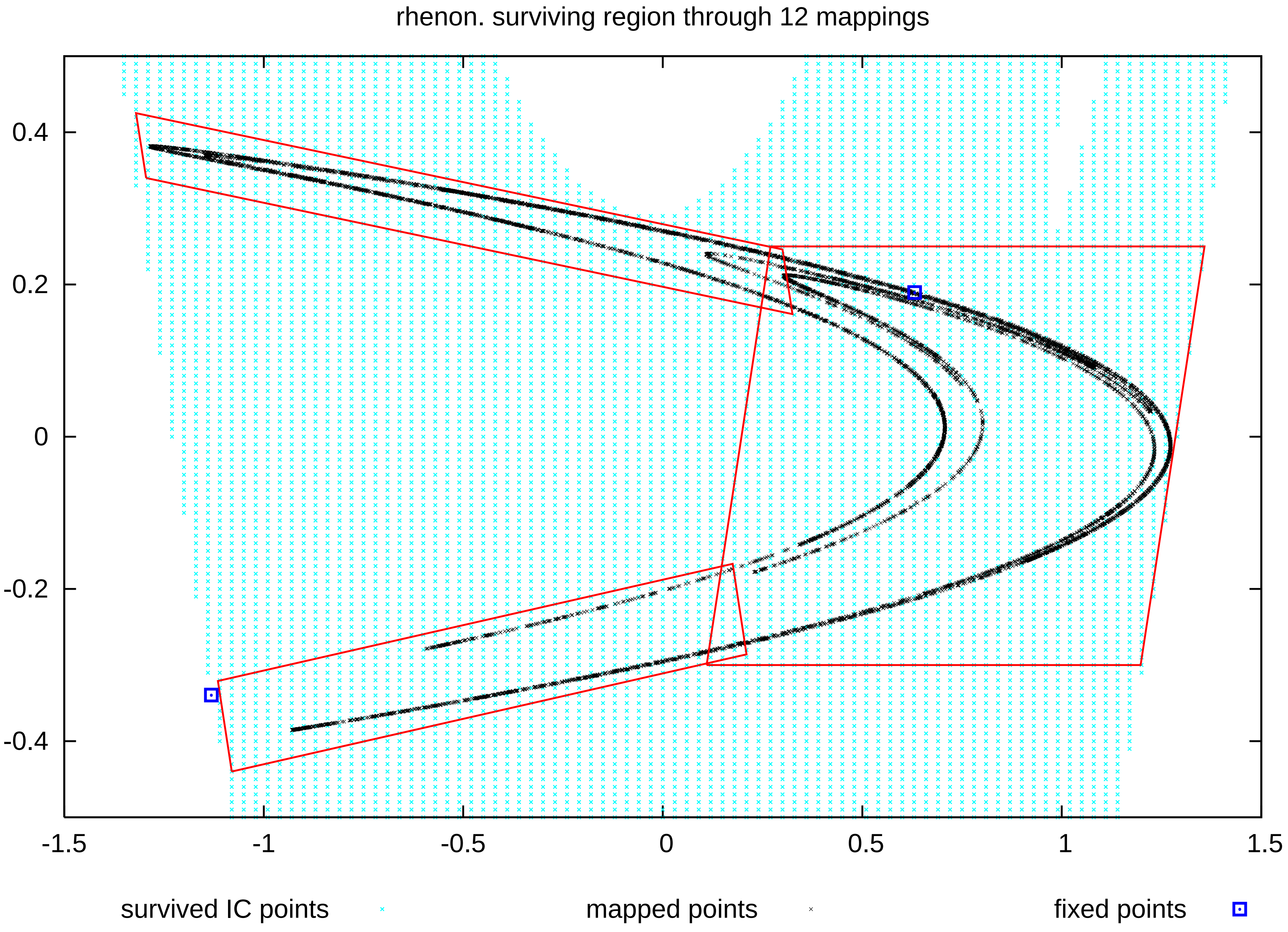
rhenon. surviving region through 12 mappings
0.4
0.2
0
-0.2
-0.4
-1.5
-1
-0.5
0
0.5
1
1.5
survived IC points
mapped points
fixed points

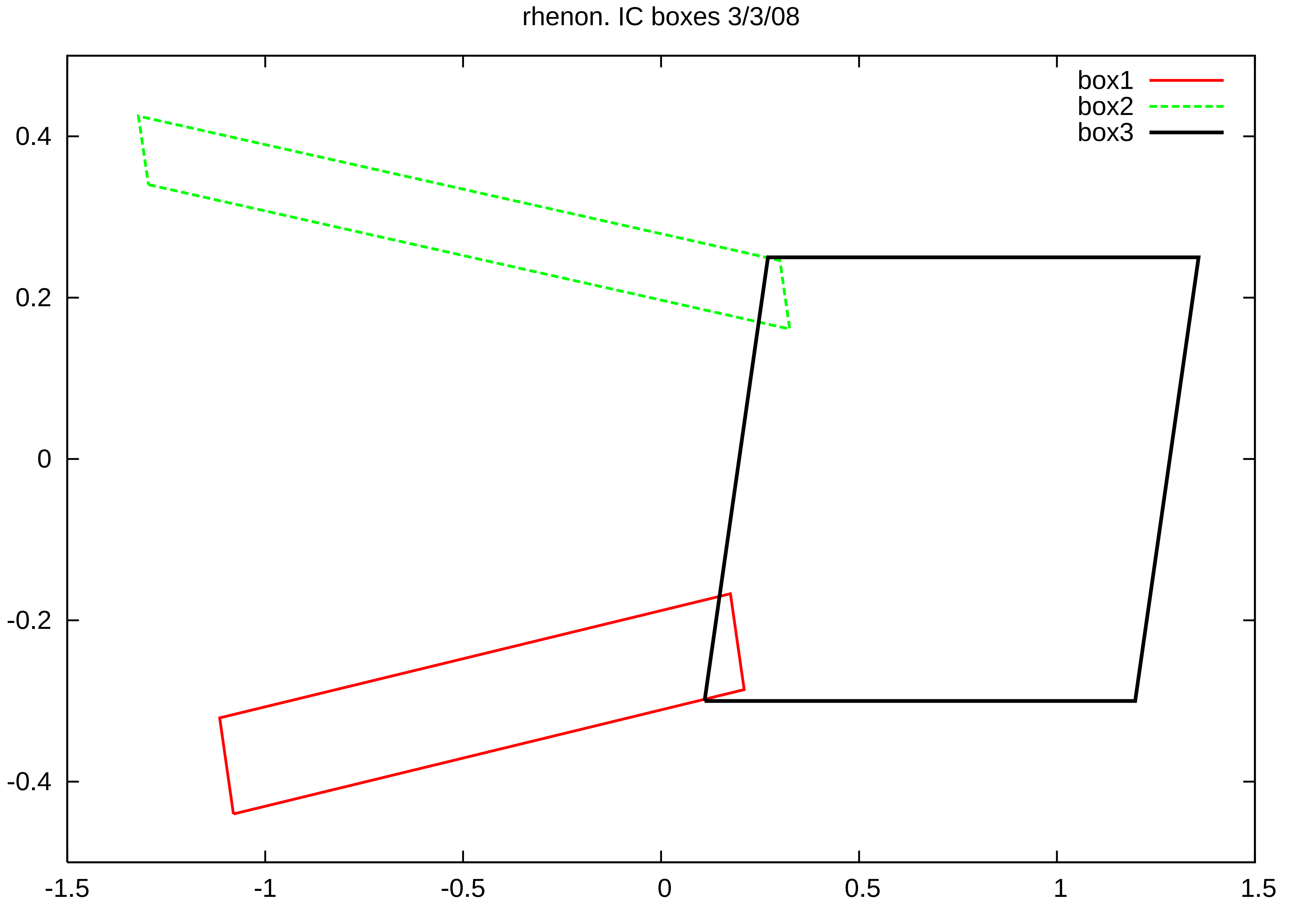
rhenon. IC boxes 3/3/08
box1
box2
box3
0.4
0.2
0
-0.2
-0.4
-1.5
-1
-0.5
0
0.5
1
1.5

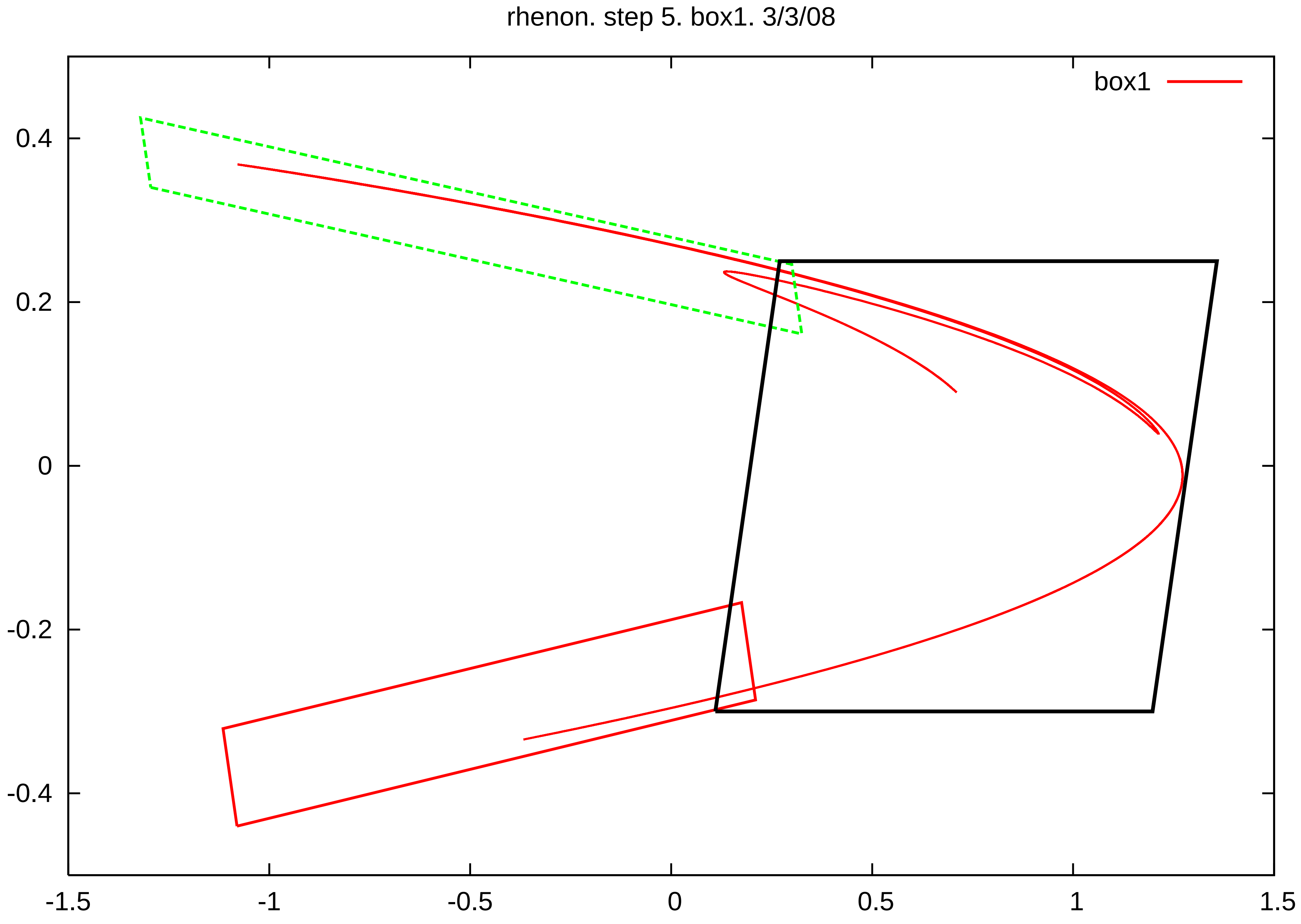

rhenon. step 5. box1. 3/3/08
box1
0.4
0.2
0
-0.2
-0.4
-1.5
-1
-0.5
0
0.5
1
1.5

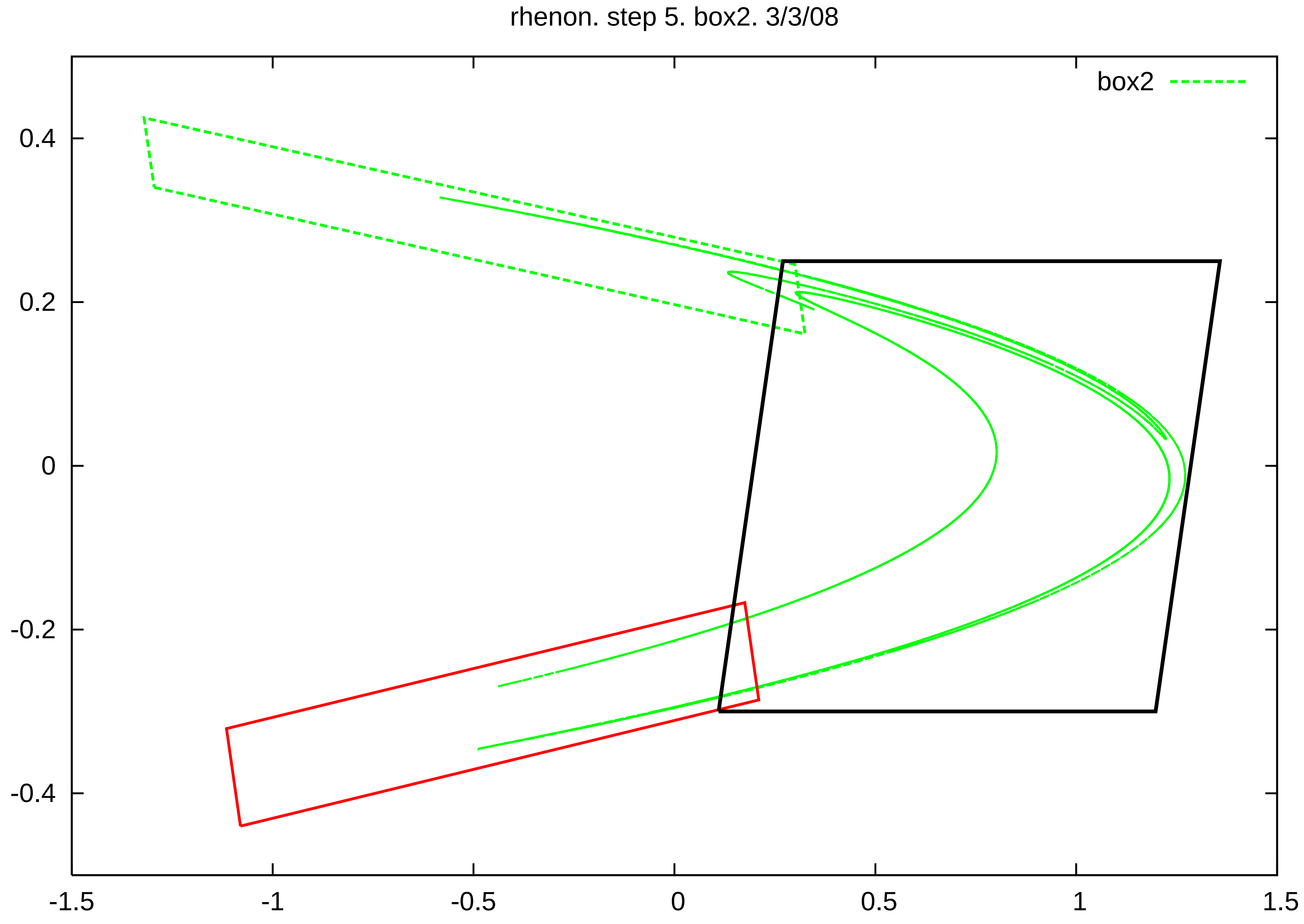
rhenon. step 5. box2. 3/3/08
box2
0.4
0.2
0
-0.2
-0.4
-1.5
-1
-0.5
0
0.5
1
1.5

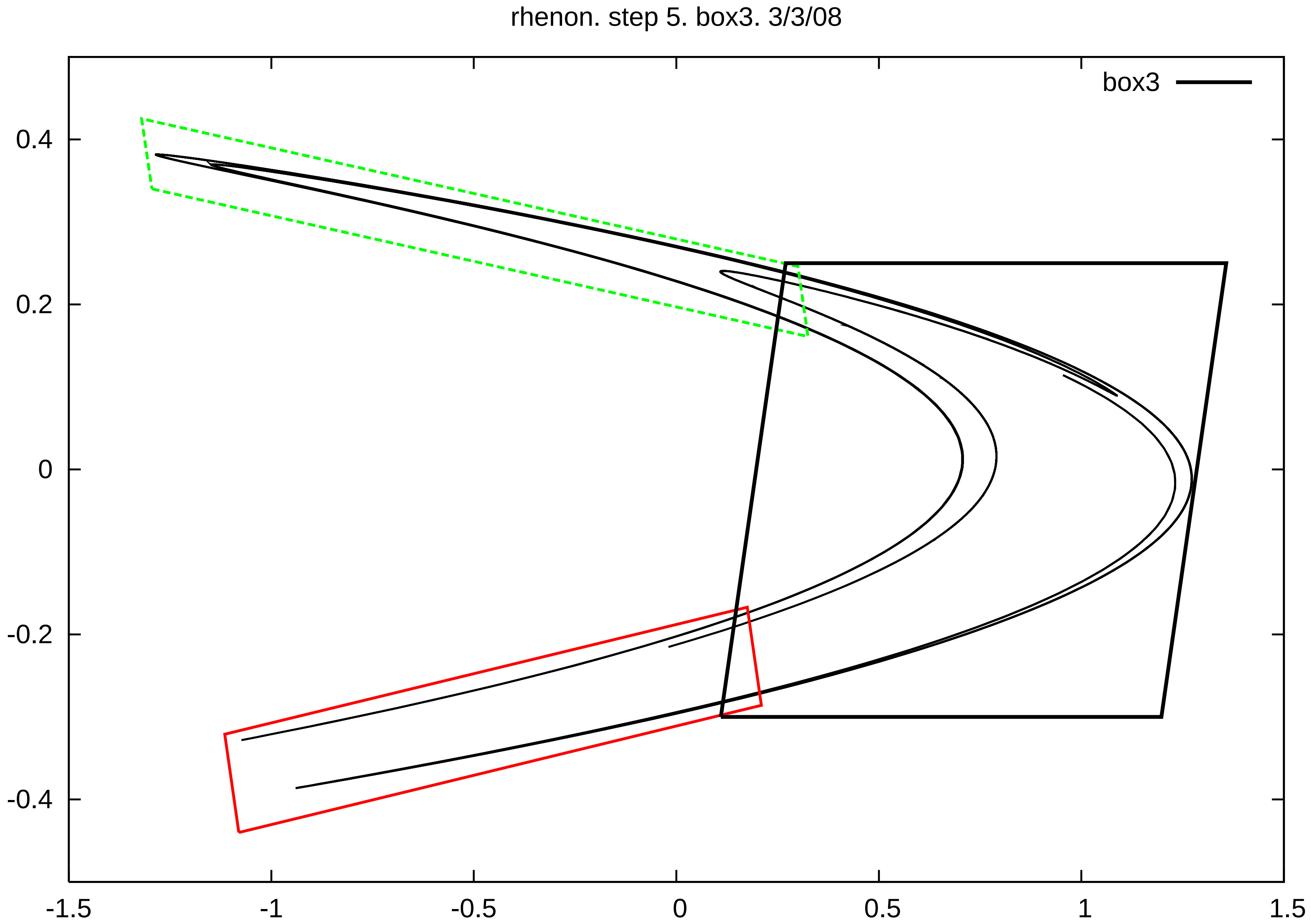
rhenon. step 5. box3. 3/3/08
box3
0.4
0.2
0
-0.2
-0.4
-1.5
-1
-0.5
0
0.5
1
1.5

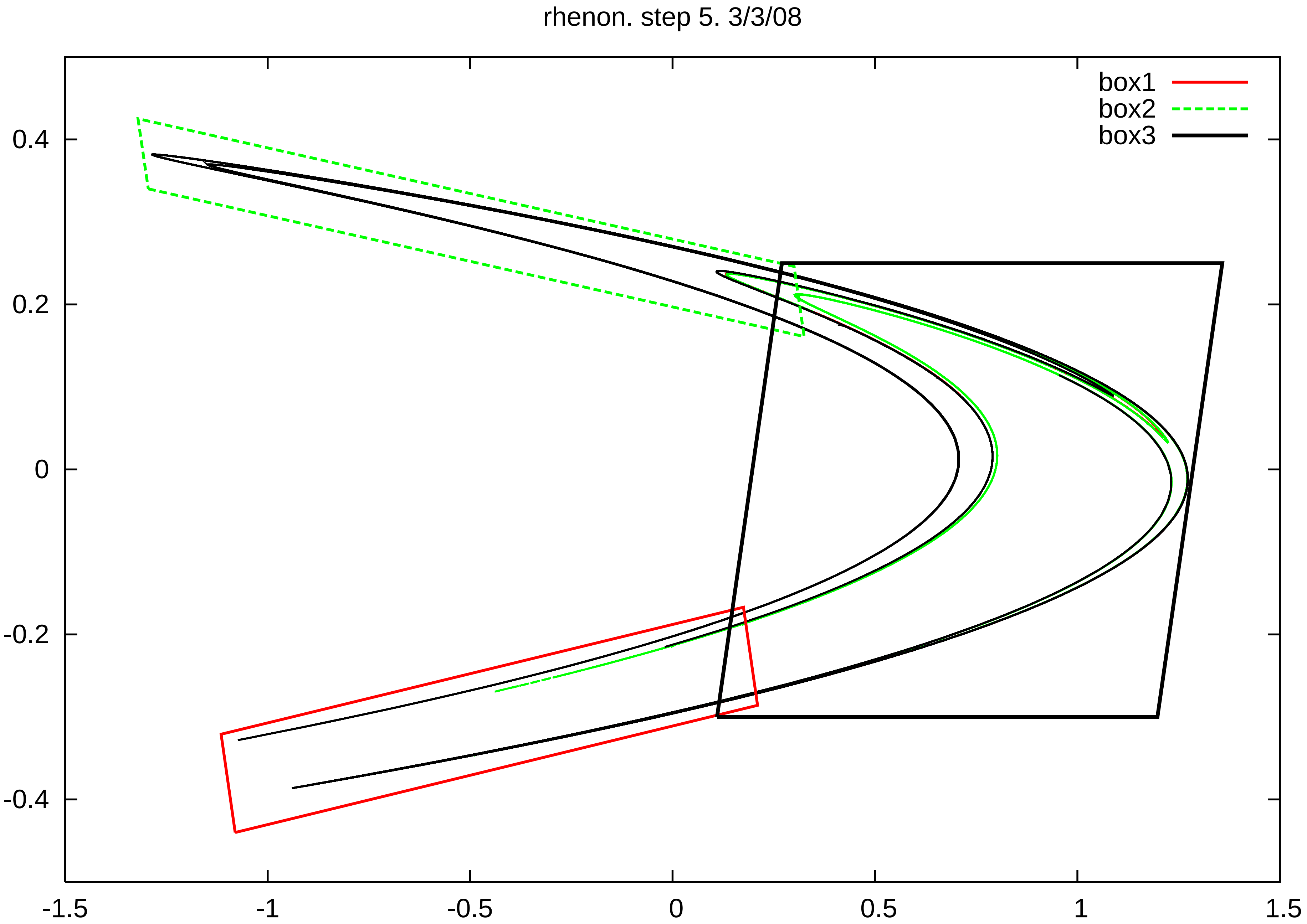

rhenon. step 5. 3/3/08
box1
box2
box3
0.4
0.2
0
-0.2
-0.4
-1.5
-1
-0.5
0
0.5
1
1.5

rhenon: Number of Objects

To carry out multiple mappings of the Henon map, Taylor model objects underwent the domain decomposition.

Number of Taylor model objects used for multiple mappings:

	n	w	for 5 steps	for 7 steps
box1	33	17	3	1386
box2	21	11	148	1691
box3	33	17	8	2839

Normal Form Methods

Iterative order-by-order coordinate transfomation to simplify dynamics around a fixed point. Assume we have TM representation of

1. Discrete Systems: One rigorous iteration of nonlinear map
2. Continuous Systems: Rigorous Flow representation of suitable time step Δt

Result: Except for resonances, obtain a coordinate transformation that up to order n **linearizes** the motion

- Elliptic case $\lambda_{i+1} = \bar{\lambda}_i$: spiral motion in $(\lambda_i, \lambda_{i+1})$ plane
- Elliptic unity case $\lambda_{i+1} = \bar{\lambda}_i$ and $|\bar{\lambda}_i| = 1$: circular motion, radius-dependent rotation frequency
- Hyperbolic case, i.e. $\lambda_i > 1$ real for $i = 1, ..., k$, $\lambda_i < 1$ for $i = 1, ..., v$: motion along hyperpolae, $\vec{e}_i$ axis expanded or contracted by λ_i

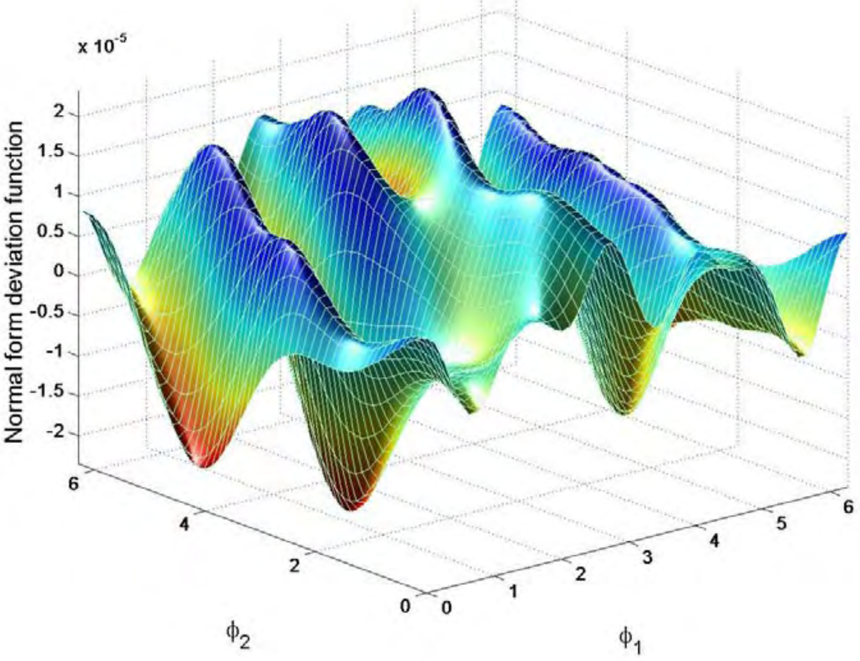
x 10^-5
Normal form deviation function
2
1.5
1
0.5
0
-0.5
-1
-1.5
-2
6
4
2
0
0
1
2
3
4
5
6
ϕ2
ϕ1

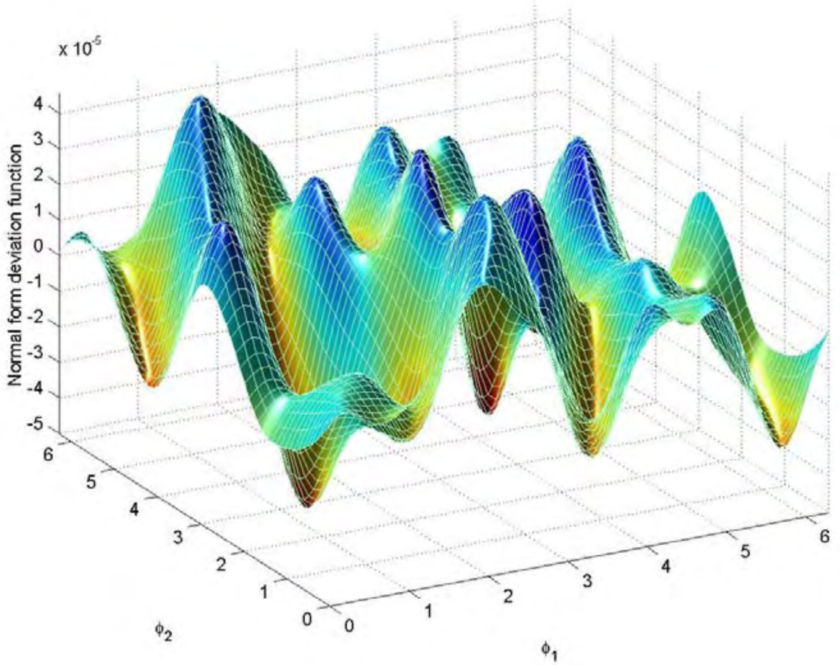
x 10^-5
Normal form deviation function
4
3
2
1
0
-1
-2
-3
-4
-5
6
5
4
3
2
1
0
φ2
0
1
2
3
4
5
6
φ1

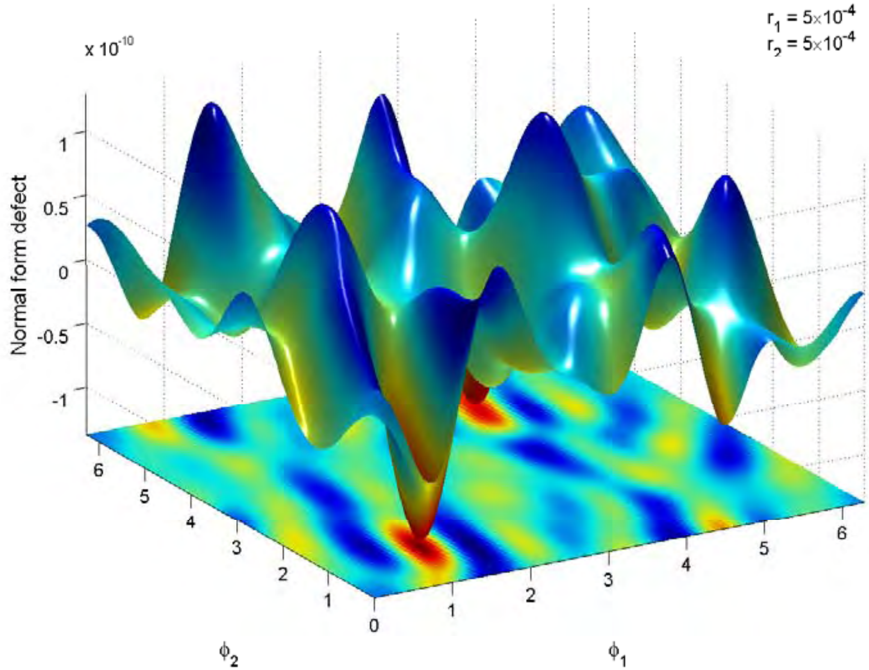

Fig. 9. Projection of the normal form defect function. Dependence on two angle variables for the fixed radii $r_1 = r_2 = 5 \cdot 10^{-4}$

Region	Boxes studied	CPU-time	Bound	Transversal Iterations
$[0.2, 0.4] \cdot 10^{-4}$	82,930	30,603 sec	$0.859 \cdot 10^{-13}$	$2.3283 \cdot 10^{8}$
$[0.4, 0.6] \cdot 10^{-4}$	82,626	30,603 sec	$0.587 \cdot 10^{-12}$	$3.4072 \cdot 10^{7}$
$[0.6, 0.9] \cdot 10^{-4}$	64,131	14,441 sec	$0.616 \cdot 10^{-11}$	$4.8701 \cdot 10^{6}$
$[0.9, 1.2] \cdot 10^{-4}$	73,701	13,501 sec	$0.372 \cdot 10^{-10}$	$8.0645 \cdot 10^{5}$
$[1.2, 1.5] \cdot 10^{-4}$	106,929	24,304 sec	$0.144 \cdot 10^{-9}$	$2.0833 \cdot 10^{5}$
$[1.5, 1.8] \cdot 10^{-4}$	111,391	26,103 sec	$0.314 \cdot 10^{-9}$	$0.95541 \cdot 10^{5}$

Table 8
Global bounds obtained for six radial regions in normal form space for the Tevatron. Also computed are the guaranteed minimum transversal iterations.

Normal Form Methods

Iterative order-by-order coordinate transfomation to simplify dynamics around a fixed point.

Result: Except for resonances, up to order n,

- Elliptic case $\lambda_{i+1} = \bar{\lambda}_i$: spiral motion in $(\lambda_i, \lambda_{i+1})$ plane
- Elliptic unity case $\lambda_{i+1} = \bar{\lambda}_i$ and $|\bar{\lambda}_i| = 1$: circular motion, radius-dependent rotation frequency
- Hyperbolic case (λ_i real) motion along $\vec{e}_i$ axis, expanded or contracted by λ_i

Practial use:

- Can be performed rigorously in Taylor model arithmetic
- Implemented to arbitrary order in arbitrarily many variables in COSY INFINITY

Rigorous Unstable Manifold Enclosures I

Goal: Find collection of hopefully very narrow Taylor models that contain a hopefully long stretch of unstable manifold.

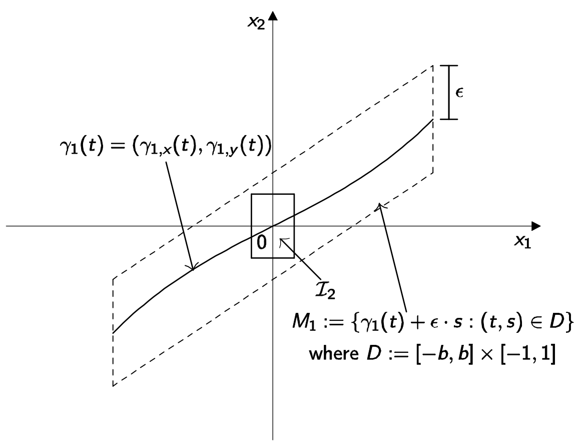

Begin with unstable manifold near fixed point:

- Obtain approximate polynomial path $\gamma(t)$ as image of normal form $\vec{e}_1$ axis
- Put "test tube" around $\gamma(t)$ to get $\gamma(t) + \varepsilon \cdot s \cdot \vec{e}_2$. Practical choice: $\varepsilon = 10^{-14}$

Rigorous Unstable Manifold Enclosures II

- Verify that $M(\gamma(t) + \varepsilon \cdot s \cdot \vec{e}_2)$ leaves "test tube" only at ends. Very useful for that:

  1. $M(\gamma(t)) =_n \gamma(\lambda_1 \cdot t)$, so orbit of γ is reproduced to order n
  2. M is contracting with λ_2 perpendicular to γ
  3. $\gamma(t) + \varepsilon \cdot s \cdot \vec{e}_2$ and its image under M can be treated rigorously in Taylor model arithmetic

After these steps, it is assured that

- The unstable manifold does NOT leave $\gamma(t) + \varepsilon \cdot s \cdot \vec{e}_2$ at top or bottom
- The unstable manifold DOES leave $\gamma(t) + \varepsilon \cdot s \cdot \vec{e}_2$ at the sides (easy to show)

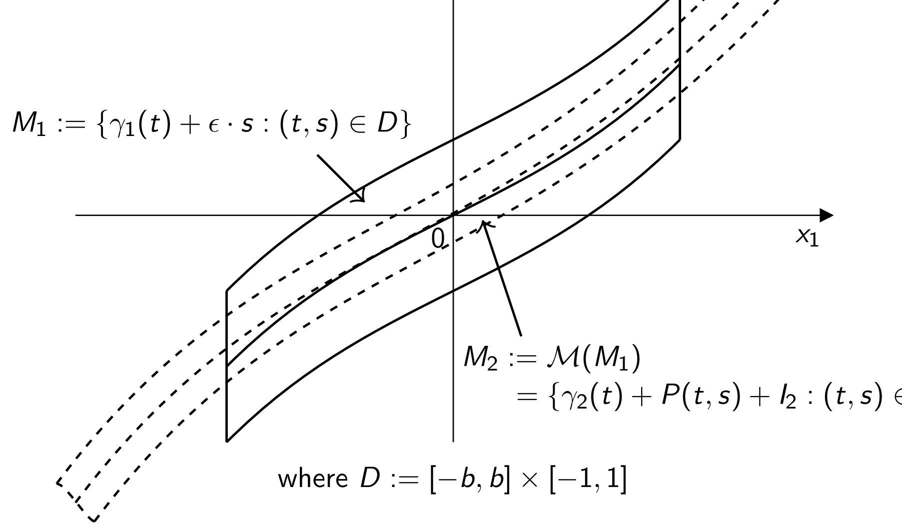
$M_1 := \{\gamma_1(t) + \epsilon \cdot s : (t, s) \in D\}$
0
x_1
$M_2 := \mathcal{M}(M_1)$
$= \{\gamma_2(t) + P(t, s) + l_2 : (t, s) \in$
where $D := [-b, b] \times [-1, 1]$

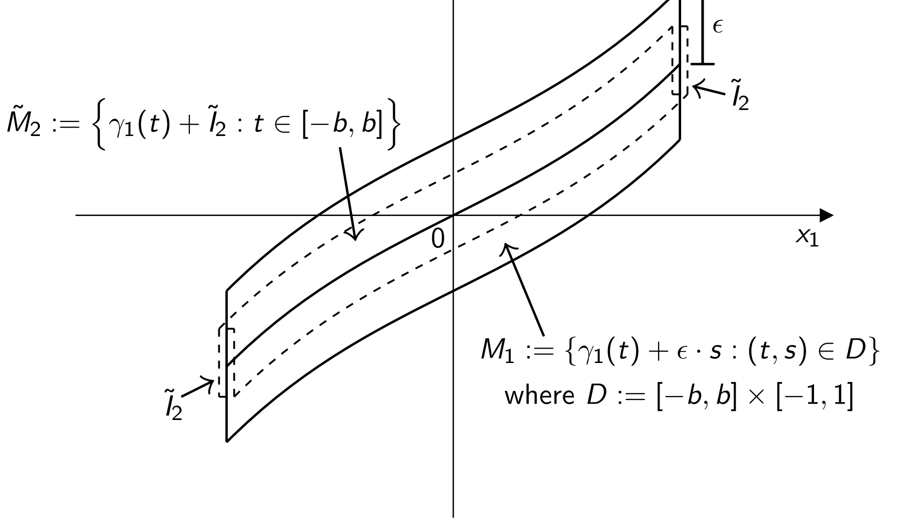

ϵ
$\tilde{I}_2$
$\tilde{M}_2 := \left\{\gamma_1(t) + \tilde{I}_2 : t \in [-b, b]\right\}$
0
x_1
$M_1 := \{\gamma_1(t) + \epsilon \cdot s : (t, s) \in D\}$
where $D := [-b, b] \times [-1, 1]$
$\tilde{I}_2$

Rigorous Unstable Manifold Enclosures III

Unstable manifold can be drawn as far as desired by

- Mapping $\gamma(t) + \varepsilon \cdot s \cdot \vec{e}_2$ through M repeatedly
- Splitting result if length $>$ tolerance

As a result, we obtain a collection of as many Taylor model as we wish, each of which

- Contains a piece of the unstable manifold
- The unstable manifold leaves through the "narrow sides"
- The unstable manifold does not leave through the "long sides"

By considering the inverse map, we can analogously obtain rigorous enclosures of the stable manifolds.

Unstable Manifold of a Henon map (a=1.4, b=0.3) represented by 450 pieces of TMs

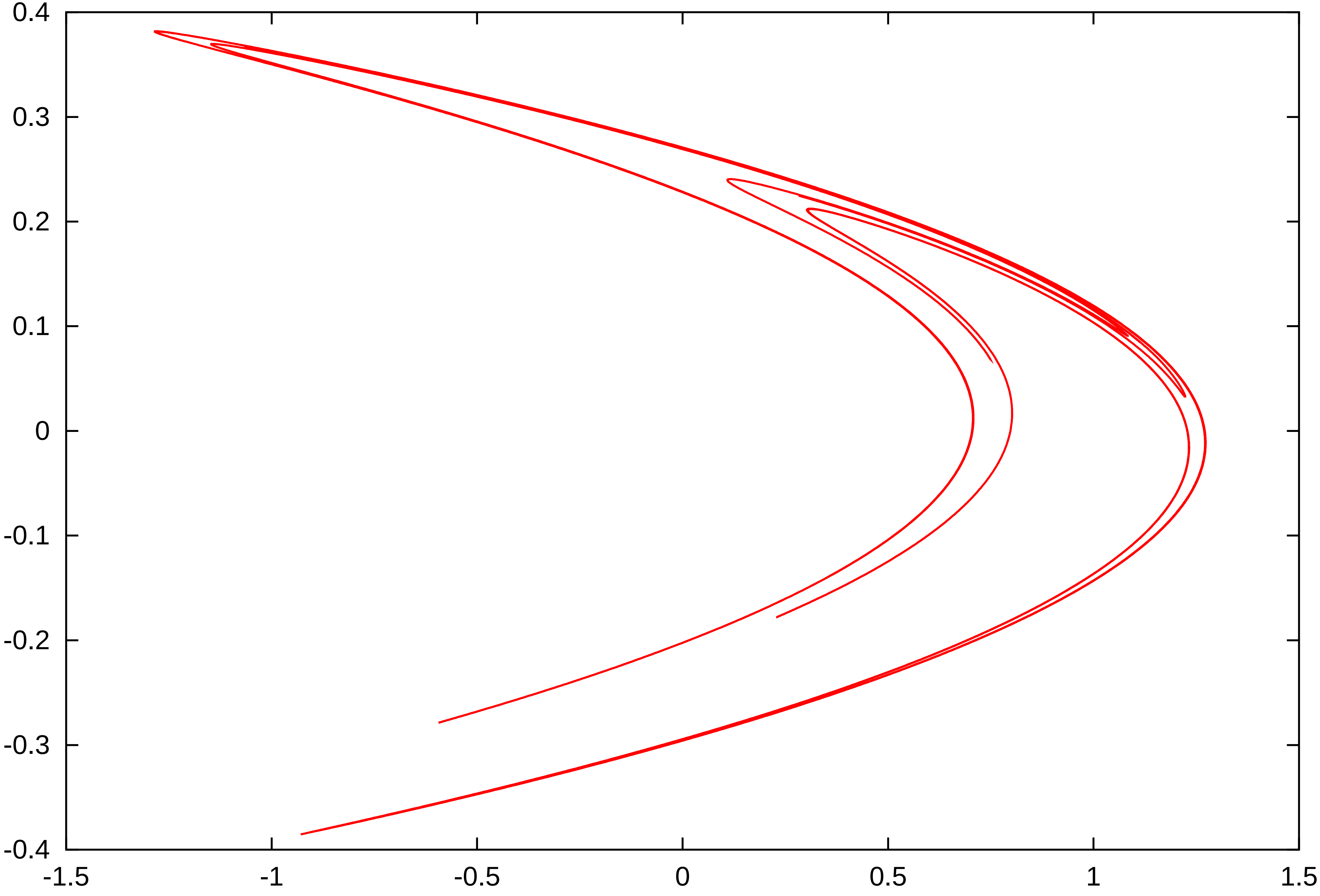

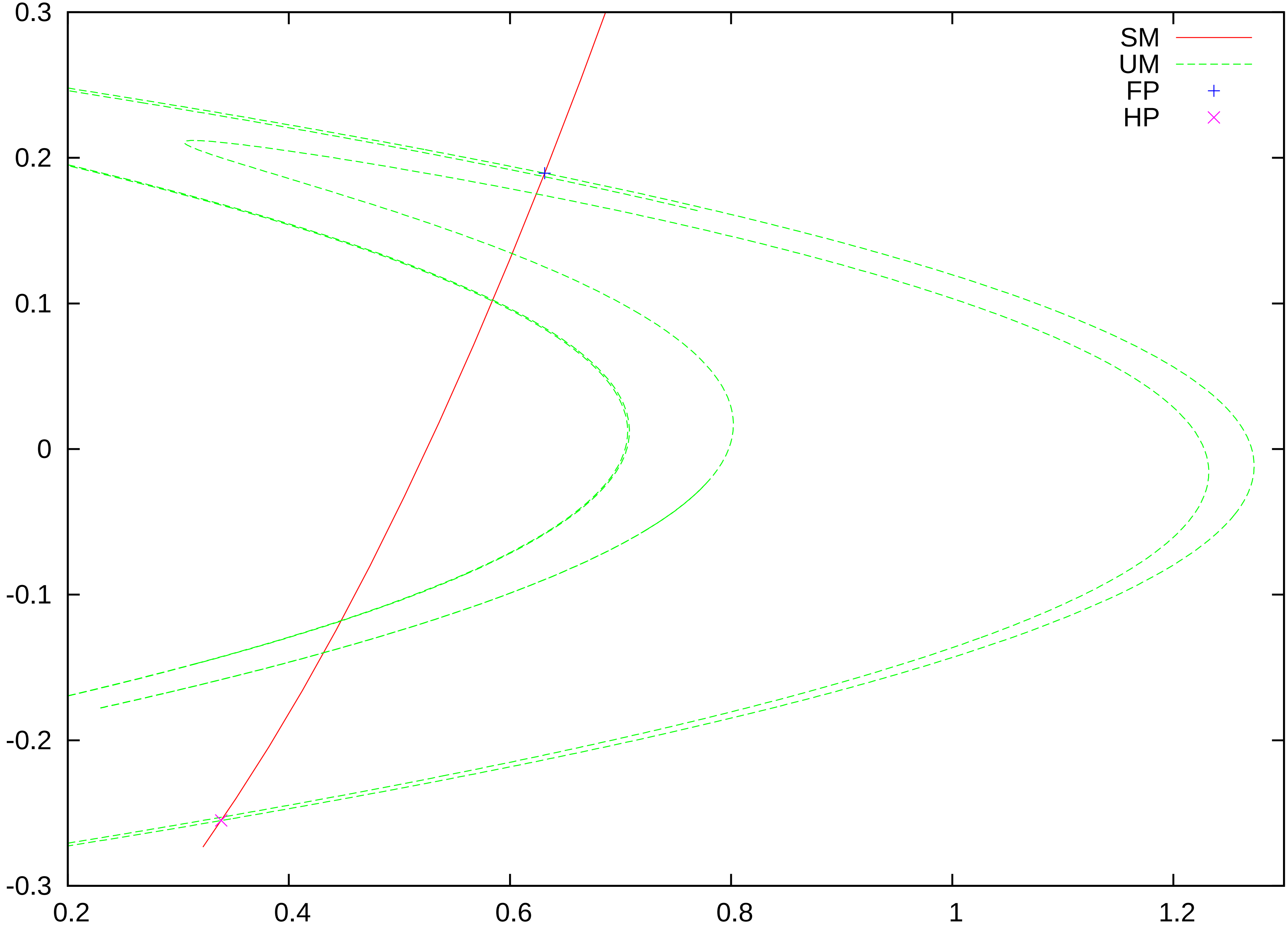

SM
UM
FP
HP
0.3
0.2
0.1
0
-0.1
-0.2
-0.3
0.2
0.4
0.6
0.8
1
1.2

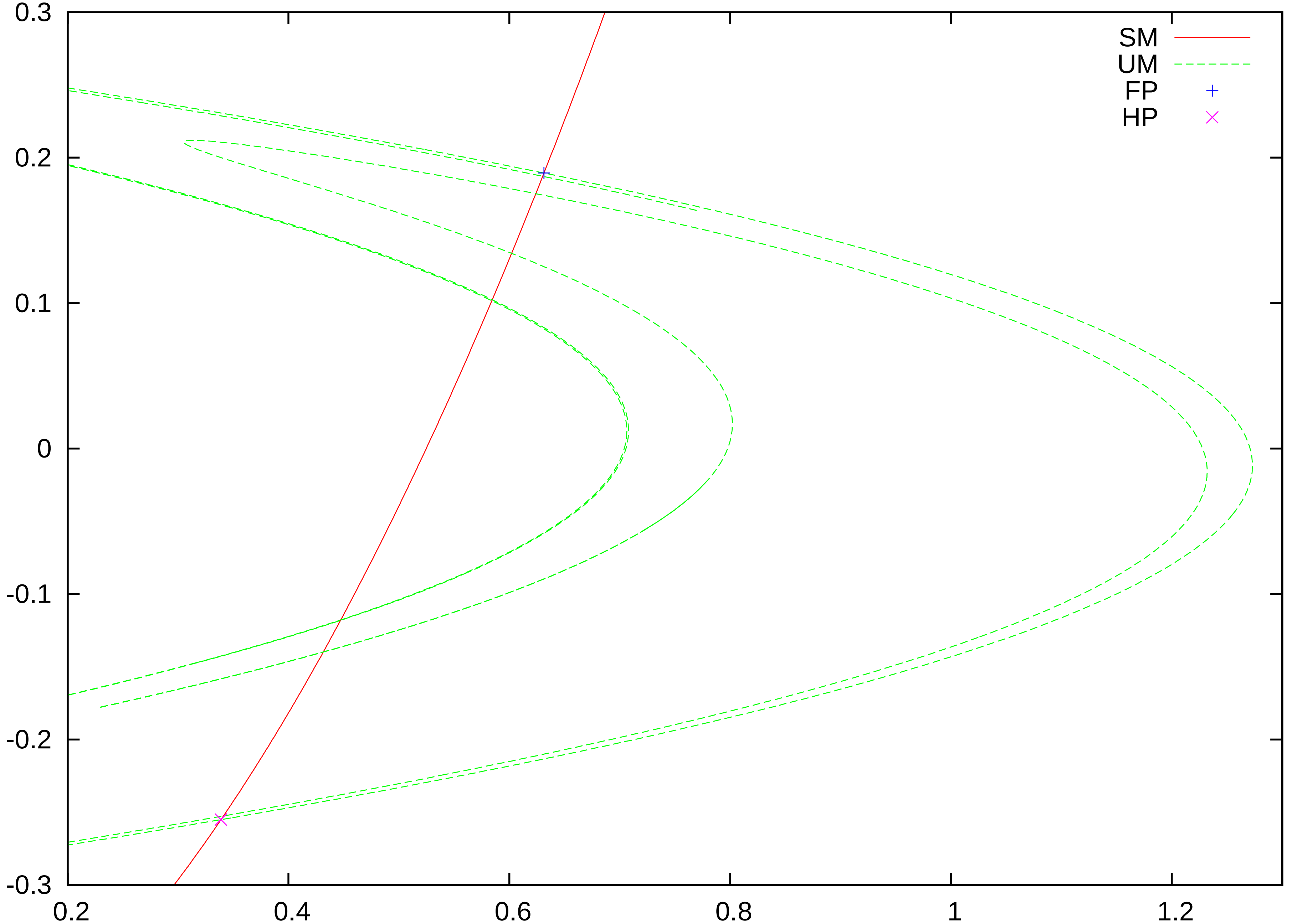

SM
UM
FP
HP
0.3
0.2
0.1
0
-0.1
-0.2
-0.3
0.2
0.4
0.6
0.8
1
1.2

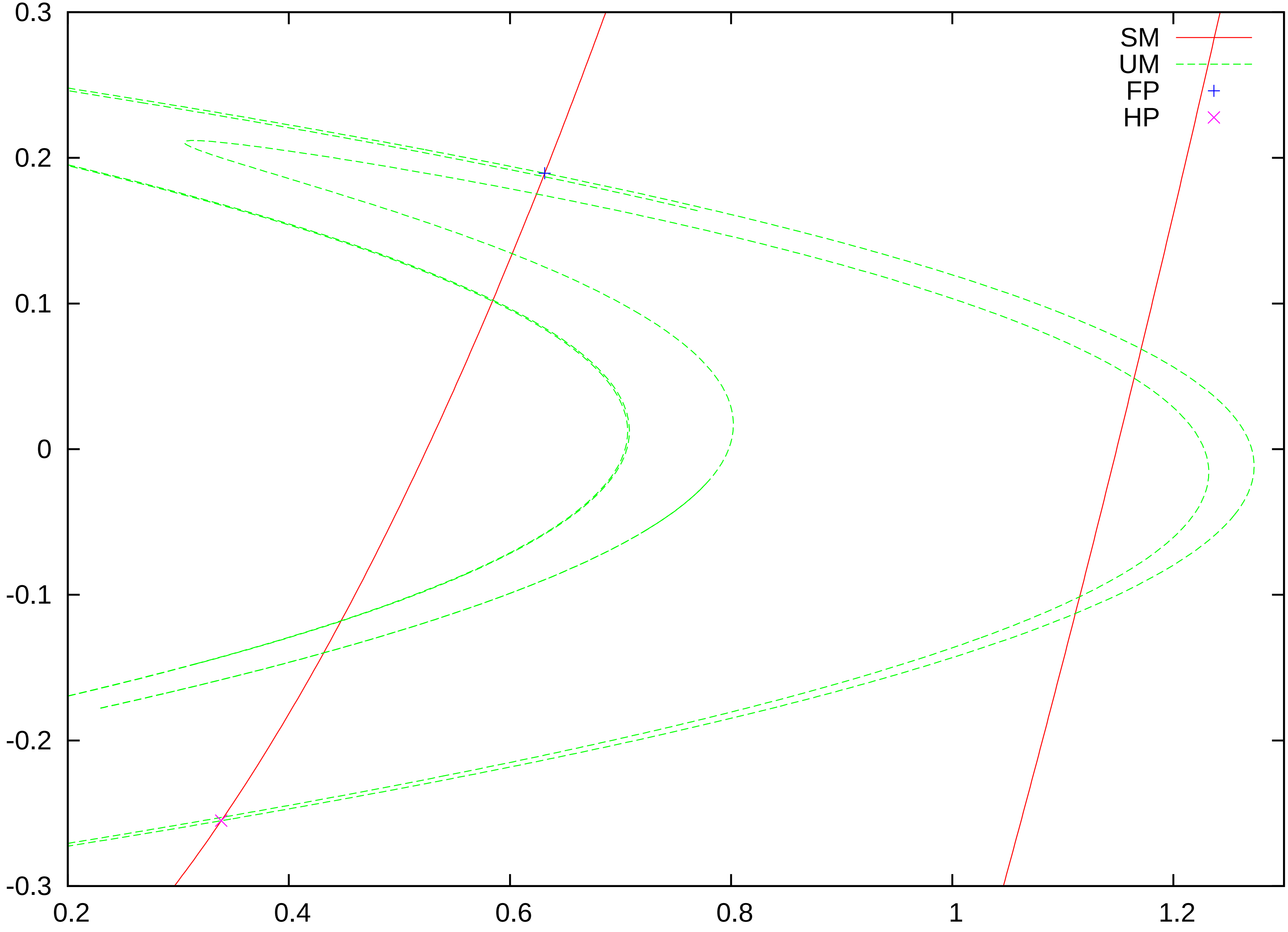

SM
UM
FP
HP
0.3
0.2
0.1
0
-0.1
-0.2
-0.3
0.2
0.4
0.6
0.8
1
1.2

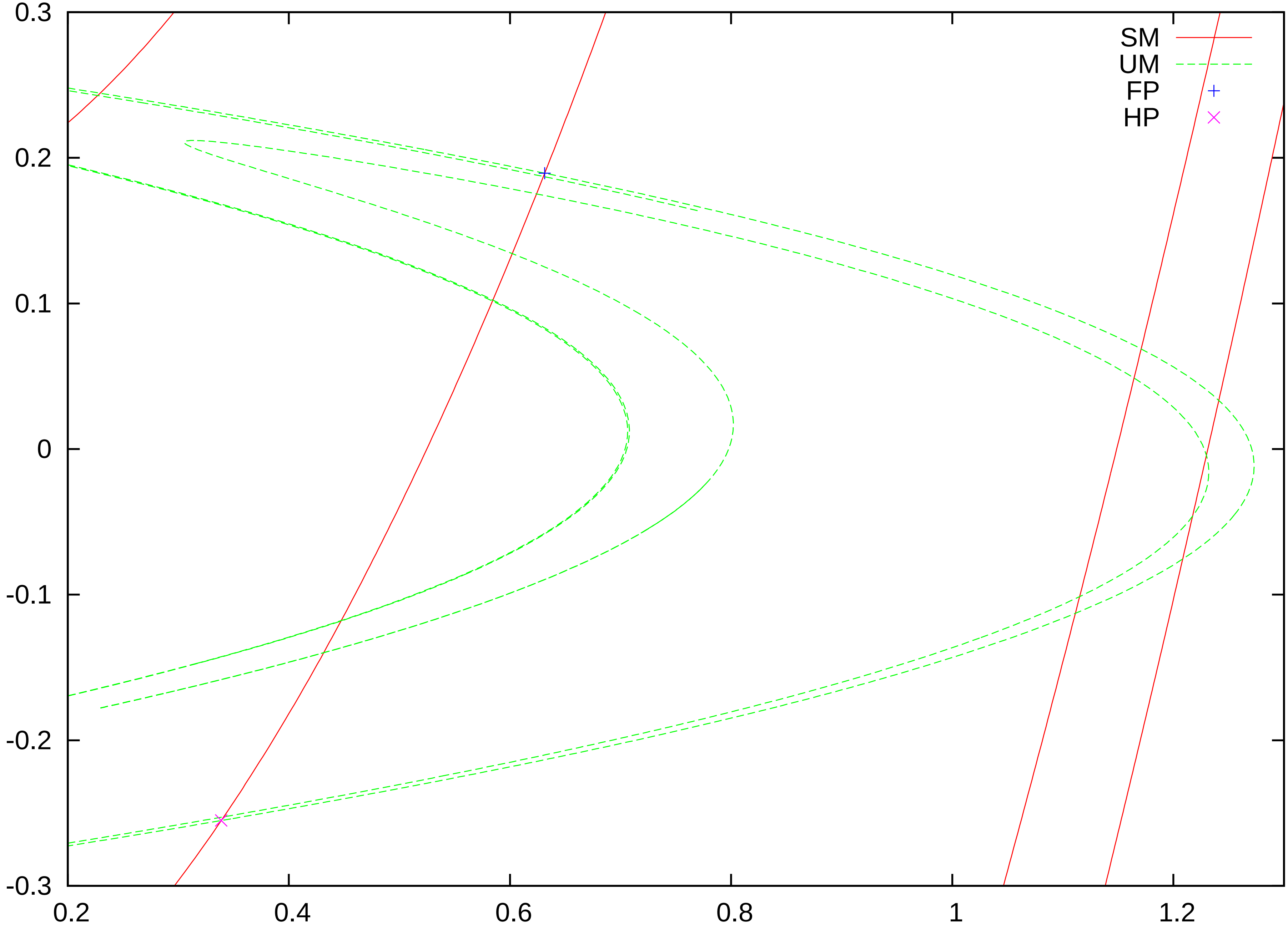
SM
UM
FP
HP
0.3
0.2
0.1
0
-0.1
-0.2
-0.3
0.2
0.4
0.6
0.8
1
1.2

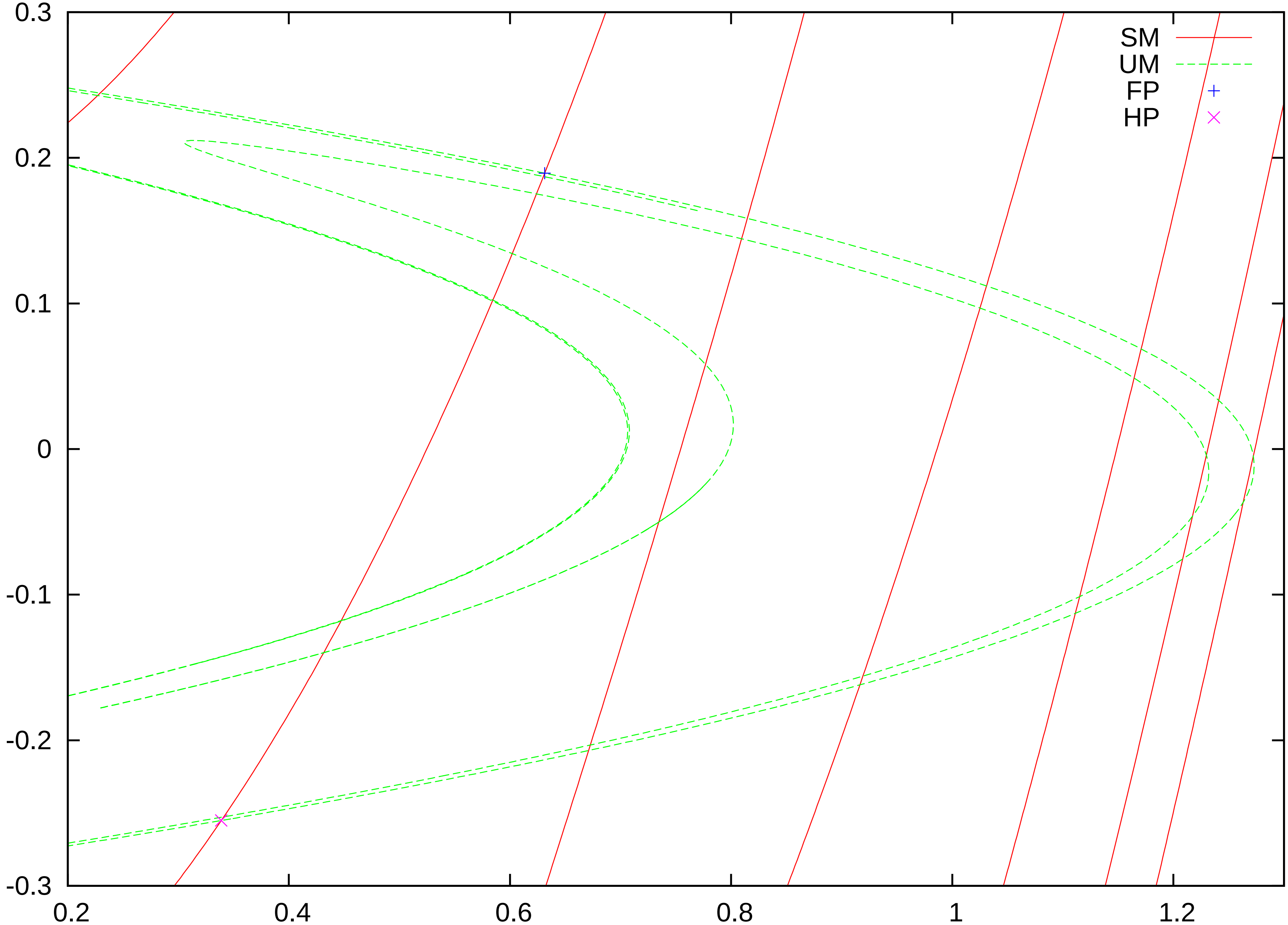

SM
UM
FP
HP
0.3
0.2
0.1
0
-0.1
-0.2
-0.3
0.2
0.4
0.6
0.8
1
1.2

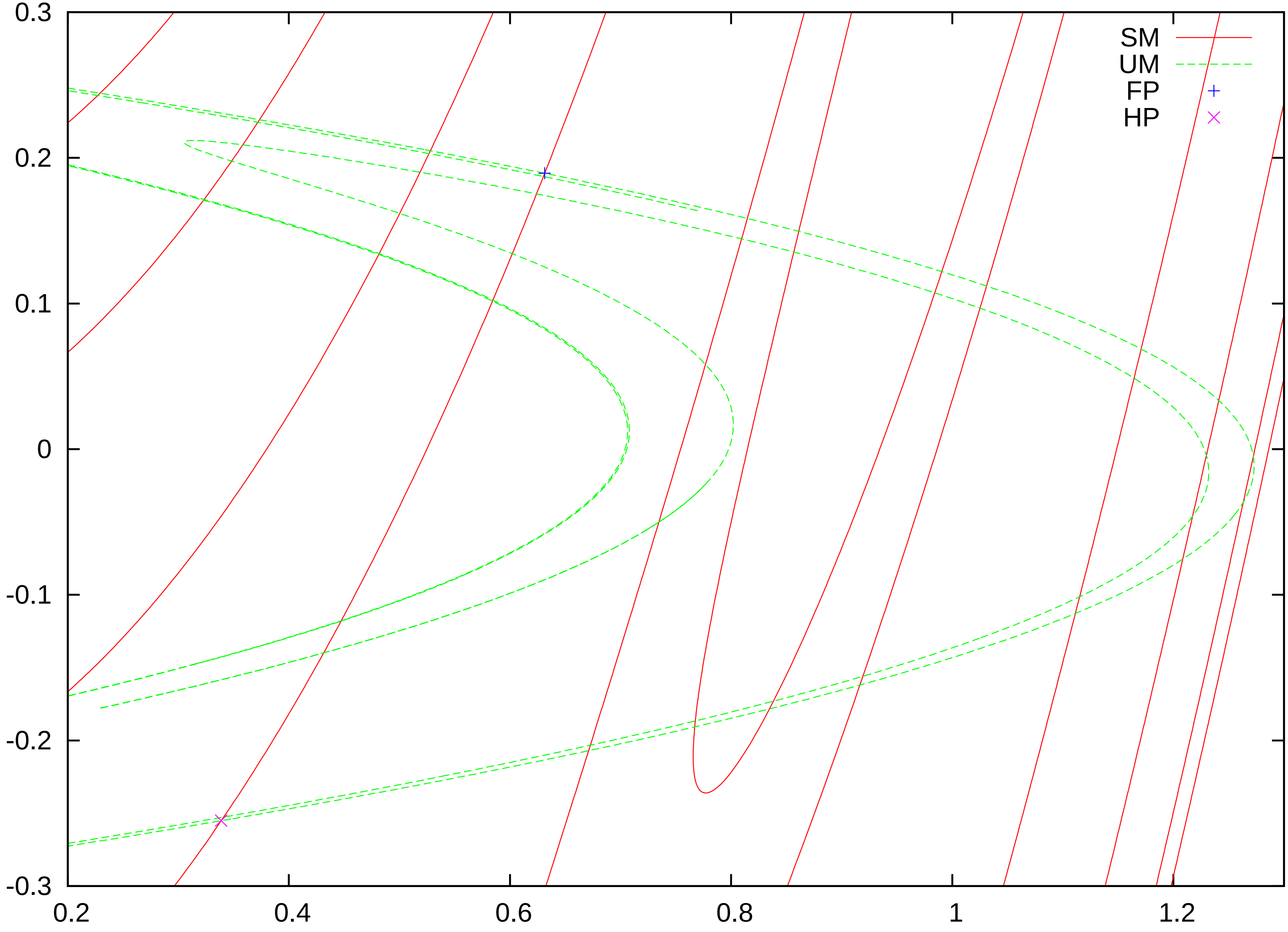

0.3
0.2
0.1
0
-0.1
-0.2
-0.3
0.2
0.4
0.6
0.8
1
1.2
SM
UM
FP
HP

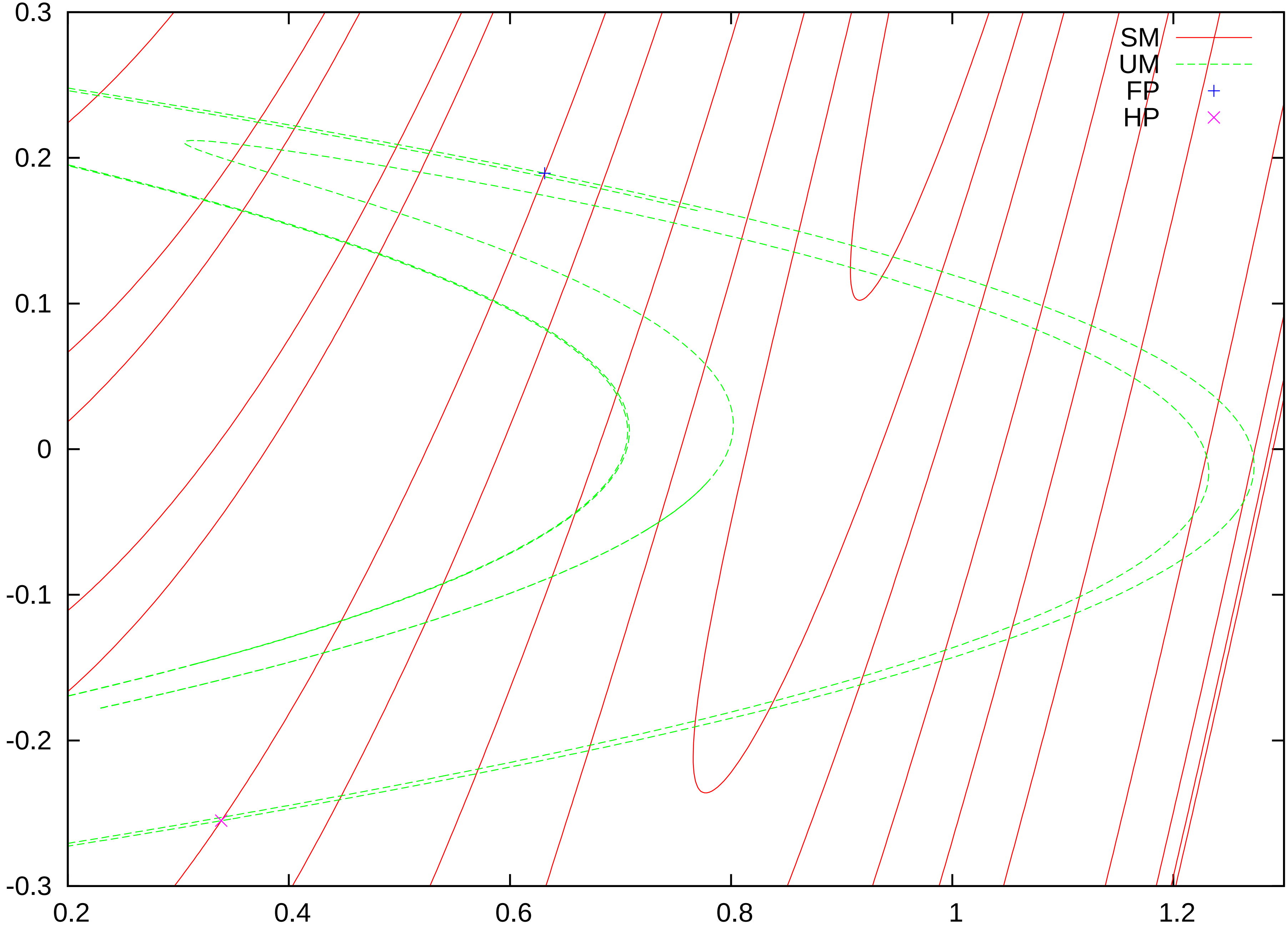

SM
UM
FP
HP
0.3
0.2
0.1
0
-0.1
-0.2
-0.3
0.2
0.4
0.6
0.8
1
1.2

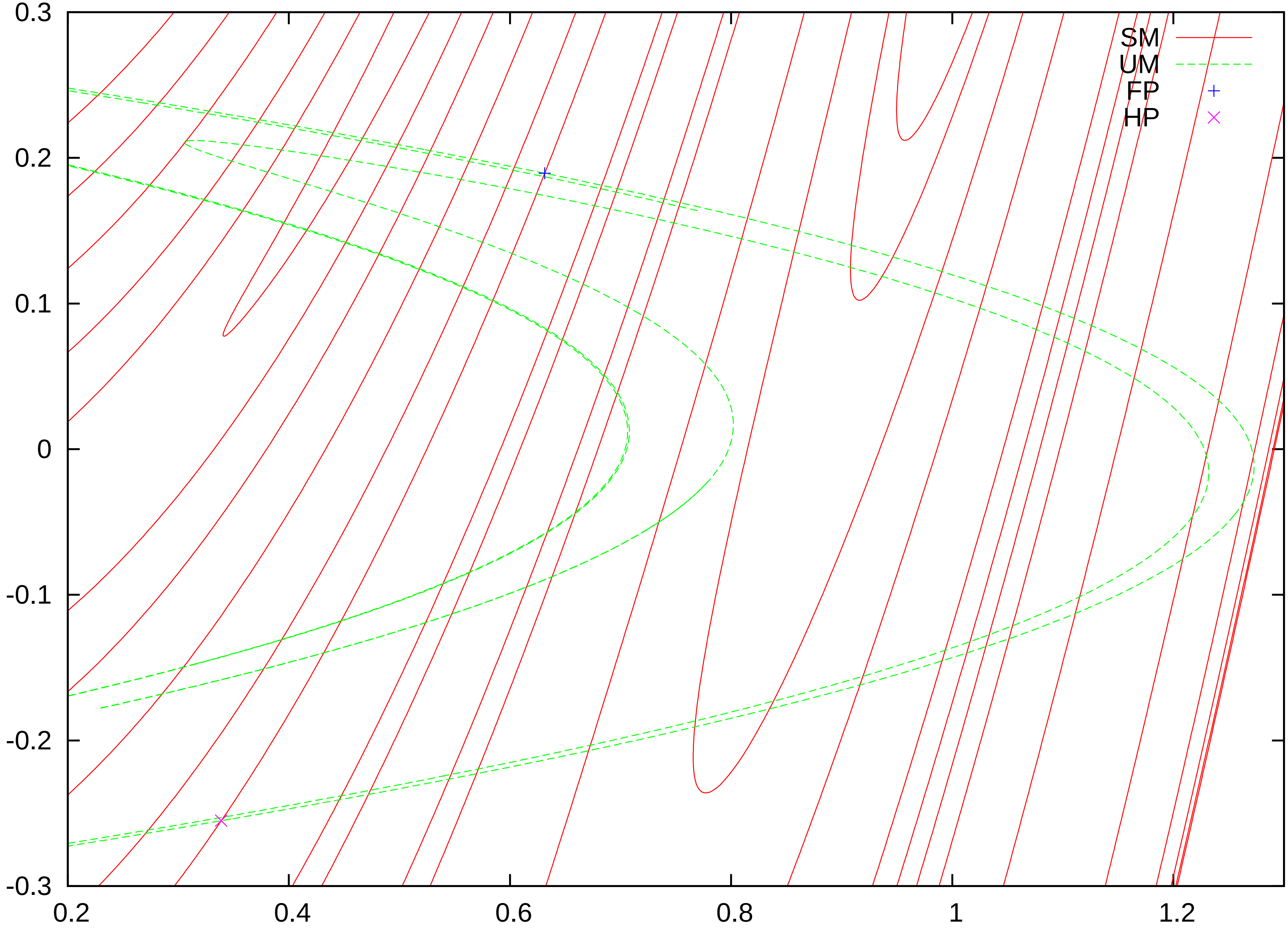

SM
UM
FP
HP
0.3
0.2
0.1
0
-0.1
-0.2
-0.3
0.2
0.4
0.6
0.8
1
1.2

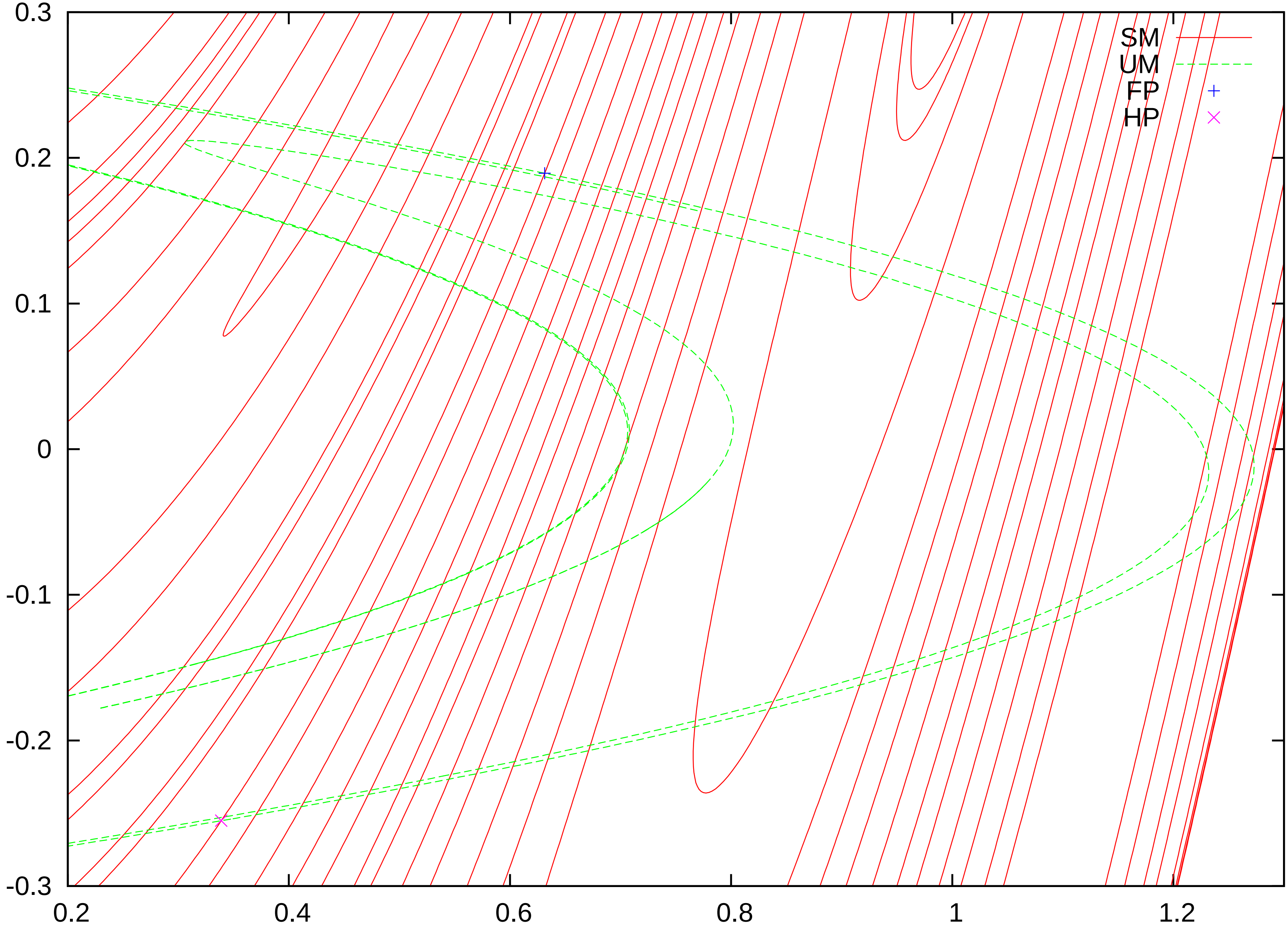
0.3
0.2
0.1
0
-0.1
-0.2
-0.3
0.2
0.4
0.6
0.8
1
1.2
SM
UM
FP
HP

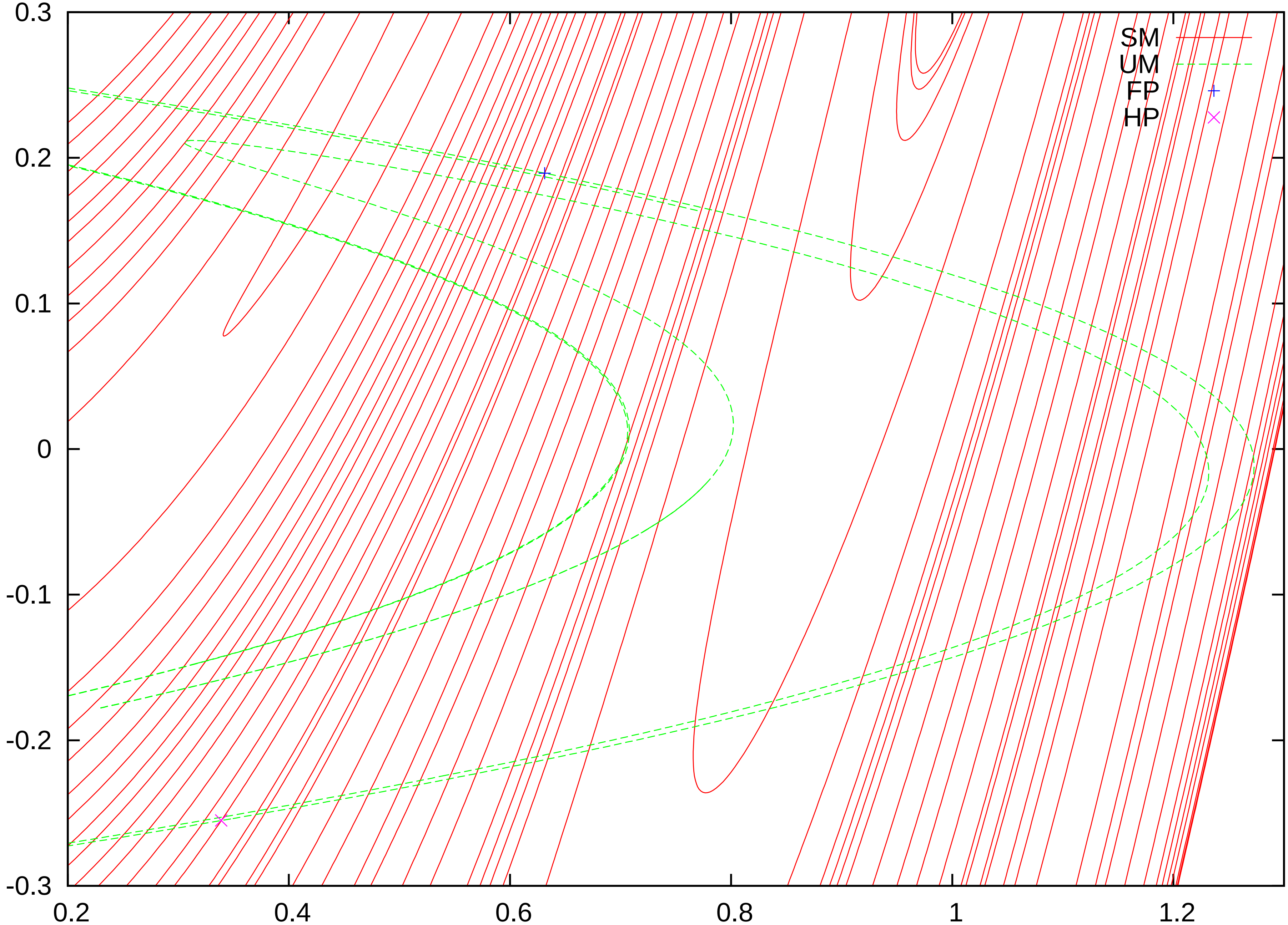

0.3
0.2
0.1
0
-0.1
-0.2
-0.3
0.2
0.4
0.6
0.8
1
1.2
SM
UM
FP
HP

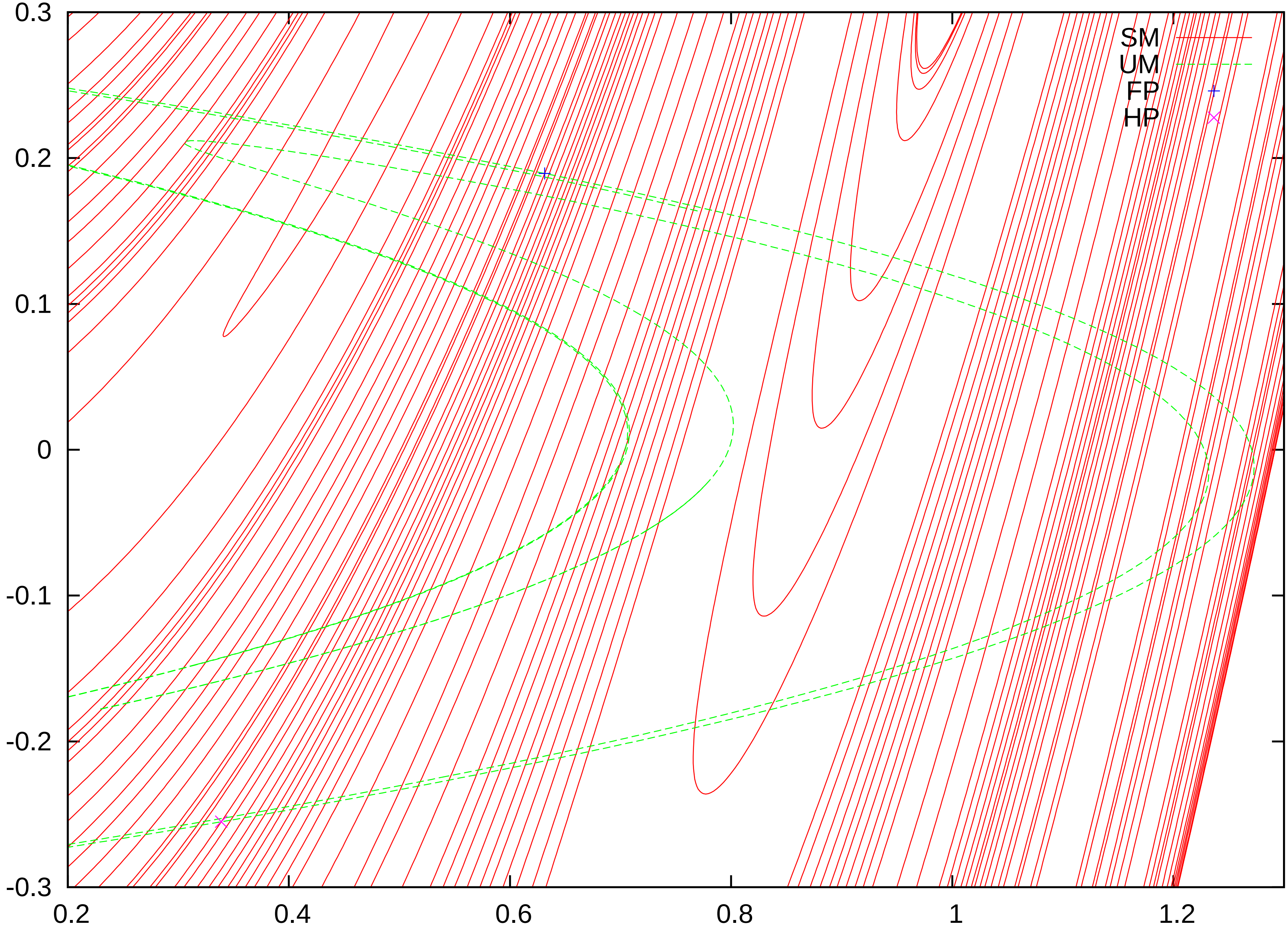

SM
UM
FP
HP
0.3
0.2
0.1
0
-0.1
-0.2
-0.3
0.2
0.4
0.6
0.8
1
1.2

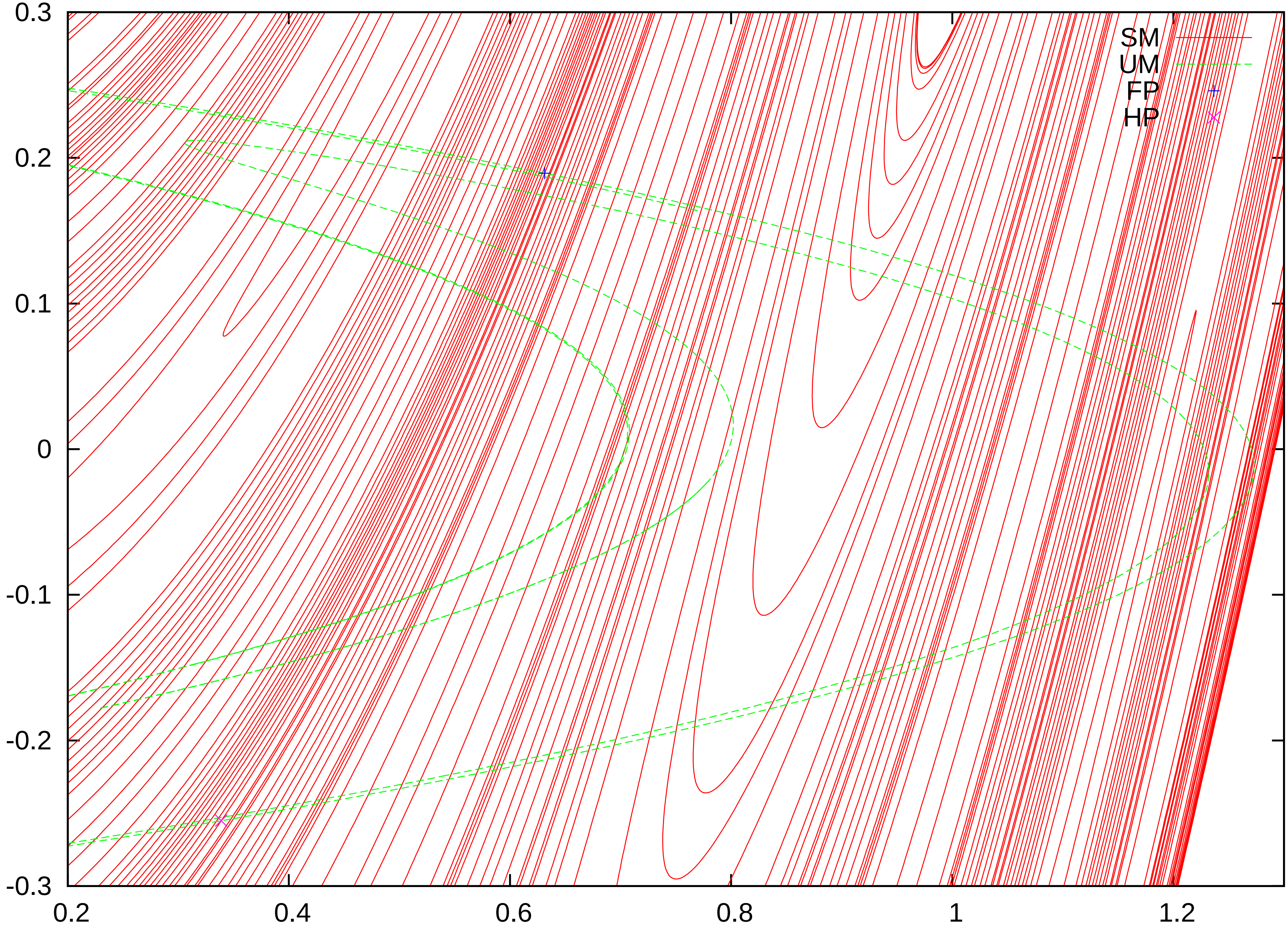
SM
UM
FP
HP
0.3
0.2
0.1
0
-0.1
-0.2
-0.3
0.2
0.4
0.6
0.8
1
1.2

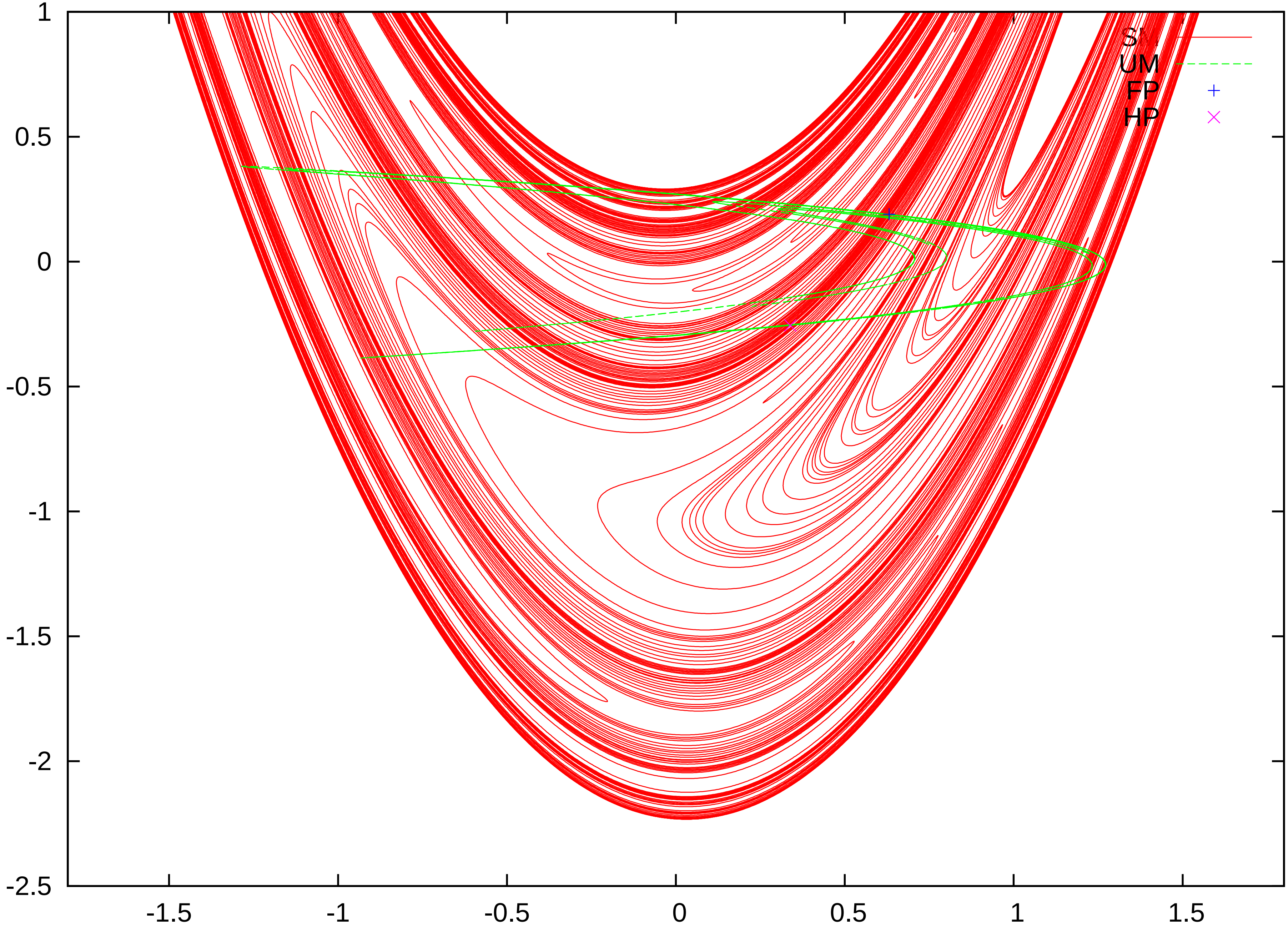
SM
UM
FP
HP
1
0.5
0
-0.5
-1
-1.5
-2
-2.5
-1.5
-1
-0.5
0
0.5
1
1.5

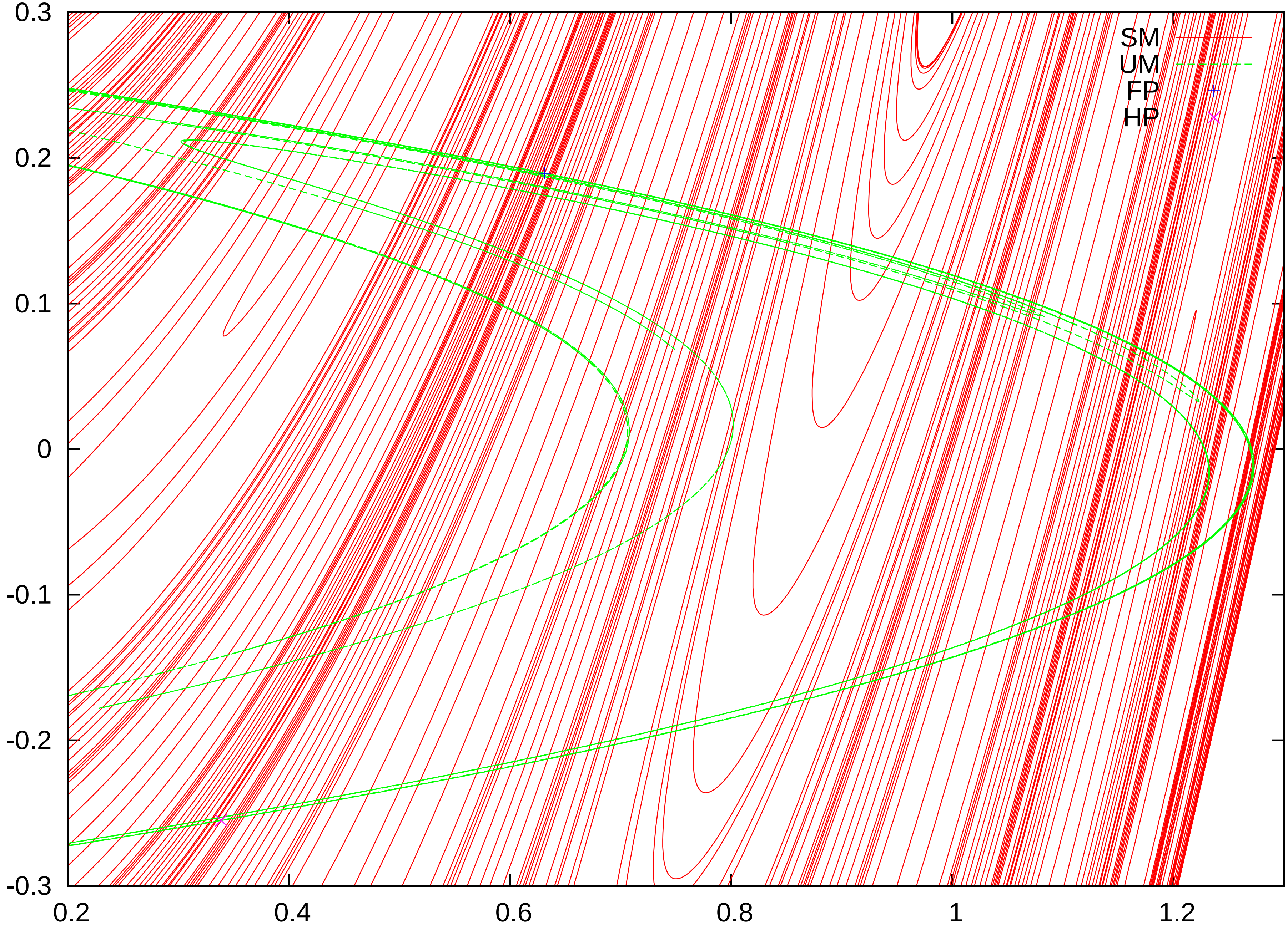

SM
UM
FP
HP
0.3
0.2
0.1
0
-0.1
-0.2
-0.3
0.2
0.4
0.6
0.8
1
1.2

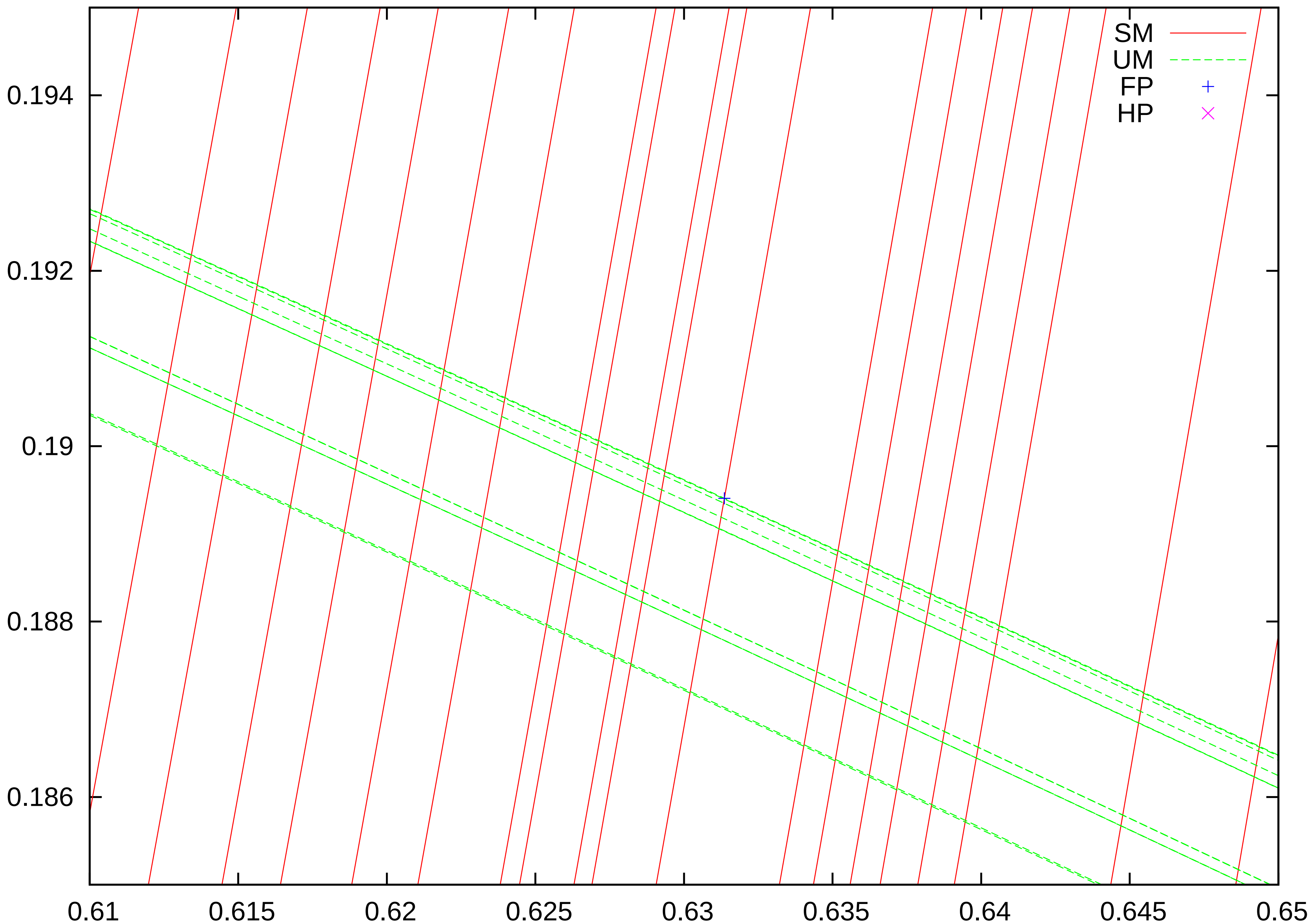

SM
UM
FP
HP
0.194
0.192
0.19
0.188
0.186
0.61
0.615
0.62
0.625
0.63
0.635
0.64
0.645
0.65

Homoclinic and Heteroclinic Points

Rigorous enclosures of the manifolds up to a certain arc length allows:

1. Rigorous enclosures of **homoclinic points** (intersections of stable and unstable manifolds of same fixed points). For example, the "Fundamental" homoclinic point H of the standard Henon map is guaranteed to satisfy

$$H \in (0.3388525493^{912819}_{878994}, -0.25511262978^{29170}_{31221}).$$

2. Rigorous enclosures of **heteroclinic points** (intersections of stable and unstable manifolds of separate fixed points). These have practical applications, for example the design of low-energy transfers in restricted three body problem.

Symbolic Dynamics

Rigorous insight into the behavior of a dynamical system can be obtained by studying symbolic dynamics. This refers to a **projection** of the dynamics into finite sets of "symbols", and study of how these evolve under map. Prime example: determine suitable subsets of variables and study their mapping properties rigorously.

Ideal candidates:

Curvilinear Rectangles: having homoclinic points in their corners, pieces of unstable and stable manifold, respectively, as their sides.

Advantages: Their mapping properties can be rigorously understood by the knowledge of the location of **all** homoclinic points up to a certain arc length of stable and unstable manifold, as well as the **mapping properties** of these homoclinic points.

Rigorous Computational Symbolic Dynamics

Using Taylor model based flow integrators and normal form methods, can set up even very complicated symbolic dynamics. Let two initial pieces of stable and unstable manifold be given.

1. Rigorously enclose **ALL** homoclinic points of using the rigorous global optimizer COSY-GO.
2. Determine rigorous **parent-child relationships** of these homoclinic points.

This allows the rigorous determination the mapping properties of curvilinear rectangles, which can be described by the so-called incidence matrix. The largest eigenvalue of it is a lower bound of the topological entropy.

Note: probably the first such attempt at a rigorous dynamics was done by Piotr Zgliczynski for the Henon map, proving that it follows a horseshoe dynamics, with

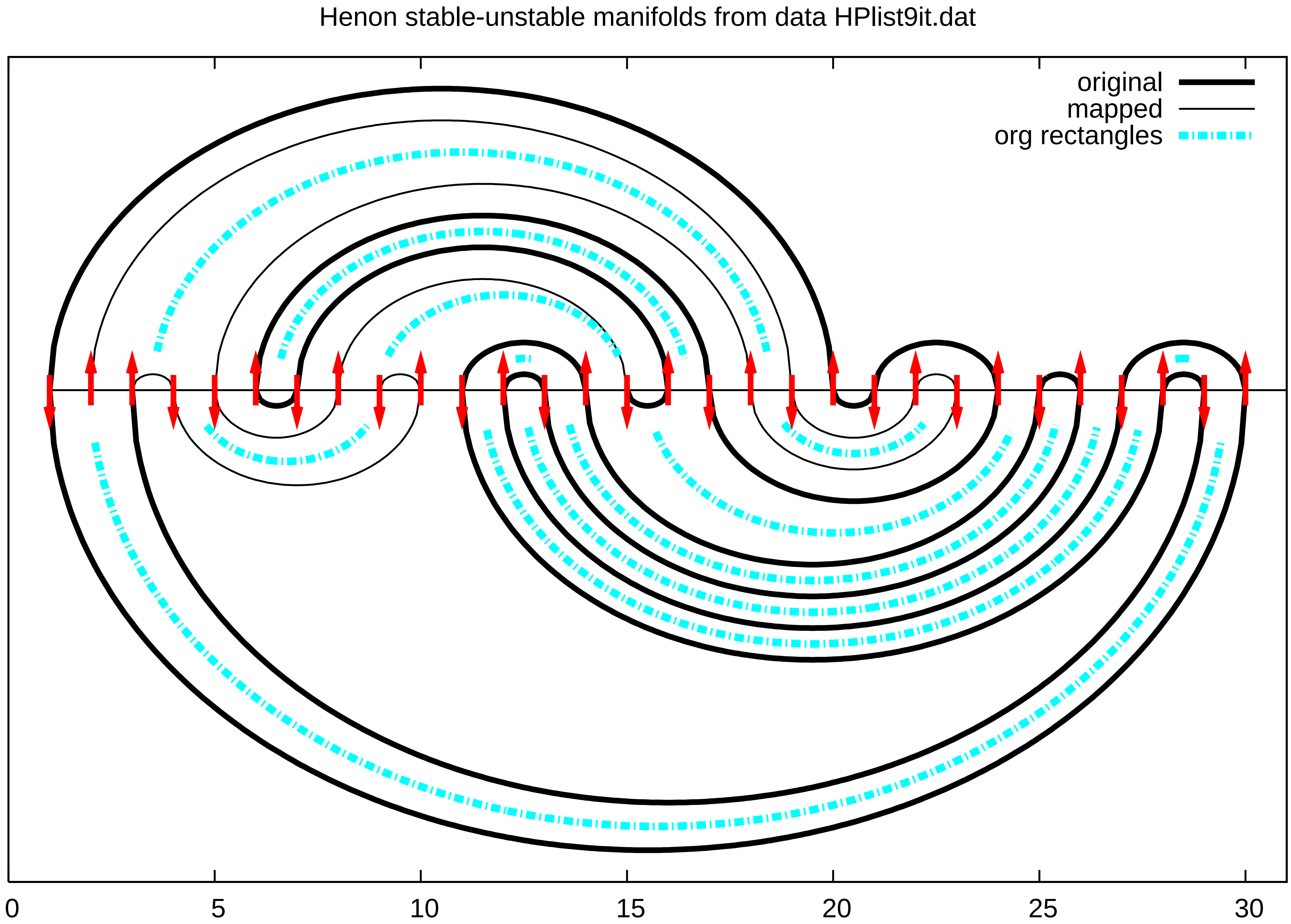
Henon stable-unstable manifolds from data HPlist9it.dat
original
mapped
org rectangles
0
5
10
15
20
25
30

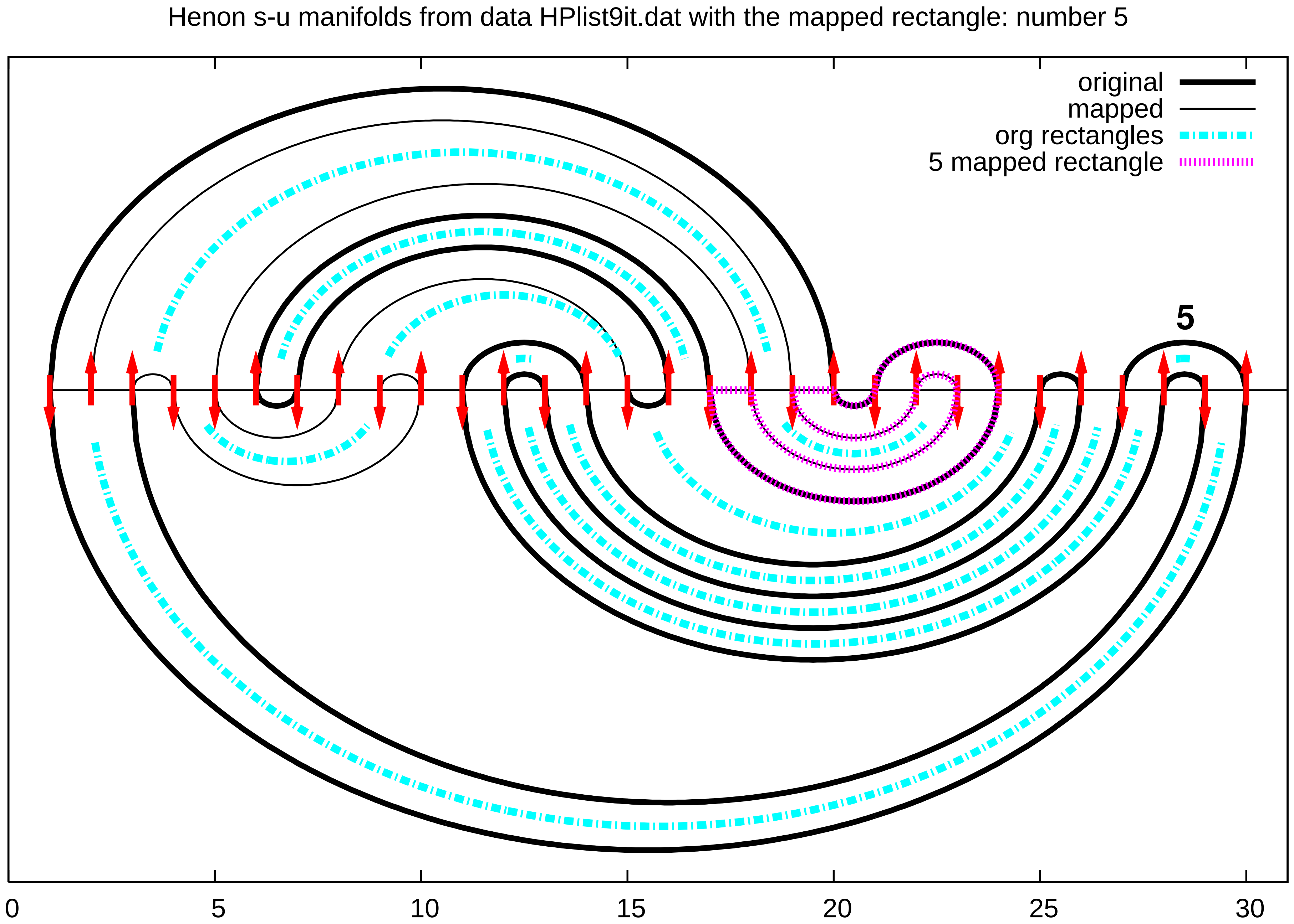

Henon s-u manifolds from data HPlist9it.dat with the mapped rectangle: number 5
original
mapped
org rectangles
5 mapped rectangle
5
0
5
10
15
20
25
30

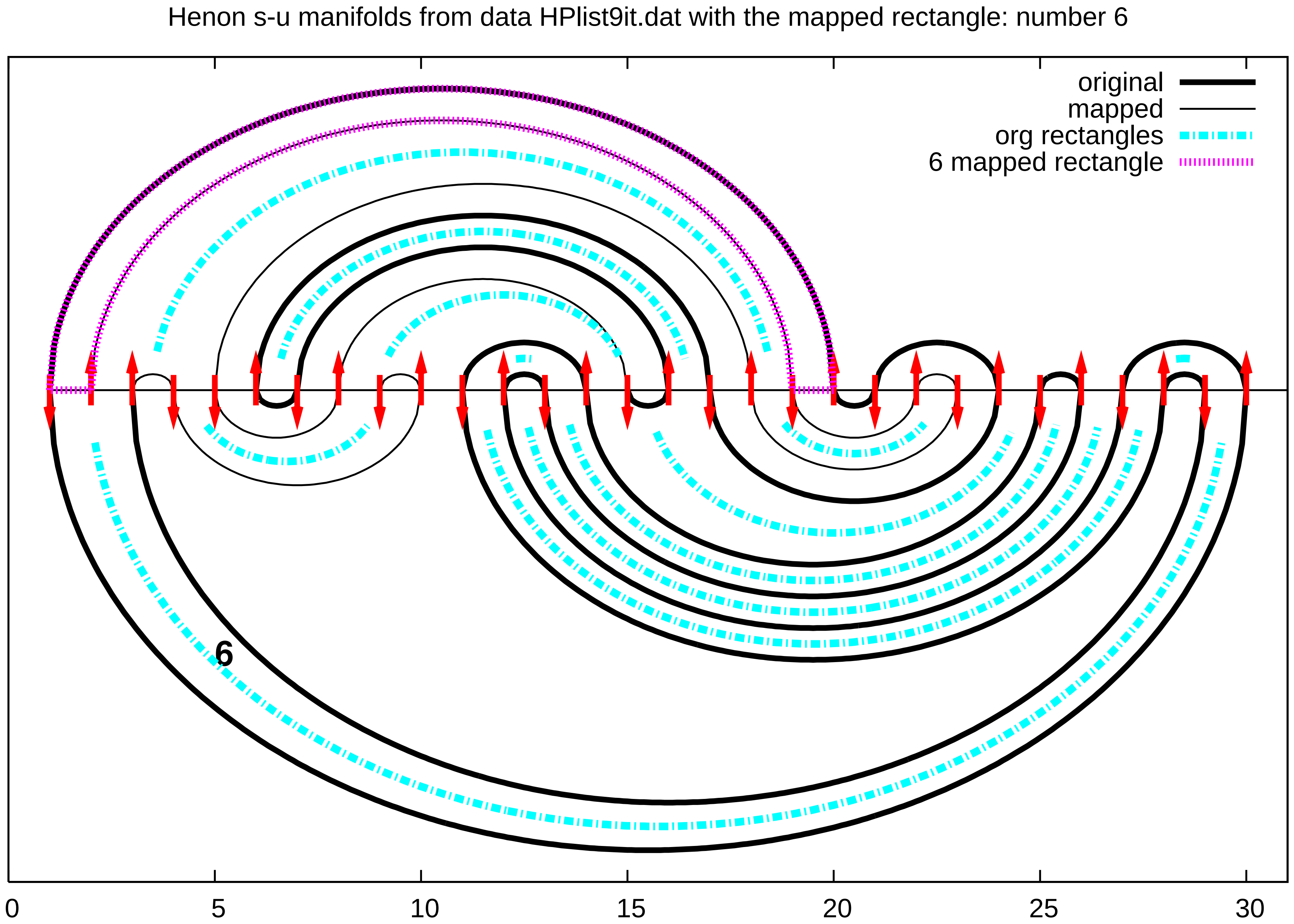

Henon s-u manifolds from data HPlist9it.dat with the mapped rectangle: number 6
original
mapped
org rectangles
6 mapped rectangle
6
0
5
10
15
20
25
30

Henon s-u manifolds from data HPlist9it.dat with the mapped rectangle: number 1

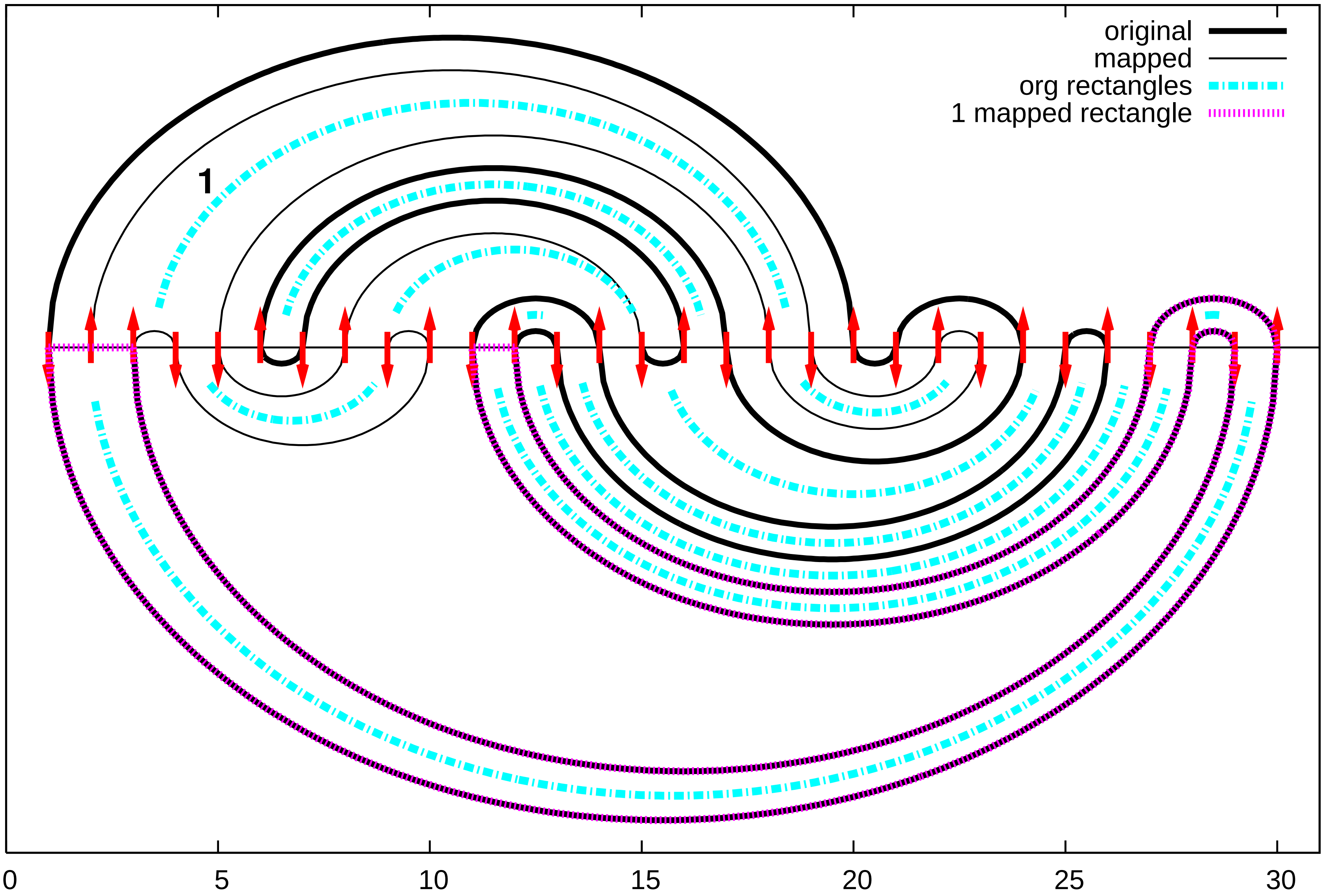

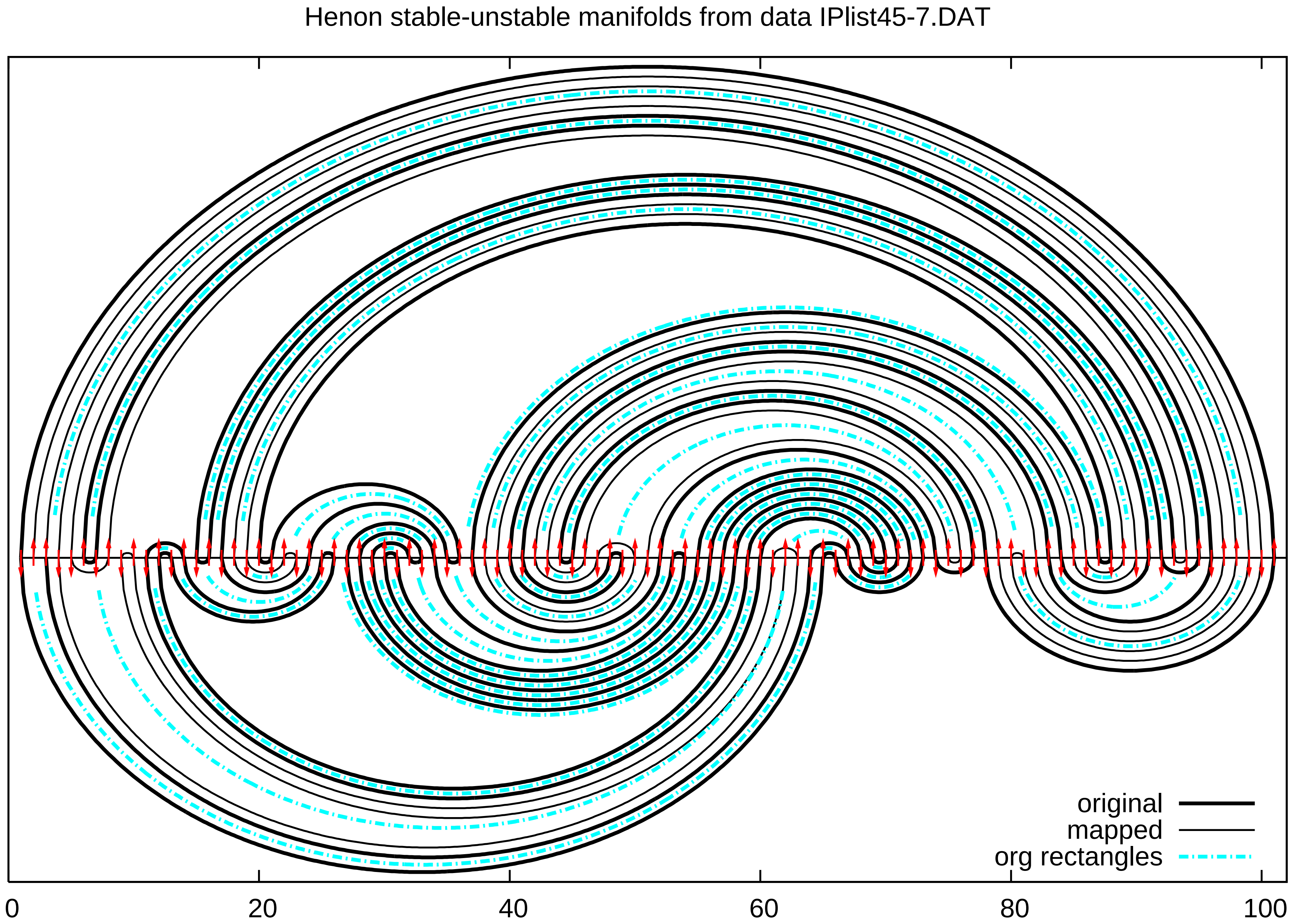

Henon stable-unstable manifolds from data IPlist45-7.DAT
original
mapped
org rectangles
0
20
40
60
80
100

Henon s-u manifolds from data IPlist45-7.DAT with the mapped rectangle: number 1

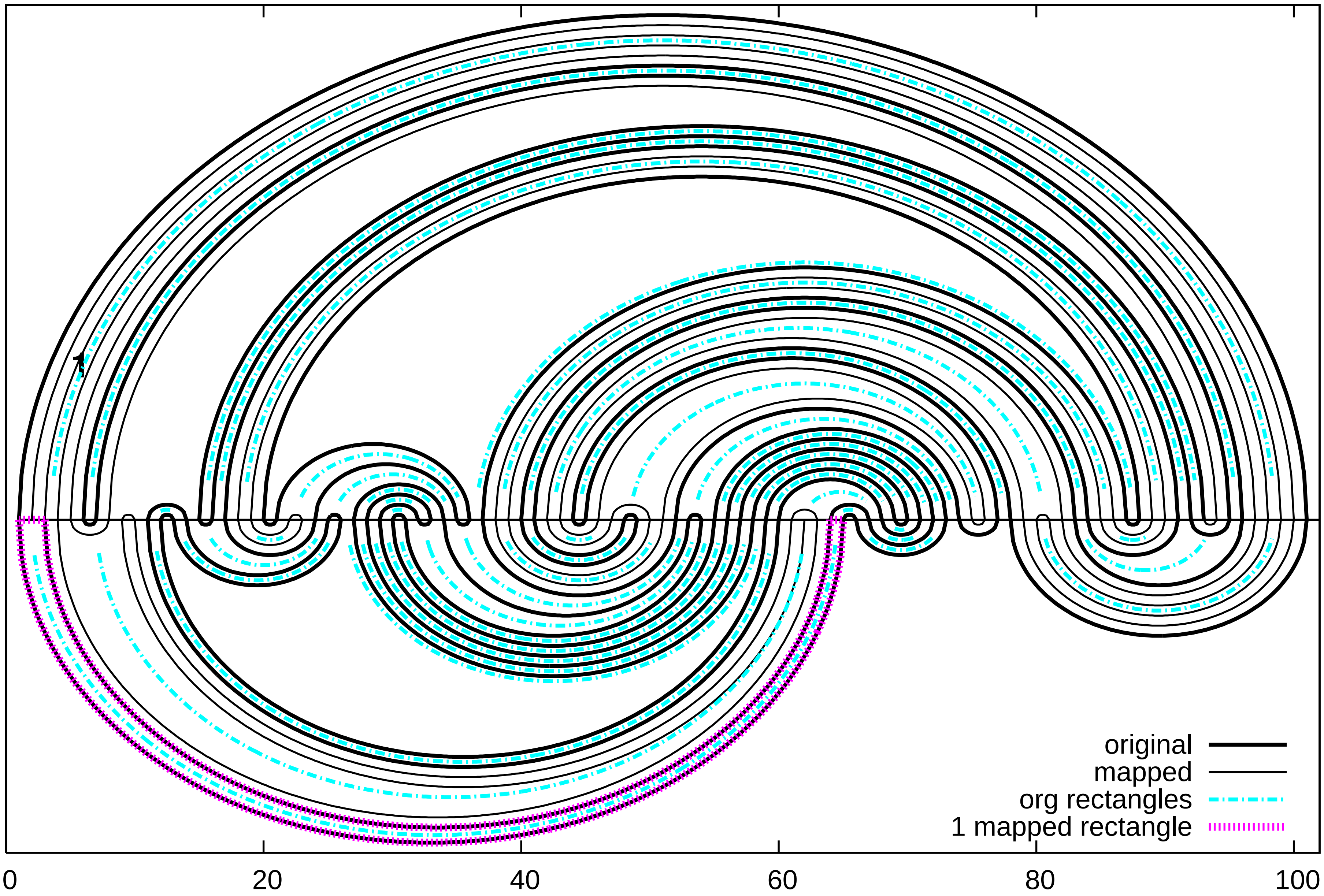

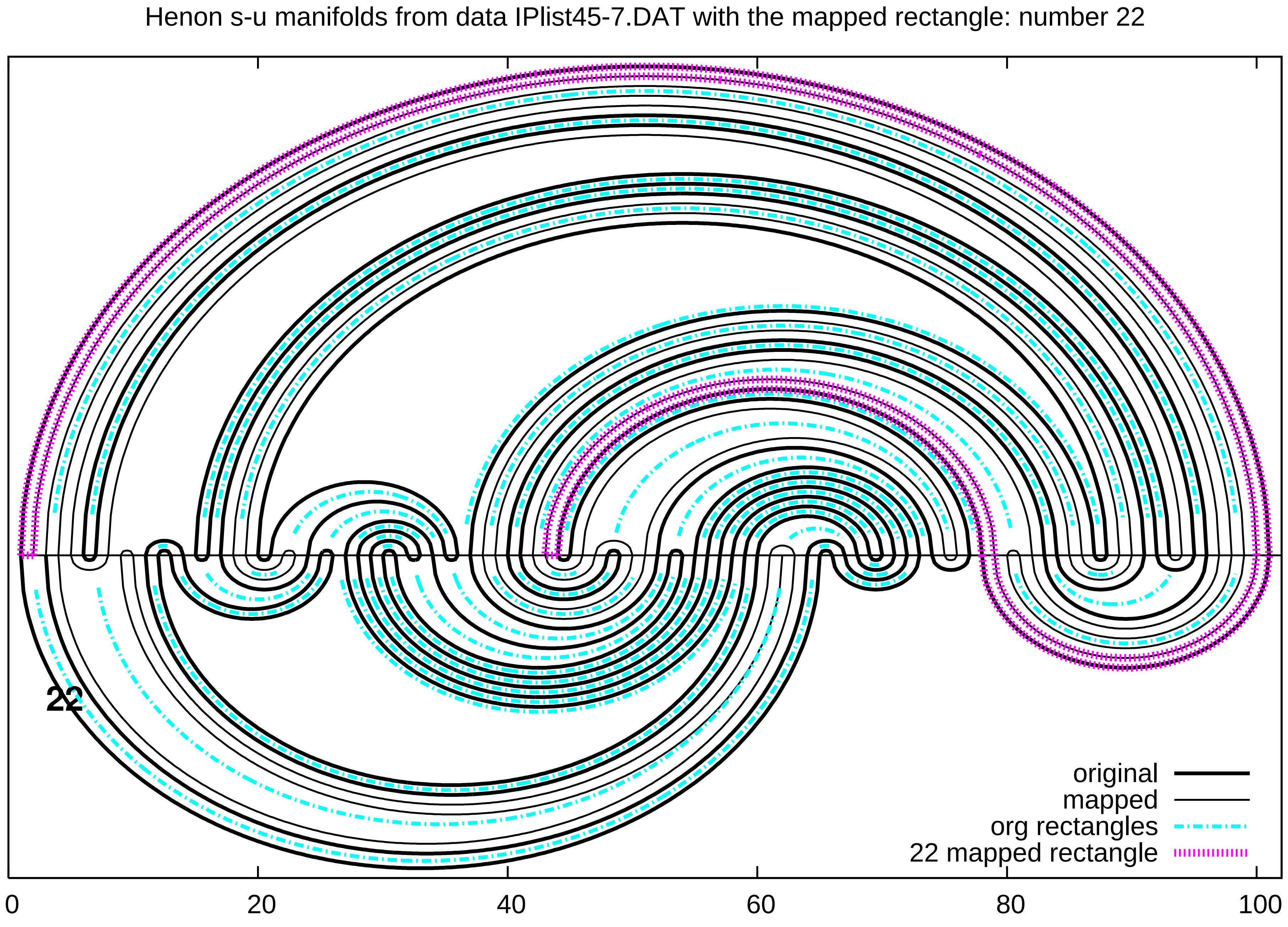

Henon s-u manifolds from data IPlist45-7.DAT with the mapped rectangle: number 22
22
original
mapped
org rectangles
22 mapped rectangle
0
20
40
60
80
100

Henon s-u manifolds from data IPlist45-7.DAT with the mapped rectangle: number 40

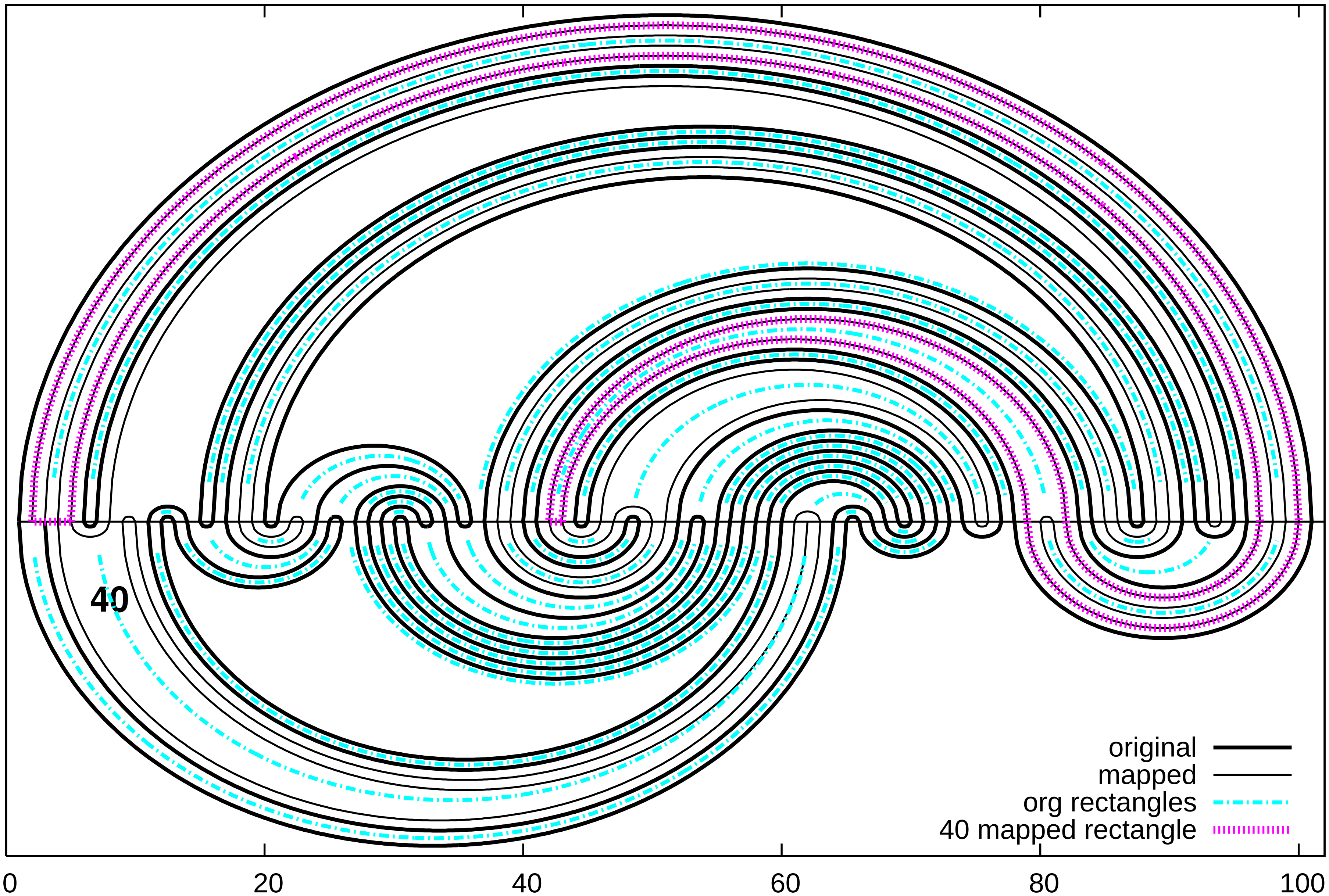

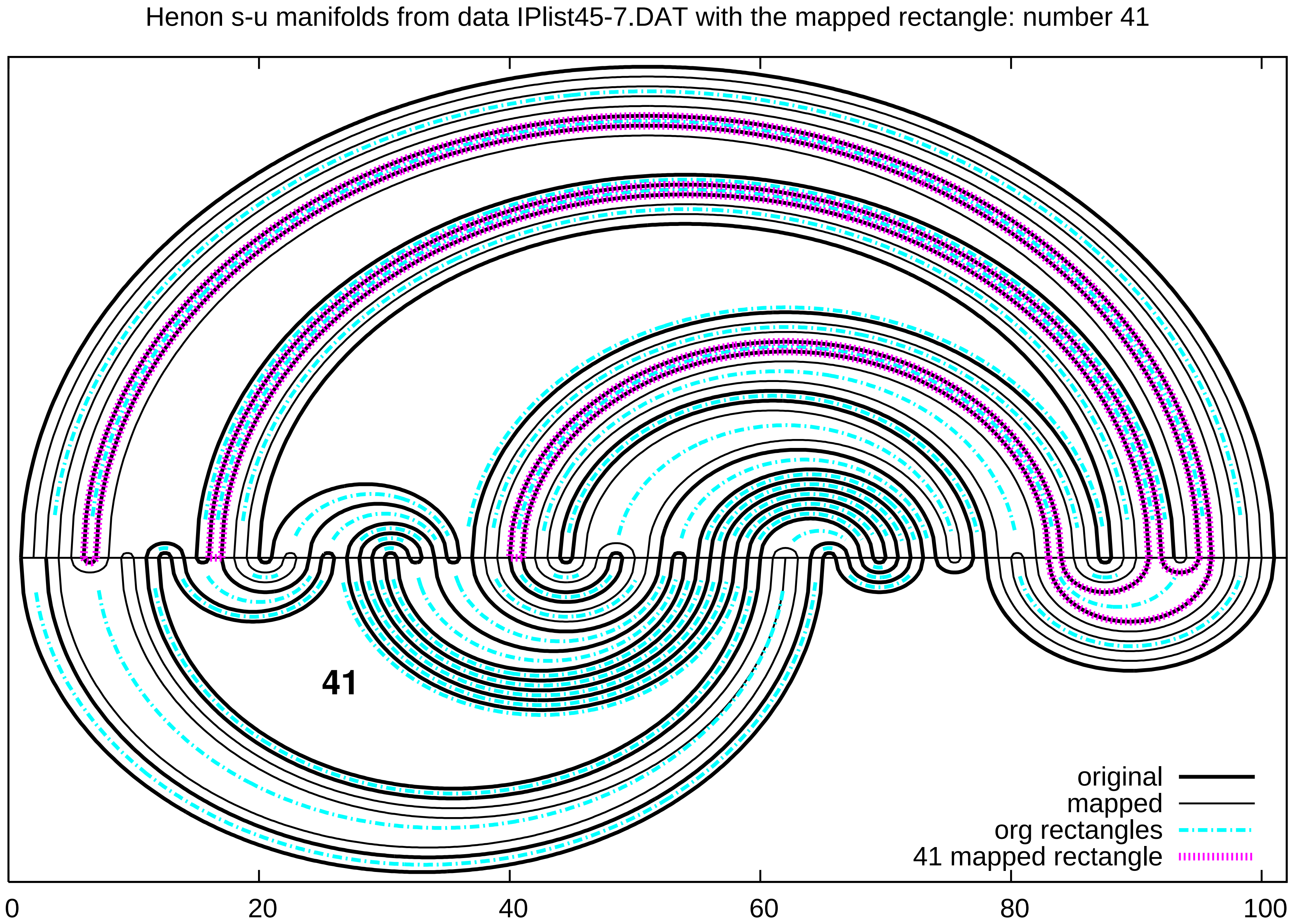
Henon s-u manifolds from data IPlist45-7.DAT with the mapped rectangle: number 41
41
original
mapped
org rectangles
41 mapped rectangle
0
20
40
60
80
100

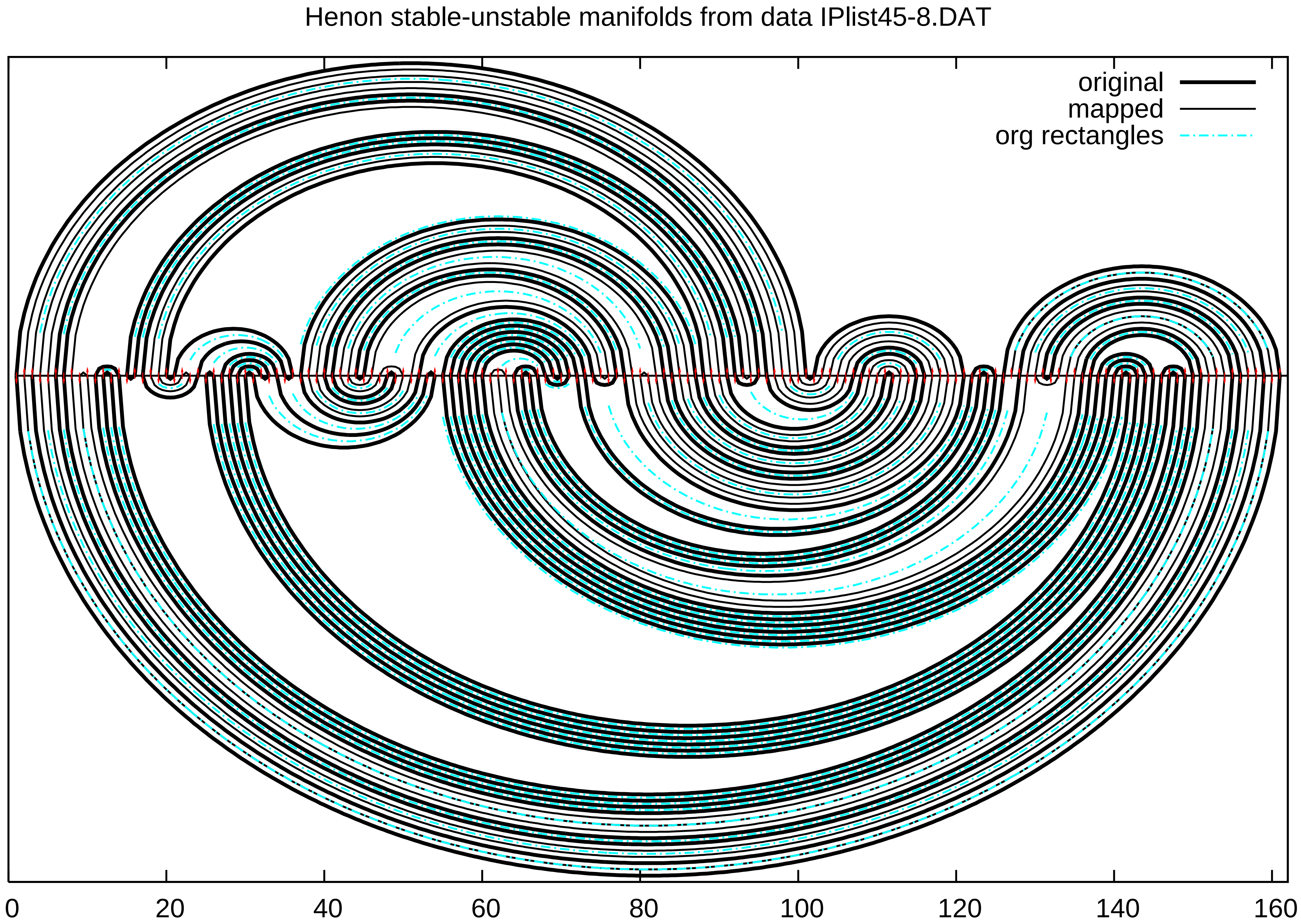
Henon stable-unstable manifolds from data IPlist45-8.DAT
original
mapped
org rectangles
0
20
40
60
80
100
120
140
160

Henon s-u manifolds from data IPlist45-8.DAT with the mapped rectangle: number 1

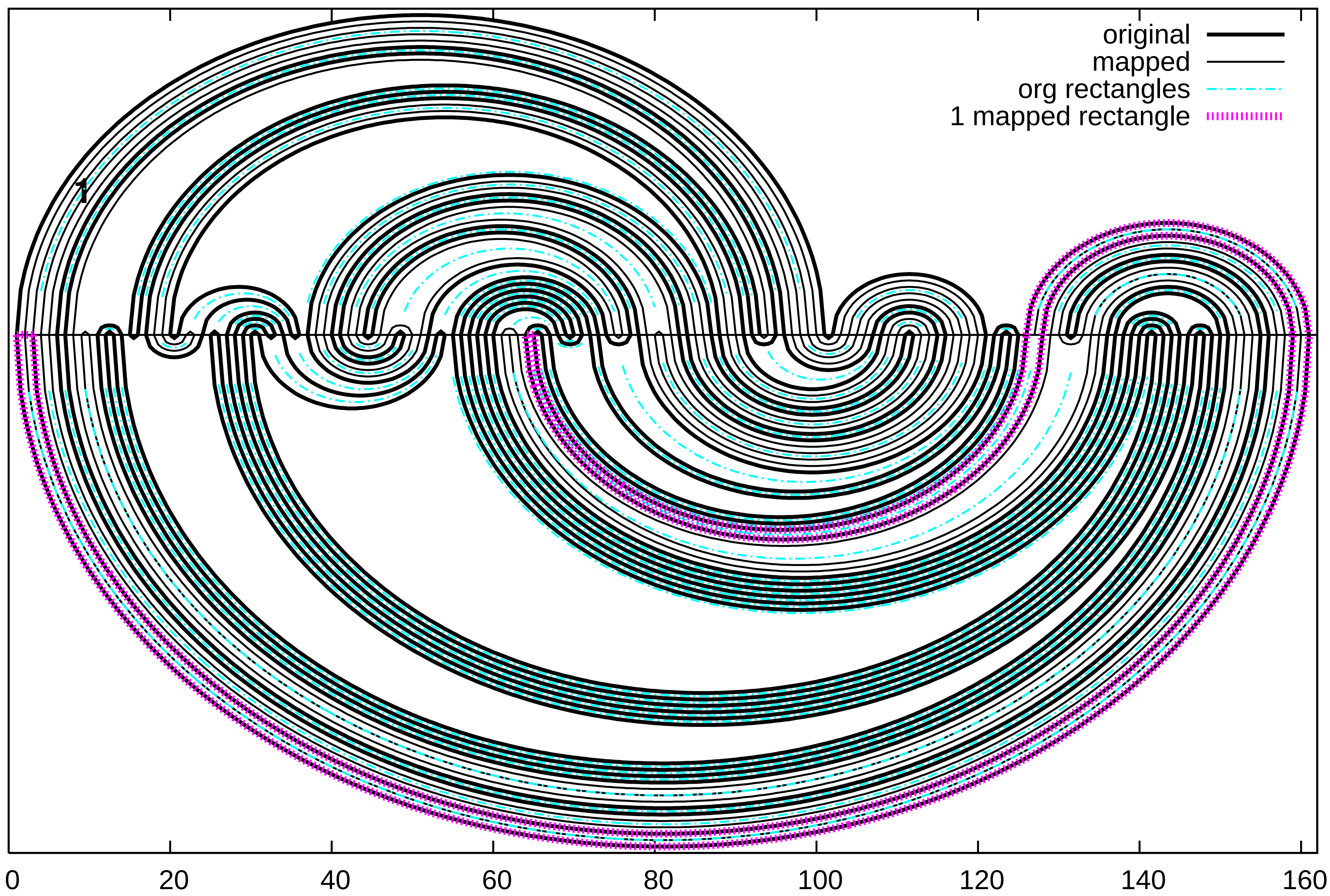

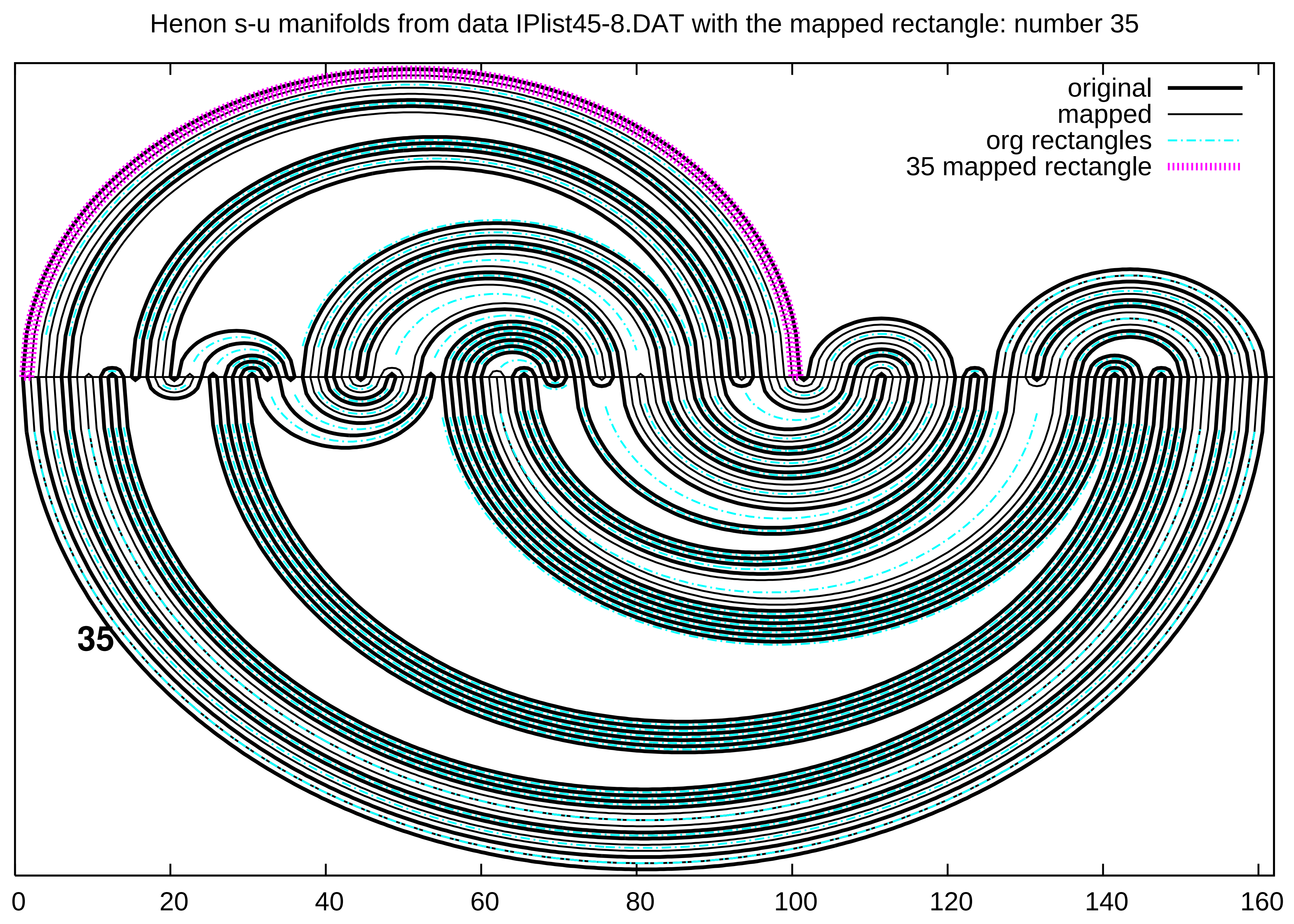
Henon s-u manifolds from data IPlist45-8.DAT with the mapped rectangle: number 35
original
mapped
org rectangles
35 mapped rectangle
35
0
20
40
60
80
100
120
140
160

Henon s-u manifolds from data IPlist45-8.DAT with the mapped rectangle: number 67

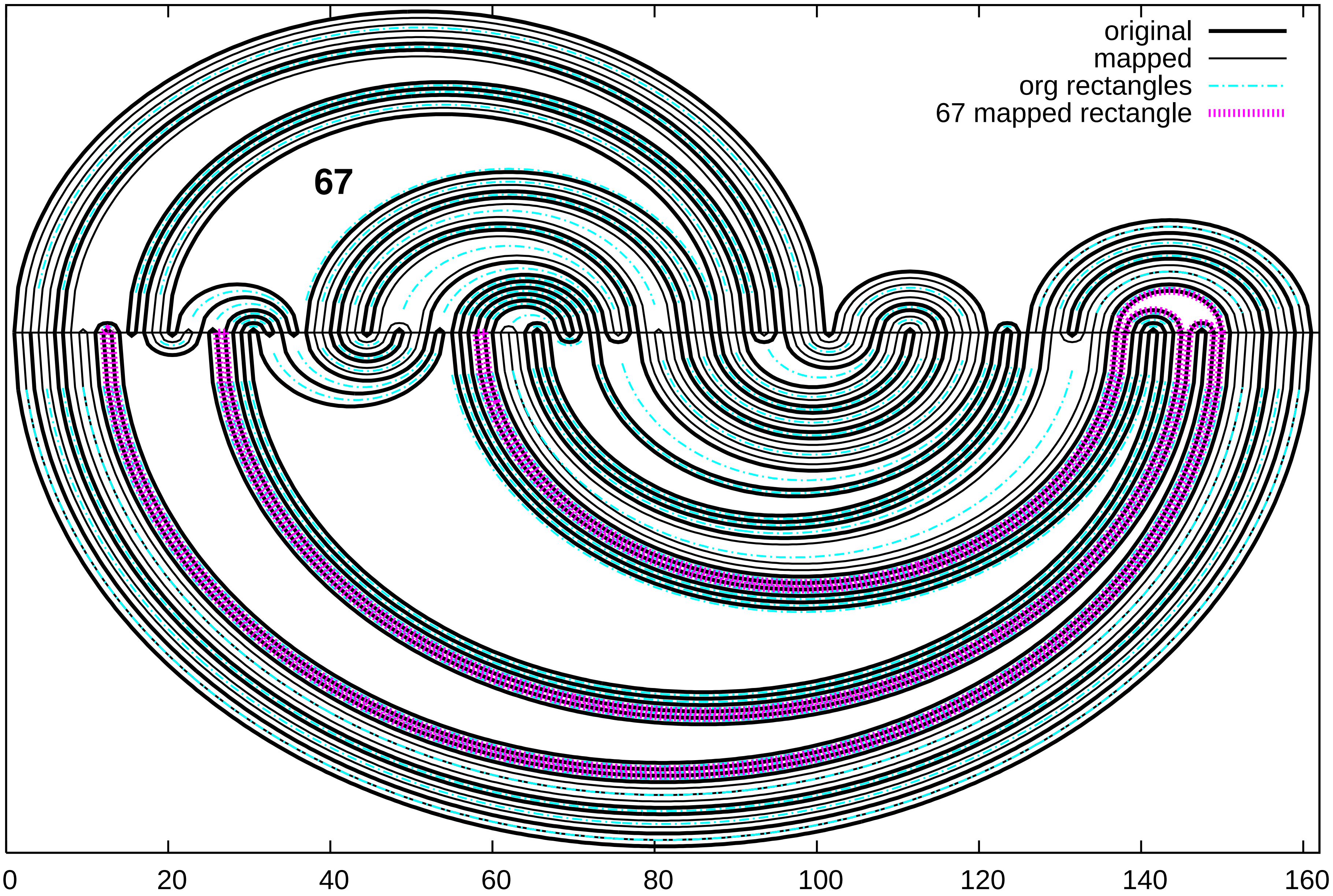

Galias' Subshift:

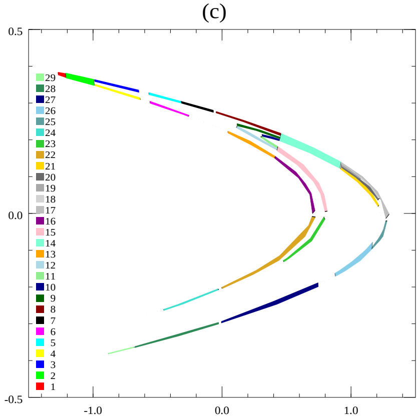

Figure 3: (a) Symbolic dynamics on 8 symbols, initial quadrangles, (b) Symbolic dynamics on 8 symbols, improved quadrangles, (c) Symbolic dynamics on 29 symbols

Figure: Galias Subshift with $h(H) > 0.430$, 29 symbols

Galias-Zgliczynski periodic table:

Table 7. Periodic orbits for the Hénon map belonging to the trapping region. Q_n, number of periodic orbits with period n; P_n, number of fixed points of h^n; $\mathrm{H}_n(h) = n^{-1}\log(P_n)$, estimation of topological entropy based on P_n.

n	Q_n	P_n	$\mathrm{H}_n(h)$
1	1	1	0.000 00
2	1	3	0.549 31
3	0	1	0.000 00
4	1	7	0.486 48
5	0	1	0.000 00
6	2	15	0.451 34
7	4	29	0.481 04
8	7	63	0.517 89
9	6	55	0.445 26
10	10	103	0.463 47
11	14	155	0.458 49
12	19	247	0.459 12
13	32	417	0.464 08
14	44	647	0.462 31
15	72	1 081	0.465 71
16	102	1 695	0.464 71
17	166	2 823	0.467 39
18	233	4 263	0.464 32
19	364	6 917	0.465 35
20	535	10 807	0.464 40
21	834	17 543	0.465 35
22	1 225	27 107	0.463 98
23	1 930	44 391	0.465 25
24	2 902	69 951	0.464 81
25	4 498	112 451	0.465 21
26	6 806	177 375	0.464 85
27	10 518	284 041	0.465 07
28	16 031	449 519	0.464 85
29	24 740	717 461	0.464 95
30	37 936	1139 275	0.464 86

Figure: Galias Periodic Table

Entropy Estimates from Trellis Untangling

1. 161 HP's, Pure Rectangles, 66 Symbols, 94 Crossings: 0.4131

Entropy Estimates from Trellis Untangling

1. 161 HP's, Pure Rectangles, 66 Symbols, 94 Crossings: 0.4131
2. 161 HP's, Rect +Hexagons, 77 Symbols, 110 Crossings: 0.4309

Entropy Estimates from Trellis Untangling

1. 161 HP's, Pure Rectangles, 66 Symbols, 94 Crossings: 0.4131
2. 161 HP's, Rect +Hexagons, 77 Symbols, 110 Crossings: 0.4309
3. 267 HP's, Pure Rectangles, 119 Symbols, 185 Crossings: 0.4131
4. 267 HP's, Rect +Hexagons, 130 Symbols, 205 Crossings: 0.4402

Entropy Estimates from Trellis Untangling

1. 161 HP's, Pure Rectangles, 66 Symbols, 94 Crossings: 0.4131
2. 161 HP's, Rect +Hexagons, 77 Symbols, 110 Crossings: 0.4309
3. 267 HP's, Pure Rectangles, 119 Symbols, 185 Crossings: 0.4131
4. 267 HP's, Rect +Hexagons, 130 Symbols, 205 Crossings: 0.4402
5. 437 HP's, Pure Rectangles, 218 Symbols, 346 Crossings: 0.4282
6. 437 HP's, Rect +Hexagons, 229 Symbols, 366 Crossings: 0.4499

Entropy Estimates from Trellis Untangling

1. 161 HP's, Pure Rectangles, 66 Symbols, 94 Crossings: 0.4131
2. 161 HP's, Rect +Hexagons, 77 Symbols, 110 Crossings: 0.4309
3. 267 HP's, Pure Rectangles, 119 Symbols, 185 Crossings: 0.4131
4. 267 HP's, Rect +Hexagons, 130 Symbols, 205 Crossings: 0.4402
5. 437 HP's, Pure Rectangles, 218 Symbols, 346 Crossings: 0.4282
6. 437 HP's, Rect +Hexagons, 229 Symbols, 366 Crossings: 0.4499
7. 707 HP's, Pure Rectangles, 381 Symbols, 603 Crossings: 0.4417
8. 707 HP's, Rect +Hexagons, 392 Symbols, 621 Crossings: 0.4536

Galias' Subshift:

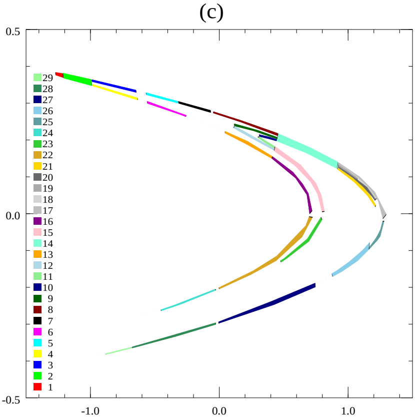

Figure 3: (a) Symbolic dynamics on 8 symbols, initial quadrangles, (b) Symbolic dynamics on 8 symbols, improved quadrangles, (c) Symbolic dynamics on 29 symbols

Figure: Galias Subshift with $h(H) > 0.430$, 29 symbols

Galias-Zgliczynski periodic table:

Table 7. Periodic orbits for the Hénon map belonging to the trapping region. Q_n, number of periodic orbits with period n; P_n, number of fixed points of h^n; $\mathrm{H}_n(h) = n^{-1}\log(P_n)$, estimation of topological entropy based on P_n.

n	Q_n	P_n	$\mathrm{H}_n(h)$
1	1	1	0.000 00
2	1	3	0.549 31
3	0	1	0.000 00
4	1	7	0.486 48
5	0	1	0.000 00
6	2	15	0.451 34
7	4	29	0.481 04
8	7	63	0.517 89
9	6	55	0.445 26
10	10	103	0.463 47
11	14	155	0.458 49
12	19	247	0.459 12
13	32	417	0.464 08
14	44	647	0.462 31
15	72	1 081	0.465 71
16	102	1 695	0.464 71
17	166	2 823	0.467 39
18	233	4 263	0.464 32
19	364	6 917	0.465 35
20	535	10 807	0.464 40
21	834	17 543	0.465 35
22	1 225	27 107	0.463 98
23	1 930	44 391	0.465 25
24	2 902	69 951	0.464 81
25	4 498	112 451	0.465 21
26	6 806	177 375	0.464 85
27	10 518	284 041	0.465 07
28	16 031	449 519	0.464 85
29	24 740	717 461	0.464 95
30	37 936	1139 275	0.464 86

Figure: Galias Periodic Table

Entropy Estimates from Trellis Untangling

1. 161 HP's, Pure Rectangles, 66 Symbols, 94 Crossings: 0.4131
2. 161 HP's, Rect +Hexagons, 77 Symbols, 110 Crossings: 0.4309
3. 267 HP's, Pure Rectangles, 119 Symbols, 185 Crossings: 0.4131
4. 267 HP's, Rect +Hexagons, 130 Symbols, 205 Crossings: 0.4402
5. 437 HP's, Pure Rectangles, 218 Symbols, 346 Crossings: 0.4282
6. 437 HP's, Rect +Hexagons, 229 Symbols, 366 Crossings: 0.4499
7. 707 HP's, Pure Rectangles, 381 Symbols, 603 Crossings: 0.4417
8. 707 HP's, Rect +Hexagons, 392 Symbols, 621 Crossings: 0.4536

Outlook

1. Current Computations take a few minutes for HP's, and a few seconds for symbolic dynamics
2. Expect we can go to 100,000 HP's
3. Other Symbolic Dynamics with Taylor Model Symbols

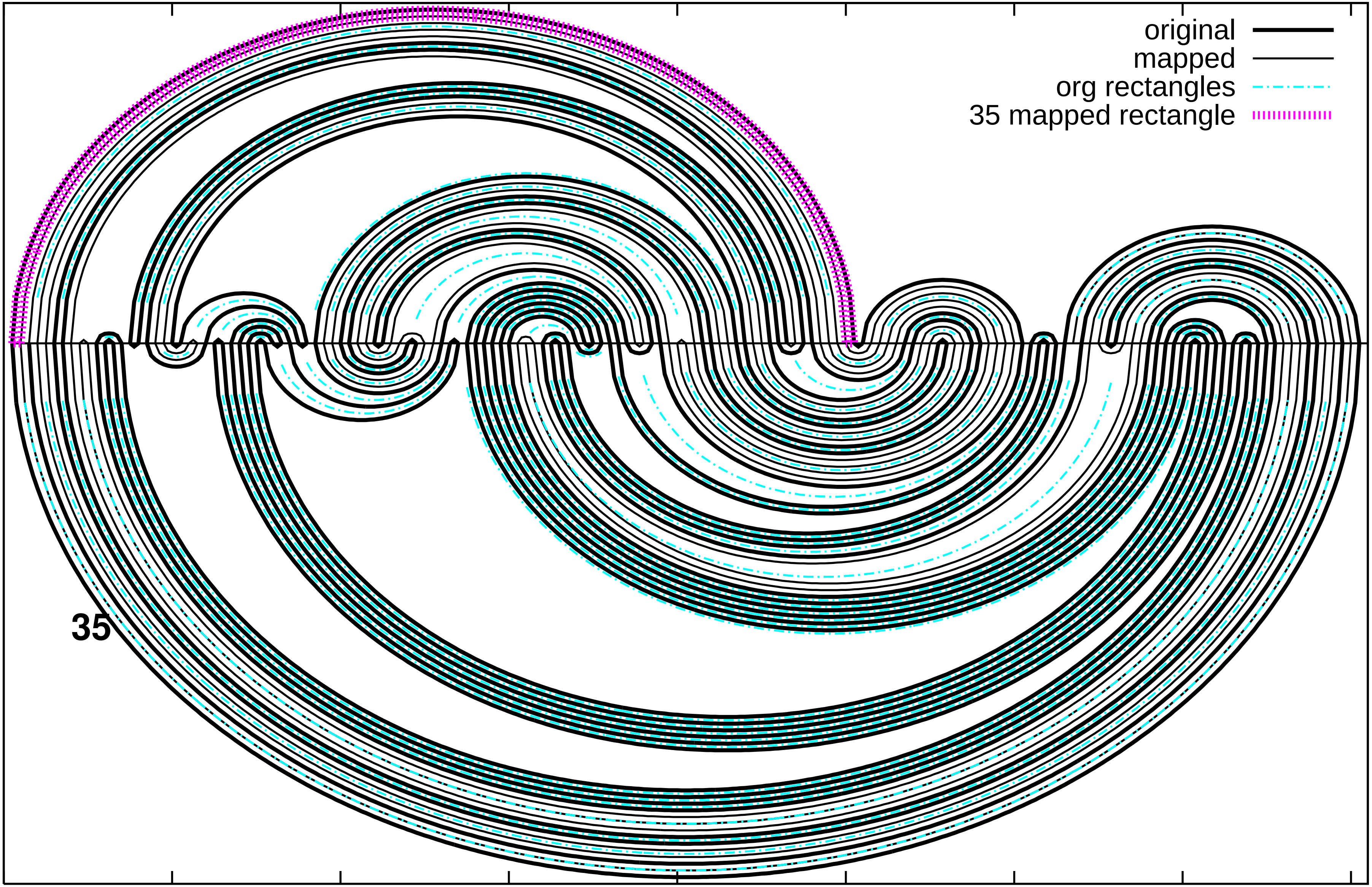
original
mapped
org rectangles
35 mapped rectangle
35